

# **"The interaction between bentonite and water vapor"**

Von der Fakultät für Georessourcen und Materialtechnik  
der Rheinisch-Westfälischen Technischen Hochschule Aachen

zur Erlangung des akademischen Grades eines  
Doktors der Naturwissenschaften

genehmigte Dissertation

vorgelegt von **M.Sc.**

**Michel Heuser**

aus Wetzlar

**Berichter** Univ.-Prof. Dr. rer. nat. Helge Stanjek  
Prof. Dr. rer. nat. Ralf Diedel

Tag der mündlichen Prüfung: 16. Februar 2018

Diese Dissertation ist auf den Internetseiten der Hochschulbibliothek online verfügbar.

## Reviewer

**Prof. Dr. rer. nat. Helge Stanjek**

Head of Department  
Clay and Interface Mineralogy  
EMR - Energy and Mineral Resources Group  
RWTH Aachen University  
Bunsenstraße 8  
52072 Aachen

**Prof. Dr. rer. nat. Ralf Diedel**

Head of Research and Development  
Stephan Schmidt KG  
Bahnhofstraße 92  
65599 Dornburg-Langendernbach

## Head of the examination comitee

**Prof. Dr. rer. nat. Georg Roth**

Head of Department  
Institute for Christallography  
RWTH Aachen University  
Jägerstraße 17-19  
52066 Aachen

## Acknowledgements

At this point I would like to say – Thank you!

My thanks go to all those people who supported direct or indirect the preparation of this study, including the professional and mental assistance.

I would in particular like to thank my parents for their encouragement and the mental assistance especially in the last years.

My partner in life should be thanked for her tireless commitment and pushing me forward to finish this work.

Dennis Künkel should be thanked for the very helpful promotion especially during all laboratory experiments and measurements.

Further thanks go to my former colleague Dr. rer. nat. Christian Weber, who always had an open mind and door for scientific exchange.

My doctoral supervisor Prof. Dr. rer. nat. Helge Stanjek should be thanked for the assessment of this thesis and the possibility and financial support for the preparation of this dissertation.

I would like to thank Prof. Dr. rer. nat. Ralf Diedel for his encouragement and his professional competence as reviewer.

Furthermore, the author thanks S&B Industrial Minerals and Stephan Schmidt KG for supplying the bentonites and the Department of Engineering Geology and Hydrogeology RWTH for the possibility to measure water adsorption. A last thank goes to Dr. Othmar Latief (Duravit AG, formerly Stephan Schmidt KG) for the assistance and performance of rheology measurements.

This research was funded partially within the special program Geotechnologien (grant no. 03G0707A) of the German Federal Ministry of Education and Research (BMBF).

## Declaration

I hereby declare that, except where specific reference is made to the work of others, the contents of this dissertation are original and have not been submitted in whole or in part for consideration for any other degree or qualification in this, or any other university. This dissertation is entirely the result of my own work, and includes nothing, except where explicitly mentioned, which is the outcome of work done in collaboration.

Parts of this dissertation have already been published under the reference below. Corresponding text passages were adopted literally in entirety or in parts from:

Heuser, M., Weber, C., Stanjek, H., Chen, H., Jordan, G., Schmahl, W.W., and Natzeck, C. (2014) The interaction between bentonite and water vapor. I: Examination of physical and chemical properties. *Clays and Clay Minerals*, **62**, 188-202.



---

(Michel Heuser, M.Sc.)



## Abstract

The influence of water vapor on bentonites or smectites, respectively, is of interest in many different fields of applied mineralogy like nuclear waste sealing or casting in foundry industry. The water vapor affects the smectite surface and perhaps its structure, which leads probably to a change of its properties in a mostly unfavorable way. Therefore, the influence of hot water vapor (200 °C) on the physico-chemical, mineralogical, and electrokinetic parameters and properties of smectite-group minerals has been studied.

After the steam treatment, turbidity measurements, methylene blue sorption, water adsorption, and cation exchange capacity were measured on both untreated and treated samples. Mineralogical changes were checked by X-ray diffraction (XRD), X-ray photon spectroscopy (XPS) was done on *O*, *Al*, and *Si*, respectively. Only few parameters showed differences between vapor-treated and raw samples.

The measurement of sedimentation volumes (SV) resulted in a decreased SV after the treatment. As shown by XRD and XPS, the crystalline structure of smectite remained unaffected by the steam treatment. Equivalent sphere diameters (ESD) were not systematically affected by the steam treatment. Differences in cation exchange capacity (CEC) between unprocessed and treated samples were observed, but only for smectites with monovalent interlayer cations.

From the variety of different measurements and its results, the conclusion is that due to the steam treatment the charge properties at or near the particle surface of smectite change.

While most of physico-chemical and mineralogical properties remained unaffected by water vapor, electrokinetic, rheological, and surface properties react due to exposure of smectite to hot water vapor.

The first physico-chemical and mineralogical experiments suggested that monovalent smectites offered changes after steaming, whereas the divalent smectites remained unaffected. This statement is partially true in terms of the experiments of this work.

As well the magnitude of the dynamic mobility and isoconductive point, as viscosity and shear stress, derived from electrokinetics and conductometric titrations, potentiometric titrations and rheological measurements react due to the exposure of smectite to water vapor.

However, not only the sodium smectite showed changes comparing unprocessed and vapor treated samples - also the calcium smectite offered almost differences. The comparison of dynamic mobility of this work with electrokinetic potentials of sulfated polystyrene particles, obtained from streaming potentials in plugs (Lyklema & Minor, 1998), indicates a modification of the surface conductance of the smectite particles due to the steam treatment.

The idea of a surface charge modification of the smectite due to the exposure to hot water vapor was confirmed by the experiments and its results of this work. Furthermore, the author speculates about a dissolution process of amorphous silica from the rough smectite surface, which was indicated by the determination of fractal dimension and the measurement of silicon. This process would influence the diffuse double layer and hence, electrokinetic parameters, like dynamic mobility and surface conductance.

After all performed experiments and calculated parameters a clear statement about the interaction of bentonite or smectite with water vapor is finally only conditionally available. However, a lot of ideas and potential declarations were given, resulting in the assumption, that water vapor or steam affects the surface structure and its charge conditions of the smectite particles.

## Kurzfassung

Der Einfluss von Heißdampf (Wasserdampf) auf Bentonite bzw. Smektiten ist für einige Industriesparten von erheblicher Bedeutung. Dazu zählen unter anderem die atomare Endlagerung bei Verwendung von Bentonit als Schadstoffbarriere und die Gießereitechnik im Rahmen des Gießens in bentonitgebundene Formstoffe.

Der Heißdampf wirkt sich auf die Oberfläche des Smektiten aus und verändert möglicherweise deren Struktur. Dies führt zu einer Verschlechterung der geotechnischen und höchstwahrscheinlich auch elektro-kinetischen Eigenschaften des Smektiten. Daher wurde die Auswirkung des Einflusses von Heißdampf bei einer Temperatur von 200 °C im Hinblick auf die vormalig genannten Eigenschaften auf Smektitgruppenminerale untersucht.

Nach Abschluss der Heißdampfbehandlung wurden Messungen der Turbidität (Partikelgröße), der Methylenblau-Sorption, der Wasseraufnahme und der Kationenaustauschkapazität, sowohl an unbehandelten, als auch an den jeweiligen dampfbehandelten Smektiten durchgeführt. Die Veränderungen der mineralogischen Eigenschaften wurden mittels der Röntgenbeugungsanalyse (XRD) und der Röntgenphotoelektronenspektroskopie (XPS) untersucht. Dies geschah im Fall von XPS im Hinblick auf die Bindungen bzw. Bindungsenergien zwischen *O*, *Al* bzw. *Si*. Nur wenige der zunächst gemessenen Parameter zeigten Unterschiede zwischen unbehandelten und dampfbehandelten Smektitproben.

Im Folgenden wurde das Sedimentvolumen (SV) einiger unbehandelter und dampfbehandelter Smektiten untersucht, mit dem Ergebnis einer Erniedrigung des Sedimentvolumens nach der Heißdampfbehandlung. Die XRD- und XPS-Messungen belegen die Annahme, dass die kristalline Struktur des Smektiten nicht von der Heißdampfbehandlung beeinflusst wird. Die Partikelgröße zeigt zwar deutliche, jedoch keine systematischen Veränderungen nach der Dampfbehandlung. Im Rahmen der Messungen der Kationenaustauschkapazität wurden ebenfalls Unterschiede zwischen unbehandelten und dampfbehandelten Smektiten fest gestellt, allerdings nur für Proben, die mit einem einwertigen Zwischenschichtkation belegt wurden.

Basierend auf der Bandbreite der durchgeführten Messungen und deren Ergebnissen entstand die Schlussfolgerung, dass im Zuge der Heißdampfbehandlung die Ladungseigenschaften an oder nahe der Smektitoberfläche beeinflusst werden.

Während die meisten physiko-chemischen und mineralogischen Eigenschaften der Smektiten nicht auf die Dampfbehandlung reagieren, zeigen die elektro-kinetischen, rheologischen und oberflächennah bestimmten Parameter eine Reaktion im Rahmen der Exposition der Smektiten mit Heißdampf.

Basierend auf den physiko-chemischen und mineralogischen Experimenten kann daher zusammengefasst werden, dass Smektiten mit einem einwertigen Zwischenkation auf die Dampfbehandlung reagieren. Diejenigen mit einem zweiwertigen Zwischenschichtkation zeigen hingegen keine Beeinflussung durch Heißdampf. Diese Annahme wird zumindest teilweise durch die bisherigen Experimente bestätigt.

Im Folgenden wurden weitere Versuche durchgeführt. Sowohl die Magnitude der dynamischen Mobilität, der isokonduktive Punkt und die Protonierung der Smektitoberfläche, als auch Viskosität und Scherspannung, die mittels elektro-kinetischer und rheologischer Messungen bestimmt wurden, zeigten eine Veränderung im Rahmen der Dampfbehandlung.

Allerdings wurden diese Unterschiede nicht nur bei Smektiten mit einem einwertigen Zwischenschichtkation beobachtet, sondern auch beispielsweise bei Kalzium-Smektit. Der Vergleich der Ergebnisse der Messungen der dynamischen Mobilität mit den elektro-kinetischen Potentialen an Polystyren-Partikeln, die basierend auf Strömungspotentialen ermittelt wurden (Lyklema & Minor, 1998), führten zu der Annahme, dass die Oberflächenleitfähigkeit auf die Heißdampfbehandlung reagiert.

Die Idee einer Modifizierung der Ladungseigenschaften an der Smektitoberfläche wird auch von weiteren Messungen bestätigt.

Darüber hinaus besteht die Annahme, dass ein Auflösungsprozess von amorpher Kieselsäure von der rauen Smektitoberfläche stattfindet. Dies wurde mittels der Bestimmung der fraktalen Dimension und der Messung von Silizium im Wasser der Autoklaven nach der Dampfbehandlung bestätigt. Dieser Prozess würde einen Einfluss auf die diffuse Doppelschicht und somit auf

elektro-kinetische Parameter (dynamische Mobilität und Oberflächenleitfähigkeit) ausüben. Nach Abschluss aller durchgeführten Experimente und den daraus berechneten Parametern ist eine klare Aussage über die Auswirkung der Heißdampfbehandlung auf Smektite nur bedingt möglich. Allerdings wurden eine Fülle von Ideen und potentiellen Erklärungen gesammelt, die zu der Aussage führen, dass der Heißdampf die Oberflächenstruktur und die Ladungseigenschaften an der Smektitoberfläche beeinflusst und verändert.

# Contents

<b>Abstract / Kurzfassung</b>	<b>5</b>
<b>List of Figures</b>	<b>10</b>
<b>List of Tables</b>	<b>11</b>
<b>1 Introduction</b>	<b>13</b>
1.1 Problem . . . . .	13
1.2 Clay mineralogy . . . . .	14
1.2.1 Clays and clay minerals . . . . .	14
1.2.1.1 General structure of clay minerals . . . . .	14
1.2.1.2 The 1:1 layer . . . . .	15
1.2.1.3 The 2:1 layer . . . . .	15
1.2.2 Smectite Group . . . . .	16
1.2.2.1 Structure . . . . .	16
1.2.2.2 Classification . . . . .	18
1.2.3 Bentonite . . . . .	19
1.2.3.1 History and definition . . . . .	19
1.2.3.2 Origin and use of bentonites . . . . .	19
1.2.3.3 Modification of bentonites . . . . .	20
1.3 Previous work . . . . .	21
1.3.1 Foundry technology . . . . .	21
1.3.2 Nuclear waste sealing . . . . .	23
1.3.3 Interaction of water vapor with minerals and mineral surfaces . . . . .	24
1.3.4 Summary . . . . .	25
1.4 Approach and benefit . . . . .	25
<b>2 Materials and Methods</b>	<b>27</b>
2.1 Sample materials . . . . .	27
2.2 Sample preparation and purification . . . . .	28
2.2.1 Fractionation . . . . .	28
2.2.2 Preparation of homoionic forms . . . . .	28
2.2.3 Dialysis and freeze-drying . . . . .	28
2.2.4 Steam treatment . . . . .	29
2.3 Colorimetry . . . . .	29
2.4 Sedimentation experiments . . . . .	30
2.4.1 Preliminary sedimentation experiments . . . . .	30
2.4.2 Sedimentation volume . . . . .	30
2.5 Solution chemistry . . . . .	30
2.6 Chemical characterization (XRF) . . . . .	30
2.7 Mineralogical characterization (XRD) . . . . .	31
2.8 Surface-near chemistry (XPS) . . . . .	31
2.9 Particle size . . . . .	31
2.10 Nitrogen Sorption . . . . .	32
2.10.1 Adsorption and Desorption Isotherms and specific surface area . . . . .	32
2.10.2 Surface roughness . . . . .	32
2.11 Water adsorption . . . . .	33
2.12 Cation exchange capacity (CEC) . . . . .	33
2.13 Methylene blue sorption (MBS) . . . . .	33
2.14 Electrokinetics . . . . .	33
2.14.1 Conductometric titrations . . . . .	33
2.14.2 Dynamic mobility . . . . .	34
2.14.3 Potentiometric titrations . . . . .	34

2.15 Rheology . . . . .	35
<b>3 Results</b>	<b>37</b>
3.1 Foundry specific characterization (S&B) . . . . .	37
3.2 Chemical characterization . . . . .	38
3.2.1 Raw material . . . . .	38
3.2.2 Clay fraction ( $< 2 \mu\text{m}$ ) . . . . .	38
3.3 Mineralogical characterization . . . . .	40
3.3.1 Raw Material . . . . .	40
3.3.2 Clay fraction ( $< 2 \mu\text{m}$ ) . . . . .	41
3.3.2.1 Mineralogical composition . . . . .	41
3.3.2.2 Lattice parameters . . . . .	41
3.4 Colorimetry . . . . .	44
3.5 Sedimentation experiments . . . . .	45
3.5.1 Preliminary sedimentation experiments . . . . .	45
3.5.2 Sedimentation volume . . . . .	45
3.6 Solution chemistry . . . . .	48
3.6.1 Ionic inventory . . . . .	48
3.6.2 Silicon and Aluminum . . . . .	48
3.6.3 Electric conductivity and pH . . . . .	48
3.7 Surface-near chemistry . . . . .	49
3.8 Particle size . . . . .	51
3.9 Nitrogen sorption . . . . .	52
3.9.1 Adsorption and desorption isotherms and specific surface area . . . . .	52
3.9.2 Surface roughness . . . . .	54
3.10 Water adsorption . . . . .	57
3.11 Cation exchange capacity . . . . .	58
3.12 Methylene blue sorption . . . . .	59
3.12.1 Vis-spectra of dye dispersions . . . . .	59
3.12.2 Time dependent band intensity . . . . .	61
3.12.3 Time dependent MB area . . . . .	64
3.13 Electrokinetics . . . . .	67
3.13.1 Conductometric titrations . . . . .	67
3.13.2 Dynamic mobility . . . . .	68
3.13.3 Potentiometric titrations . . . . .	70
3.14 Rheology . . . . .	71
3.14.1 Viscosity . . . . .	71
3.14.2 Shear stress . . . . .	72
<b>4 Discussion</b>	<b>75</b>
4.1 Steam Treatment . . . . .	75
4.1.1 Temperature . . . . .	75
4.1.2 Duration . . . . .	76
4.1.3 Solid to liquid ratio . . . . .	77
4.1.4 Cooling down . . . . .	77
4.1.5 Drying . . . . .	77
4.2 Discussion of measured parameters . . . . .	78
4.3 Impact on foundry technology . . . . .	90
<b>5 Outlook</b>	<b>92</b>
<b>References</b>	<b>95</b>
<b>Lebenslauf / Curriculum vitae</b>	<b>104</b>

## List of Figures

1	Usage of bentonites . . . . .	13
2	Structure of the tetrahedral sheet . . . . .	14
3	Structure of the octahedral sheet . . . . .	15
4	Structural built up of natural clay minerals . . . . .	15
5	Structure of montmorillonite . . . . .	17
6	Distinction between di- and tri-octahedral smectites . . . . .	18
7	Cast experiment performed at the IfG . . . . .	22
8	Principle of the measurement of wet tensile strength . . . . .	23
9	Pressure digestion vessel / Autoclave . . . . .	29
10	Results of the XRD measurements . . . . .	42
11	Detailed view on the (001)-reflection of smectites . . . . .	43
12	Results of colorimetry in the $La^*b^*$ color space . . . . .	44
13	Sedimentation volume (SV) of selected samples . . . . .	45
14	Preliminary sedimentation experiments of BeW-Na . . . . .	46
15	Preliminary sedimentation experiments of BeC-Ca . . . . .	47
16	pH of unprocessed and treated samples . . . . .	49
17	Equivalent sphere diameters of smectites . . . . .	51
18	Ad-/desorption isotherms of unprocessed and treated samples . . . . .	52
19	Rouquerol plots of unprocessed and steam treated samples . . . . .	53
20	BET surface area plots of unprocessed and steam treated samples. . . . .	54
21	T-plots of unprocessed and steam treated samples. . . . .	55
22	Determination of fractal dimensions . . . . .	56
23	Results of the water adsorption experiments . . . . .	57
24	Cation exchange capacities of unprocessed and treated smectites . . . . .	58
25	Methyleneblue spectra of bentonites . . . . .	60
26	Time dependent changes of MB-spectra of BeD-Na and BeD-K . . . . .	61
27	Time dependent changes of MB-spectra of BeD-Ca and BeD-Mg . . . . .	62
28	Time dependent changes of MB-spectra of Namorit S-Mg and Volclay-Na . . . . .	63
29	MBS, time-dependent area below sorption curves for BeD-Na and BeD-K . . . . .	64
30	MBS, time-dependent area below sorption curves for BeD-Ca and BeD-Mg . . . . .	65
31	MBS, time-dependent area below sorption curves for Namorit S-Mg and Volclay-Na . . . . .	66
32	Results of the conductometric titrations . . . . .	67
33	Particle shape $n$ of unprocessed and vapor treated smectites . . . . .	68
34	Magnitude of the dynamic mobility $u_d^*$ depending on electrolyte concentration . . . . .	69
35	Potentiometric titrations of A: BeW-Na and B: BeC-Ca. . . . .	70
36	Dynamic viscosity of the bentonite dispersion . . . . .	71
37	Shear stress of the bentonite dispersion . . . . .	72
38	Specific volumes of 5 g of the clay after heating . . . . .	76
39	Orientation of methylene blue complex . . . . .	79
40	Viscosity in relation to the particle shape $n$ for various shear rates . . . . .	82
41	Electrokinetic potentials of sulfated polystyrene particles . . . . .	83
42	Particle shape $n$ depending on pH of the sodium and calcium smectite dispersions . . . . .	85
43	Scatter plots of measured parameters . . . . .	88

## List of Tables

1	Classification of smectites after Güven (1988). . . . .	18
2	Origin and condition of raw materials. . . . .	27
3	Foundry specific properties and parameters of raw bentonites . . . . .	37
4	Chemical composition of raw bentonites . . . . .	38
5	Chemical composition and structural formulae of bentonite samples . . . . .	39
6	Mineralogical composition of raw bentonites . . . . .	40
7	Aqueous concentrations of silicon and aluminum . . . . .	48
8	Characteristic peak parameters measured by XPS . . . . .	50
9	Specific surface areas (SSA) calculated after BET-theory from Nitrogen sorption. . . . .	54
10	Fractality of unprocessed and treated smectites . . . . .	57
11	Measured and theoretical band positions of MBS-kinetics . . . . .	59
12	Temperature of steam treatments of previous work and this study. . . . .	75
13	Duration of steam treatments of previous work and this study. . . . .	76
14	Solid to liquid ratio of steam treatments performed in previous work and this study. . . . .	77
15	Comparison of different parameters of unprocessed and treated smectites . . . . .	82
16	Comparison of calculated and measured relative viscosity of unprocessed and treated smectites. . . . .	86
17	Values of $D$ and $r$ from this work compared with others. . . . .	87

---

# Chapter 1

## Introduction



# 1 Introduction

## 1.1 Problem

Industrial and technical applications of clay minerals and bentonites encompass among other things, like agronomy and iron ore pelletization, geotechnical application and use in contaminant removal i.e. adsorbents (Mellah & Chegrouche (1997); Gitipour *et al.* (1997)), drilling or reinforcing fluids and additives (Erdoğan & Demirci (1996); Luckham & Rossi (1999)), landfill and dump technology (Ashmawy *et al.* (2002); Scalia & Benson (2011)), ceramics in material science (Zhu *et al.* (2002); Fahrenholtz (2008)), and moulding in foundry technology (Baier (1991); Beeley (2001)), see Figure 1. Other special applications in chemistry, technical, and medical science are reported and developed actually.

Bentonites contain by various definition  $>50$  wt.% of smectite-group minerals such as montmorillonite, beidellite, and/or nontronite (Grim & Güven (1978); Murray (2007); EUBA (2009)). In terms of foundry applications smectite-contents  $>70$  wt.% are preferred and applied (Grefhorst, 2006).

Additional in bentonite containing minerals among others are quartz, feldspars, micas, kaolinite, anatase, cristobalite, opal, and volcanic glasses (Delano *et al.* (1994); Ufer *et al.* (2008); Christidis & Huff (2009)).

The physical and chemical properties of bentonites vary with the amount of smectite-group minerals and mainly with its properties and parameters such as particle size and morphology, type and hydration state of the interlayer cations, surface properties (i.e. sorption of anions, zeta-potential), and the presence of free water in the pore space (Montes-H. *et al.* (2003); Kaufhold *et al.* (2010)).

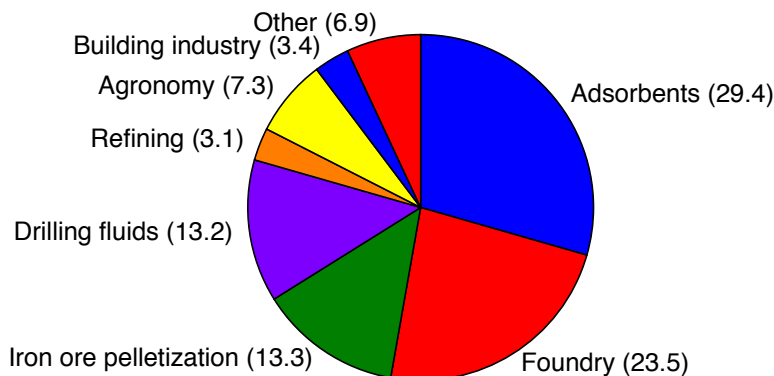


Figure 1: Usage of bentonites (values in %). The world production is in the order of  $13 \cdot 10^6$  t (Harvey & Lagaly, 2006).

In view of figure 1 bentonite applications and use in foundry industry amounts up to 23.5 % of the world production of bentonites - a percentage which is not negligible compared to the proportion of other areas of application.

With regard to foundry technology, moulding or so called green sands consist of a refractory material, usually sand including mainly the mineral quartz (for special applications zircon or chromite sand is used), bentonite as binding material, special additives like lustrous carbon producers, and (normal not deionized) water (Träger & Bührig-Polaczek (2000); Beeley (2001); Recknagel & Dahlmann (2009)).

Smectite-group minerals in connection with water enclose the surface of the quartz particles and contribute to plasticity and stability of the moulding sand. During casting, the liquid water in the moulding sand evaporates, moves along the temperature gradient in the outer areas of the mould, and condenses to liquid water in temperature fields around or beneath  $100^\circ\text{C}$ . During

this transport process, water vapor affects the mineral particles of the bentonite-sand-mixture and probably their surface properties. While a change of the surface properties of quartz by water vapor seems to be unlikely, an affection of the smectite particles by water vapor and a resultant change of its surface properties is conceivable.

This transport process may be part and could lead to the so-called "monday-production" of castings resulting in casting defects (i.e. cavity, blowholes, bubbles, scabbing or sintered core irons) and hence, significant additional expenses and significant additional costs for the foundry and its customers.

Therefore, it should be part and aim of this study to look for a connection between water vapor and changing properties of bentonites, with special regard to foundry technology (see chapter 1.4).

## 1.2 Clay mineralogy

### 1.2.1 Clays and clay minerals

#### 1.2.1.1 General structure of clay minerals

Phyllosilicates and in particular clay minerals consist of a continuous tetrahedral sheet (figure 2). In each tetrahedron a cation ( $\text{Si}^{4+}$ ,  $\text{Al}^{3+}$ , and  $\text{Fe}^{3+}$ ) is located in the center and coordinated to four oxygen atoms (figure 2, left). Three corners of every tetrahedra are connected to adjacent tetrahedra with the basal oxygen atoms ( $\text{O}_b$ ) leading to a hexagonal ring network in crystallographic  $a, b$ -direction. Apical located oxygen atoms ( $\text{O}_a$ ) are related to the octahedral sheet (figure 3).

The octahedral layer consists of edge shared octahedrons forming (pseudo-) hexagonal sheets. In the center of every octahedron a cation (common:  $\text{Al}^{3+}$ ,  $\text{Fe}^{3+}$ ,  $\text{Mg}^{2+}$ , and  $\text{Fe}^{2+}$ , also observed:  $\text{Li}^+$ ,  $\text{Mn}^{2+}$ ,  $\text{Co}^{2+}$ ,  $\text{Ni}^{2+}$ ,  $\text{Cu}^{2+}$ ,  $\text{Zn}^{2+}$ ,  $\text{V}^{3+}$ ,  $\text{Cr}^{3+}$ , and  $\text{Ti}^{4+}$ ) is located, surrounded by oxygen atoms at the  $\text{O}_a$ - and  $\text{O}_b$ - positions and OH, F, Cl, and O at the  $\text{O}_{oct}$ -position. The before listed anions at  $\text{O}_{oct}$  have no connection to the apical oxygen atoms  $\text{O}_a$  of the tetrahedra. The occupation of the octahedral positions (except the cation position) leads to two different orientations of the octahedron (*cis* and *trans*) depending on the location of the octahedral anionic position  $\text{O}_{oct}$  (figure 3, left).

Corners of the tetrahedra, which are not integrated in the tetrahedral sheet (apical oxygen positions  $\text{O}_a$ ) share octahedral oxygen atoms at  $\text{O}_a$  and  $\text{O}_b$  positions and form a three-dimensional structure of repeating TO- or TOT-layers, which are described as 1:1 or 2:1 layer structures respectively. In some cases in between two or more TOT-sandwiches a further octahedral sheet is located leading to a 2:1:1 layer structure (figure 4).

Detailed information about the structure of clay minerals could be further read at Brigatti *et al.* (2006).

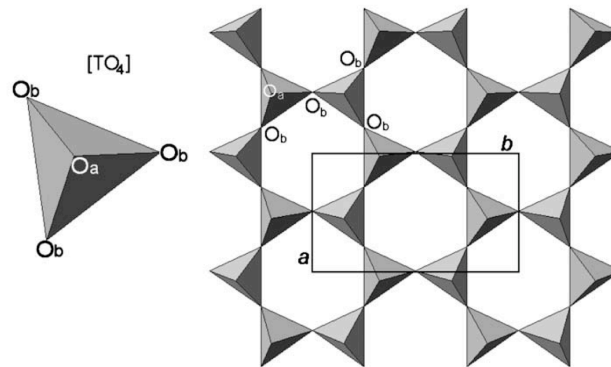


Figure 2: Left: Tetrahedron; Right: tetrahedral sheet,  $\text{O}_a$  - apical oxygen atom,  $\text{O}_b$  - basal oxygen atom,  $a$  and  $b$  - unit-cell parameters (Extract from Brigatti *et al.* (2006)).

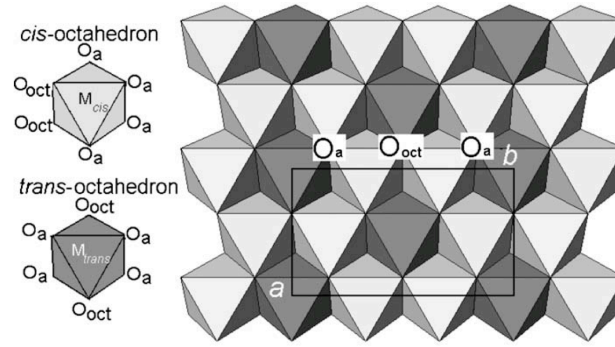


Figure 3: Left:  $O_{oct}$  (OH, F, Cl, and O) orientation in *cis*-octahedron and *trans*-octahedron; Right: location of *cis*- and *trans*-sites in the octahedral sheet.  $O_a$  - apical oxygen atom,  $O_b$  - basal oxygen atom,  $a$  and  $b$  - unit cell parameters (Extract from Brigatti *et al.* (2006)).

### 1.2.1.2 The 1:1 layer

The minerals of the 1:1 layer sheet silicates are built up of repeating TO-sandwiches each consisting of one tetrahedral and one octahedral sheet (figure 4, left). Based on the occupancy of the octahedral sheet two major groups could be distinguished: the dioctahedral species (figure 6, right) of the Kaolin group and the trioctahedral species (figure 6, left) of the Serpentine group. A description of the differences between di- and tri-octahedral species is given in chapter 1.2.2.2. Further explanations are not part of this study due to the application of only bentonites or smectites respectively.

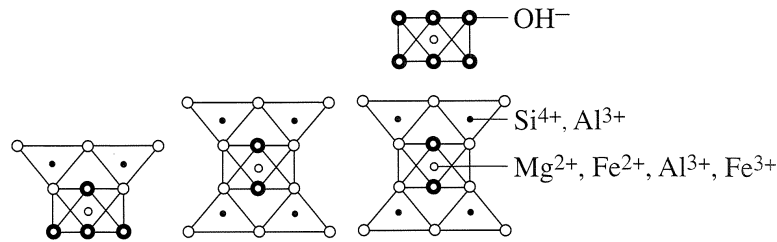


Figure 4: Structural built up of natural clay minerals: 1:1 layer (TO), 2:1 layer (TOT), and 2:1:1 layer (Extract from Wenk & Bulakh (2004)).

### 1.2.1.3 The 2:1 layer

The minerals of the 2:1 layer sheet silicates consist of repeating TOT-sandwiches (figure 4, middle and right). As described above in chapter 1.2.1.2, the occupancy of the octahedral sheet determines the differentiation between di- and tri-octahedral species (figure 6).

Based on its structure and variations six minerals or mineral groups respectively within the 2:1 layer clay minerals can be distinguished:

- Pyrophyllite Group:
  - dioctahedral: Pyrophyllite, trioctahedral: Talc
  - both layer structures are electrically neutral
  - no charge balancing interlayer cation is present
  - TOT sandwiches are kept together by van der Waals attraction
- Mica Group:
  - di- and trioctahedral species are present (Muscovite and Phlogopite series)

- charge balancing by an unhydrated interlayer cation, commonly  $K^+$ ,  $Na^+$ ,  $Ca^{2+}$ , or  $Ba^{2+}$
- Illite:
  - dioctahedral phyllosilicate ("clay mica") available in soil and sedimentary rocks
  - structure is similar to Muscovite
  - interlayer is occupied by poorly hydrated  $K^+$ – cations
  - non-expandable layer with a great variation in chemical composition
- Chlorite:
  - built up on repeating negatively charged TOT sandwiches with a positively charged octahedral sheet as interlayer
  - TOT sandwiches and the octahedral interlayer are connected by H-bonds
  - common Chlorites are usually trioctahedral species
- Vermiculite:
  - trioctahedral phyllosilicate with hydrated interlayer cations (commonly:  $Na^+$ ,  $Ca^{2+}$ , and  $Mg^{2+}$ ) within TOT sandwiches
  - a negative layer charge, that originates from substitutions in tetrahedral sites
- Smectite group:

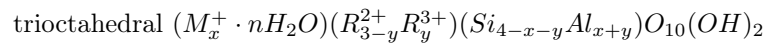
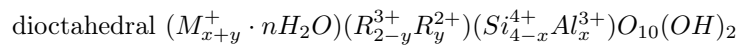
The clay minerals of the smectite group have some special characteristics leading to their distinct properties. Due to the fact that this work deals with the properties of unprocessed and water vapor treated bentonites or smectites respectively a more detailed view insight their structure is necessary. Therefore, further information about the smectite group is given in the following chapter 1.2.2.

### 1.2.2 Smectite Group

The term *smectite*, which is often used as mineral name, cannot be linked to one mineral, but represents a transcription for a group of minerals with similar structural formula and great variations in chemistry.

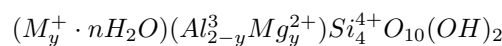
#### 1.2.2.1 Structure

The minerals of the smectite group are built up on continuous 2:1-layers in *c*-direction with an intercalated cation within every TOT-sandwich (figure 5). If the octahedral sheet is mainly occupied by trivalent cations the structure is called dioctahedral or trioctahedral, if divalent cations dominate the octahedral sheet. The general structural formula of the two different smectite species reads as follows:

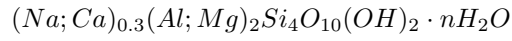


The indices  $x$  and  $y$  give information about the layer charge, which originates from tetrahedral and octahedral substitutions.  $R^{2+}$  and  $R^{3+}$  represent divalent or trivalent cations respectively and  $M^+$  indicates a monovalent interlayer cation.

The structural formula of the most common smectite mineral Montmorillonite is given by (Brigatti *et al.*, 2006):



whereas the *Handbook of Mineralogy* (Anthony *et al.*, 2013) proposes the following formula for Montmorillonite, with clearly defined interlayer cations, but open space for the occupation of the octahedral sheet with  $\text{Al}^{3+}$  and/or  $\text{Mg}^{2+}$ :



In contrast to other 2:1-layer clay minerals (see chapter 1.2.1.3), the smectite group shows three major differences leading to their very special properties:

- substitution of tetrahedral and octahedral cations
- a (negative) layer charge between 0.2 and 0.6 per half unit cell
- exchangeable interlayer cations with variable hydration state

The cationic positions of the three different sheets: octahedral, tetrahedral, and interlayer, can be dominated by several monovalent to tetravalent ions (see table 1).

Tetrahedral sites are mainly occupied by  $\text{Si}^{4+}$ ,  $\text{Al}^{3+}$ , and  $\text{Fe}^{3+}$ , whereas a substitution of  $\text{R}^{3+}$  by  $\text{Si}^{4+}$  is possible, resulting in an excess of negative charge, that influences the charge of the 2:1-layer as well as the local charge at the layer surface (Brigatti *et al.*, 2006).

The octahedral sites are dominated by  $\text{Al}^{3+}$ ,  $\text{Fe}^{3+}$ ,  $\text{Fe}^{2+}$ ,  $\text{Mg}^{2+}$ ,  $\text{Ni}^{2+}$ ,  $\text{Zn}^{2+}$ , and  $\text{Li}^{+}$ .

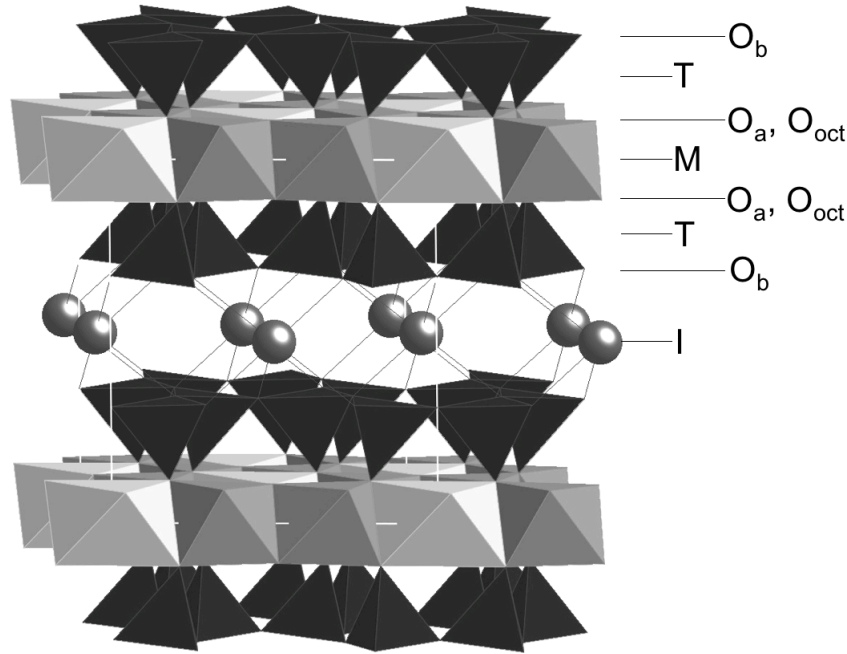


Figure 5: Structural built up of Montmorillonite:  $\text{O}_{oct}$  orientation in *cis*- and *trans*-octahedron,  $\text{O}_a$  - apical oxygen atom,  $\text{O}_b$  - basal oxygen atom, M - octahedral cation, T - tetrahedral cation, and I - interlayer cation (built with *Crystal Maker 7.2.3*).

As described above, the general structure of smectite-group minerals is shown by figure 5, although the occupation of the octahedral cationic position (figure 5, M) leads to the distinction between the different minerals of the group (see table 1). These differences are summarized in the next chapter 1.2.2.2 *Classification*.

### 1.2.2.2 Classification

The distinction between the different species of smectite-group minerals can be made with regard to the occupation of the octahedral sheet with di- or tri-valent cations, the octahedral cation or octahedral substitutions, respectively, and hence, the ratio between tetrahedral to octahedral layer charge (see Table 1, Güven (1988)).

As described above, if the octahedral sheet is mainly or completely occupied by trivalent cations (i.e.  $\text{Al}^{3+}$ ) the structure is called dioctahedral and, if divalent cations (i.e.  $\text{Mg}^{2+}$ ) dominate the octahedral sheet to a fraction of 2/3 the structure is called trioctahedral (Anthony *et al.*, 2013). The distinction between di- and trioctahedral species or sheets is illustrated in the following figure 6 (Brigatti *et al.*, 2006).

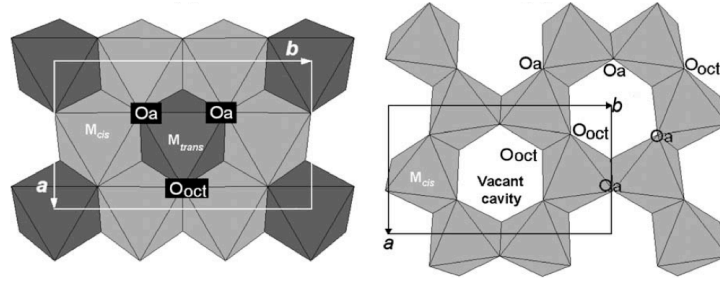


Figure 6: Left: trioctahedral sheet; Right: dioctahedral sheet.  $O_a$  - apical oxygen atoms shared with tetrahedra,  $O_{oct}$  - anionic site shared between adjacent octahedra.  $a$ ,  $b$  - unit-cell parameter (Extract from Brigatti *et al.* (2006)).

The following table 1 summarizes the different di- and trioctahedral species of smectite-group minerals depending on the octahedral cation, possible octahedral substitutions, and the ratio of tetrahedral to octahedral layer charge (Güven, 1988).

Common smectite-group minerals with a dioctahedral character are Montmorillonite, Beidelite, Nontronite, and Volkonskite. Common trioctahedral species are Stevensite/Hectorite, Saponite, and Sauconite.

Table 1: Classification of smectites after Güven (1988).

$\zeta_T/\zeta_O^*$	Dioctahedral		Trioctahedral	
	Octahedral cation	Species	Octahedral cation	Species
<1	$\text{Al} (\text{R}^{2+})^{**}$	Montmorillonite	Mg	Stevensite
			Mg (Li)**	Hectorite
			AlMgLi	Swinfordite
>1	Al	Beidelite	Mg	Saponite
	$\text{Fe}^{3+}$	Nontronite	$\text{Fe}^{2+}$	Fe-Saponite
	$\text{Cr}^{3+}$	Volkonskite	Zn	Sauconite
	$\text{V}^{3+}$	V-Smectite	Co	Co-Smectite
			Mn	Mn-Smectite

\* ratio tetrahedral to octahedral layer charge

\*\* octahedral substitutions

The most familiar and well known species is given by Montmorillonite - a mineral that is often used equally to smectite, although its name indicates a group of minerals and not one species. The structural formula of Montmorillonite was shown in chapter 1.2.2.1. Type and extent of the occupation of interlayer and octahedral sheet with mono- and di- or di- and trivalent cations are not exactly defined, resulting in a great chemical diversity of Montmorillonite structures.

### 1.2.3 Bentonite

The following chapter *Bentonite* encompasses the definition of bentonites depending on their respective application, the types and uses of natural bentonites, and the actually common modifications of bentonites by acid-, soda-, and organic-activation.

#### 1.2.3.1 History and definition

Knight introduced the term bentonite first in 1898 for a clayey material found in Ford Benton in Wyoming (USA). Other scientists, i.e. Condra (1908), Hewitt and Wherry (1917), Ross and Shannon (1926), and Wright (1968), think about the alteration process and the origin of bentonite, resulting in the following definition. Bentonite represents a clay mainly consisting of smectite-group minerals contributing to its physical properties (Grim & Güven, 1978).

Although the term bentonite is firmly connected to its origin from the alteration of volcanic ashes or tuff (see chapter 1.2.3.2), other clays with similar properties, but different origin are also named bentonite.

Another term, which is used for a material with similar mineralogical composition and physico-chemical properties, represents *fuller's earth*. It refers to a material for commercial applications and is used beside bentonite, but did not replace it.

The Wyoming bentonites are characterized by its main component a sodium smectite and became commercial importance because of its physical properties. These natural occurrences of bentonites lead to an important bentonite supporting and refining industry in Wyoming, but also in other countries worldwide with similar geological and mineralogical materials (i.e. England, Germany, Japan, and Greece; Grim & Güven (1978)).

As mentioned in the first chapter *Introduction* bentonites contain by various definition  $>50$  wt-% of smectite-group minerals such as montmorillonite, beidellite, and/or nontronite (Grim & Güven (1978); Murray (2007); EUBA (2009)), whereas minerals of the montmorillonite-beidellite series predominantly form the most important bentonites and contribute to their special physico-chemical properties. In terms of foundry applications smectite-contents  $>70$  wt-% are preferred and applied (Grefhorst, 2006).

Additional in bentonite containing minerals among others are in particular quartz and feldspars, and with minor contents micas, kaolinite, anatase/rutile, cristobalite, opal, and volcanic glasses (Delano *et al.* (1994); Ufer *et al.* (2008); Christidis & Huff (2009)).

Characteristic geographical, geological, mineralogical, and chemical data of bentonites from all over the world are presented by Grim & Güven (1978), chapter 3.

#### 1.2.3.2 Origin and use of bentonites

After Grim & Güven (1978) the origin of natural bentonites could be divided in the four following processes. The first process *Alteration of volcanic ash or tuff* was firstly suggested by Knight (1898) for a bentonite, whereas over time other origin processes were established:

- Alteration of volcanic ash or tuff
- Hydrothermal alteration of igneous rocks
- Deuteric alteration of igneous rocks
- Other origin processes, or an origin, which cannot clearly assigned to one of the first three processes

In the course of this study the originating process of the used bentonites has not been examined in detail, but most of them originated from the alteration of volcanic ash or tuff.

Further detailed information about the originating processes can be read at Grim & Güven (1978), chapter 3.6 and in Christidis & Huff (2009), and will not be discussed in this study.

The most important and naturally occurring bentonites are the sodium-, calcium-, or mixed species. The characterization of bentonites is based on the interlayer cation (Figure 5, I - interlayer cation) of the smectite-group mineral, whereas montmorillonite-beidellite structures are the most common.

The interlayer of the smectite structure is predominantly occupied by mono- and/or divalent cations or mixtures of both of them, but in most cases to an unknown extent. Most of the smectite-group minerals building up bentonites contain of sodium or calcium, rarer of potassium or magnesium as interlayer cation.

The fraction of one cation amounts up to <90 % of the interlayer positions (Steudel & Emmerich, 2013). The other 10 % are occupied by other cations. Even a secondary treatment with monoionic salts to increase the amount of one cation in the interlayer leads to the same result as stated before. Depending on the type of the interlayer cation the fraction of a monoionic occupation could decrease down to 70 % (Steudel & Emmerich, 2013).

The modification of bentonites or smectites respectively aim to increase i.a. the fraction of a monoionic interlayer to improve its physico-chemical properties (see the following chapter 1.2.3.3, soda activation).

The use of natural and modified bentonites encompasses many fields of application (see figure 1, also described in chapter 1.1).

Bentonites show a wide range of application in many industries and industrial processes. The use and application of bentonites depends on its properties and hence the physico-chemical properties of smectite-group minerals. These are i.e. viscosity, thixotropy, plasticity, shrinking, bonding strength, shear strength, water impedance, etc. (Grim & Güven, 1978).

Grim & Güven (1978) connected properties and uses of bentonites and listed them. In the following enumeration their distribution is presented (Grim & Güven (1978), chapter 5):

- Ceramics: Plasticity, green strength, drying shrinkage, dry strength, firing properties
- Foundry moulding sands: Green compression strength, dry compression strength, hot strength, flowability, permeability
- Petroleum industry : Drilling fluids, catalysts, decolorization
- Engineering applications: Plasticity, activity, water sorption, unconfined compression strength, shear strength, sensitivity, permeability, frost heaving, compressibility and consolidation, soil stabilization
- Agricultural use: cation exchange capacity, fertilizer, etc.
- Others: Adhesives, animal bedding, cement, mortar, and aggregates, clarification of alcohols, emulsifying, suspending, and stabilizing agents, fabrics, floor absorbents, food, greases, ink, medicines, pharmaceuticals, and cosmetics, paint, paper, pelletizing ores, fluxes, fuels, etc., pesticides, rubber, smectite-organic-complexes, water clarification, water impedance

The above presented enumeration, which does not already claim to completeness, demonstrates the importance of bentonites and their application. Further detailed information is given by Grim & Güven (1978) and can be read there.

### 1.2.3.3 Modification of bentonites

Actually some structural and surface modifications of bentonites are known and applied in different technical uses for i.e. sorption processes, geotechnical and foundry applications, and contaminant removal.

These are the activation or treatment of bentonites with acid, soda, or organic molecules respectively, in order to modify its physical and chemical properties.

#### *Acid activation*

The acid activation or acid treatment respectively of bentonites with hydrochloric, sulfuric, or phosphoric acid leads to delamination of the stacked TOT-sandwiches (see chapter 1.2.2.1) of the smectite-group minerals (Christidis *et al.*, 1997).

With increasing concentration of the used acid the surface area increases until an acid-specific maximum is reached and the surface area decreases with ongoing increase of the concentration of the acid.



The treatment influences not only the surface area of the smectite minerals, but also its particle size, resulting in increased sizes after the treatment (Yildiz *et al.*, 2004).

Considering the optimal concentration of the used acid, the activation or treatment process causes increased surfaces of smectites, which could be applied for i.e. sorption processes in the course of contaminant removal and bleaching agent for i.e. foods (Malhoukhi *et al.*, 2009).

#### *Soda activation*

The activation of bentonites with soda ( $\text{Na}_2\text{CO}_3$ ) or sodium carbonate, respectively represents the most common method to transform Ca-bentonites into Na-bentonites, especially in terms of foundry technology (Ohrdorf & Flachberger (2009), Ohrdorf & Flachberger (2010), and Krischey *et al.* (2015)), but also in food technology (Gougeon *et al.*, 2003) and drilling fluid technology (Erdoğan & Demirci, 1996).

The bentonite is mixed with soda, whereas the soda-concentration is of great importance for the success of the activation (common are 2-4 wt.%), and leads to a cation exchange process, resulting in a bentonite consisting of a sodium-smectite and hence, its positive influenced properties (Baier, 1991). But, as mentioned in chapter 1.2.3.2 the interlayer of a smectite-group mineral shows a monoionic occupation only up to 90 % (Steudel & Emmerich, 2013).

The aim of the soda activation are among others are increased cation exchange capacities (CEC, see chapter 2.12), higher (001)-spacing, higher water adsorption, and other positive changes of physico-chemical properties (Volzone & Garrido (1991), Erdoğan & Demirci (1996), Yıldız *et al.* (1999)).

#### *Organic activation*

The activation of bentonites with organic molecules opens a wide field of applications and space for research and development (Breen & Watson (1998), Krischey *et al.* (2015)). However, the organic activation represents a very special part of the modification of bentonites, it is actually only subordinately applied to modify bentonites for foundry technology. A further detailed discussion of the organic activation of bentonites or organoclays is therefore not part of this study.

### 1.3 Previous work

This chapter encompasses prior work regarding the interaction of water vapor with minerals, mineral surfaces, and especially in terms of two important industrial processes - foundry technology and nuclear waste sealing. For one thing, the modification of minerals and mineral surfaces by water vapor is of great interest, on the downside water vapor is used as measuring agent, but also influences the process containing surfaces of minerals and other materials.

The interaction has been studied very well over decades of research. However, in many cases the modification of materials by water vapor or steam, respectively is currently not clear, also not to what extent water vapor affects surfaces or structures of materials.

The following chapters 1.3.1 to 1.3.3 represent a major part of research and development regarding water vapor and its influence usually to minerals and mineral surfaces until today.

#### 1.3.1 Foundry technology

Prior to this work the BMBF-/DFG-founded project "HydraSmec: Understanding processes at the hot smectite-water interface for tailoring industrial bentonite applications" provided the first basic incentive to study the influence of hot water vapor on parameters and properties of bentonites.

In 2009, three cast experiments were performed at the IfG<sup>1</sup>. Moulding sand, cast iron and casting temperature have been defined previously: moulding material is quartz sand (QWF<sup>2</sup>, type F32),

<sup>1</sup>Institut für Giessereitechnik, Hansaallee 203, 40549 Düsseldorf, Germany, project partner in HydraSmec

<sup>2</sup>Quarz Werke Frechen, Kaskadenweg 40, 50226 Frechen, Germany

mixed with one of the five kinds of bentonite (S&B<sup>3</sup>, BeC, D, E, H, and W, 0.08 g/g), and with water (0.035 g/g).

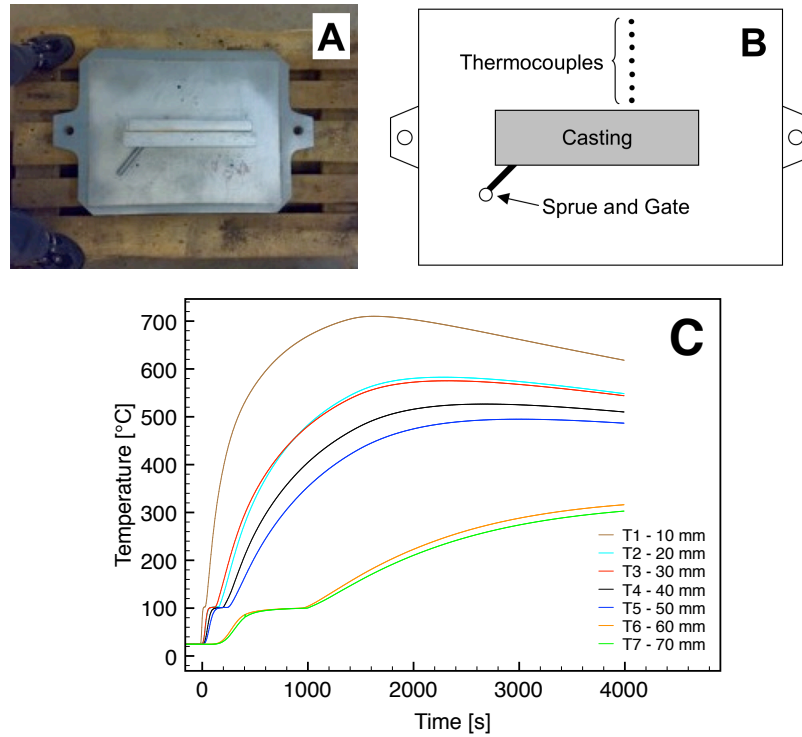


Figure 7: Cast experiment performed at the IfG. A: model before casting, B: schematic diagram of the model including the position of casting, sprue and gate, and thermocouples, and C: temperature depending on time for each of the seven installed thermocouples.

One of the experiments is shown in figure 7. The goal was to get information about the temperature distribution and gradient in the moulding sand during the casting and the cooling time. A wooden model has been formed and transferred into the negative moulding form (figure 7A). The compressibility of the moulding sand was set to 45 %.

Seven thermocouples installed in the mould with a distance of 10 mm (figure 7B) monitored the temperature during the casting (figure 7C). In total 45 kg cast iron were filled into the mould under a pouring temperature of 1400°C. During casting temperatures up to 700°C were measured, while the thermocouples at the edge of the mould monitored only 300°C. Depending on geometry of the casting the monitored temperature decreases down to 100°C and below.

As part of the casting process, liquid water in the moulding sand evaporates near the molten metal to an exceedingly hot vapor moving along the temperature gradient to cooler regions, condensing to liquid water. This region, known as condensation zone, is characterized by water contents higher than at the beginning of the casting (Grefhorst *et al.* (2005); Jordan *et al.* (2013)). During this transport process, water vapor affects the smectite particles and probably their surface properties.

A very similar process is simulated by the determination of the wet tensile strength (Grefhorst *et al.*, 2005). A temperature gradient is introduced to a moulding sand while a tensile force affects the material. Figure 8 shows the principle of the measurement (Grefhorst *et al.*, 2005). As mentioned above the liquid water in the mould evaporates, moves along the temperature gradient, and condenses in the so-called condensation zone, in which temperatures of 100°C and below are measured.

<sup>3</sup>S&B, Industrial Minerals GmbH, Schmielenfeldstraße 78, 45772 Marl, Germany

Due to the accumulation of water in this zone the strength is considerably lower than the green tensile strength. Water content, physico-chemical properties, and the intensity of conditioning of the bentonite contribute to the differences between wet and green tensile strength (Hasse, 2014).



Figure 8: Principle of the measurement of wet tensile strength at S&B Industrial Minerals: Heating up to 300 °C, forming of the condensation zone, and subsequent applying of a tensile strength.

Whether the casting with bentonite bonded moulding sand or the determination of the wet tensile strength, in both cases water vapor moves along the mould and affects the bentonite and its surface in a probably unfavorable way. This potential modification might be one controlling factor leading to a poor quality of moulding sands and therefore to an increase of casting defects (Grefhorst *et al.*, 2010), which has been observed.

### 1.3.2 Nuclear waste sealing

Besides foundry technology the influence of water vapor on bentonite is also important for the sealing of nuclear waste repositories. In terms of this applied problem several decades of research resulted in a detailed understanding of the influence of water vapor on geotechnical and mineralogical parameters of bentonite. Couture (1985b) and Couture (1985a) performed a vapor treatment at temperatures between 150 °C and 250 °C. Both permeability and its ability to swell and to fill fractures decreased greatly up to 250 °C. The reduction of swelling capacity commenced at 150 °C.

Oscarson & Dixon (1989) observed also a decrease in swelling capacity, which was not caused by an alteration of the mineralogical composition of the montmorillonite and which was influenced by physical aggregation of clay particles only to a lesser extent. Oscarson *et al.* (1990) discovered that permeability of unprocessed and treated bentonites differed, but gave no reasons. Both studies have in common that differences between unprocessed and treated bentonites were observed already for water vapor treatments starting at 110 °C. The positive aspects of untreated bentonites (such as fast swelling and low water permeability) became lost.

Güven (1990) performed a steam treatment at temperatures >260 °C resulting in a modified microstructure and a disturbance of the lamellar fabric.

Madsen (1998) studied the influence of steam on bentonite at temperatures <120 °C. XRD, IR spectroscopy, and thermogravimetry showed no significant changes due to steaming except for a slight increase of CEC. The reduction of swelling pressure was attributed to aggregation of clay particles.

Bish *et al.* (1997) examined the effects of steam on the surface properties of two sodium-smectites. No structural mineralogical changes (XRD) after their treatment were observed. Based on  $^{27}\text{Al}$ -MAS-NMR measurements they speculate about a relocation of aluminium, but the differences between spectra of unprocessed and steamed samples were only little. However, contact angles determined with polar liquids change after steaming, whereas non-polar liquids lead to no modification of contact angles. Water adsorption isotherms of untreated and steamed samples differed and the ability of samples to adsorb water decreased although with hysteresis effects. A small increase of zeta potentials after the treatment was detected.

Pusch (2000) investigated the influence of water vapor on bentonite in a temperature range

between 90°C and 110°C, leading to bulk clay expansion and aggregation. Nevertheless, the hydration rate and swelling pressure were in the same order of magnitude for untreated and steamed clay. The hydraulic conductivity increased up to 10 % due to a more heterogeneous microstructure after the treatment. Partial dissolution of smectite and precipitation of *Si* or silica respectively subsequent to cooling after the treatment induced aggregation and cementation of particles. However, silicon and aluminium concentrations were not measured in this study. Changes in physical properties were not very significant.

Pusch studied the influence of water vapor in terms of nuclear waste sealing since the middle 1960's, but mostly under geotechnical, rarer under mineralogical aspects, and in any case under the change of micro- or nano-properties of bentonites.

### 1.3.3 Interaction of water vapor with minerals and mineral surfaces

#### *Zeolithes*

The interaction of water vapor with mineral surfaces is also of interest within the field of contaminant removal by natural and synthetic zeolites (Bish & Ming, 2001). The catalytic activity of zeolite surfaces changes significantly in the presence of water vapor, accompanied by a variable sorption rate of pollutants from liquid or gaseous phases (Kikuchi *et al.*, 1996). In contradistinction it is also possible to deactivate surfaces of zeolites with vapor treatment, resulting in a decrease of pollutant adsorption (Ohtsuka & Tabata, 1999). Furthermore, dealumination, relocation of aluminium in the framework and changes in the micropore volume are related to the vapor treatment of zeolites (Grinsted *et al.* (1993); Sano *et al.* (1996); Capek *et al.* (2004)). In contrast to this study, the water vapor treatment of zeolites is usually performed at temperatures above 400 °C (see the aforementioned authors), which might cause other and stronger physico-chemical effects.

Although smectites and zeolites have many properties and applications in common, their very distinct crystal structures often lead to very different properties (Bish, 2006). To which extent observations of the water-vapor-zeolite interface can be applied to the water-vapor-smectite interface remains to be shown.

#### *Sorption isotherms and specific surface area*

The determination of sorption isotherms and specific surface areas can be measured by the use of different gases (i.e. Helium, Argon, Nitrogen) after i.e. the BET-method (Brunauer *et al.* (1938); Dogan *et al.* (2006)), but also by the use of water vapor (Kahr & Madsen (1996); Wang *et al.* (2003); Akin & Likos (2014)).

From the adsorption of water vapor under defined moisture and temperature conditions specific surface area, pore-size-distributions and sorption isotherms could be measured and calculated. Further detailed informations about physical sorption could be found at Thommes (2010) and the aforementioned references.

#### *Ceramics*

In terms of ceramics water vapor is used to modify the (surface-)structure and to influence the crystal-growth of including minerals (Bagwell & Messing (1999); Guo (1999)). Furthermore, other properties or conditions, like oxidation, corrosion, mullite formation, temperature stability, alumina volatility, and crack propagation of ceramic materials which are influenced by water vapor were studied by Jorgensen *et al.* (1961), Lee *et al.* (2003), More *et al.* (2003), Opila & Myers (2004), and Wiederhorn (1967).

Unlike bentonites, which are influenced by water vapor in a temporary unknown extent, regarding ceramics water vapor is intentional used for a special modification. Further detailed informations about the modification of ceramics could be found at the aforementioned references and are not part of this study.

#### *Surface modification*

Further technical applications of the interaction of water vapor with minerals or mineral surfaces are not known, but some properties of minerals, which are influenced by water vapor, were and

are actual part of research and development (Hofmann & Klemen (1950); Young (1958)). This are in particular physical and chemical surface structure, roughness, topography, and fractility or fractal dimensions (i.e. Anbeek (1992); Xu *et al.* (2004); Zhu *et al.* (2009)), which are assumed to interact with water vapor and offer scope for additional research, also in this study.

#### 1.3.4 Summary

The previous chapters demonstrate the wide range of the use and application of water vapor and its interaction with minerals. From the presented studies and work some properties of minerals are influenced by water vapor, some others remained unaffected. The extent of affection varied partially with the respective study and depended on many properties of the used material. However, a few changes were observed by several scientists and listed below, but a unique result and conclusion could not be derived. Furthermore, most of the older studies recognized changes in one or two parameters or properties and give no or an insufficient explanation for its observations.

In summary, the following effects with steam treatment were observed in earlier studies:

- (1) ability to swell and the swelling pressure decreased
- (2) permeability and hydraulic conductivity increased
- (3) CEC increased slightly
- (4) no structural changes are evident from XRD, IR and thermogravimetry
- (5) regarding the interaction of water vapor with zeolites dealumination occurred.

## 1.4 Approach and benefit

The aim of this study is to gain information about the interaction between bentonite or smectite respectively and hot water vapor. Earlier studies examined this relation, but with regard to the effects and mostly not regarding the alteration of smectite minerals or its surfaces.

The previous chapter 1.3 presents a review over the fields of application of water vapor to minerals or mineral surfaces, with special regard to foundry technology and nuclear waste sealing. Special attention is given to modifications on particle level triggered by water vapor and in particular to changes of the structure and the surface of a smectite-plate.

Thereby, physico-chemical, electro-kinetic, and mineralogical properties of unprocessed smectites will be measured and its results compared to those of vapor-treated species. The goal is to find a parameter reacting due to a water vapor treatment, in order to prevent that smectite particles are affected by water vapor to an actually unknown extent.

In the next chapter 2 methods to measure properties and parameters of smectites assumed to react under the influence of water vapor are presented. Afterwards, in chapter 3 the results of all measurements are shown and interpreted in chapter 4. The last chapter 5 encompasses a summary of decisive results, its interpretation and potential for further work after this study.

---

# Chapter 2

## Materials and Methods

## 2 Materials and Methods

This chapter presents the sample materials used for the experimental study, the sample preparation and purification including the vapor treatment, and the methods applied to determine several properties and parameters, which are assumed to react due to the vapor treatment. In particular experiments i.e particle size, chemistry, mineralogy, specific surface area, fractality, and charge conditions at particle scale were performed.

For fractions smaller  $2\text{ }\mu\text{m}$  the term bentonite is used in the same meaning as smectite because of its composition. Furthermore, the terms dispersion and suspension are meant to be equivalent, however some authors prefer the one, some the other description.

### 2.1 Sample materials

Five industrial bentonites used for foundry applications (Bentonite C, D, E, H, and W) and two commercial clays (Namorit S and Volclay) were used in this study (table 2). The chemical and mineralogical characterization of the raw samples is presented in chapter 3.2.1 and 3.3.1, respectively.

Based on the assumption, that only the smectite-group minerals show a significant alteration due to the vapor treatment, the raw bentonites (see table 2) were only used for a first characterization and in the following fractionized by sedimentation (see chapter 2.2.1).

Regarding the measured properties and parameters not all bentonites or smectites respectively were used for every experiment only selected samples were used. Only two samples namely BeC-Ca and BeW-Na have been utilized for most of the experiments, due to their natural occurrence as Ca- and Na-smectite respectively.

Table 2: Origin and condition of raw materials.

Sample	Origin	Distributor	Condition/Pretreatment
BeD, E, H	various	SB*	Soda activated, industrial milling, $<100\text{ }\mu\text{m}$ .
BeC, W	various	SB*	unactivated, industrial milling, $<100\text{ }\mu\text{m}$ .
Volclay	Wyoming Bentonite	SB*	Soda activated, industrial milling, $<100\text{ }\mu\text{m}$ .
Namorit S	Indian Bentonite	SSKG**/ HA***	Soda activated, industrial milling, $<63\text{ }\mu\text{m}$ .

\* S&B Industrial Minerals GmbH, Schmielenfeldstraße 78, 45772 Marl, Germany.

\*\* Stephan Schmidt KG, Bahnhofstraße 92, 65599 Dornburg-Langendernbach, Germany.

\*\*\* Hüttenes-Albertus Chemische Werke GmbH, Wiesenstraße 23/64, 40549 Düsseldorf, Germany.

The raw bentonites Be(ntonite) C, D, E, H, and W are distributed by *S&B Industrial minerals*, a well-known company in terms of different industrial minerals, especially for geotechnical and foundry applications. The bentonites BeD, E, and H are calcium-bentonites, which were soda-activated and milled until a particle size smaller  $100\text{ }\mu\text{m}$  is reached. Bentonite BeC represents an unactivated calcium-bentonite and BeW is an unactivated natural sodium-bentonite. Both show a particle size smaller  $100\text{ }\mu\text{m}$  due to industrial milling.

The Volclay, also distributed by *S&B Industrial minerals*, is characterized as Wyoming bentonite, a natural sodium bentonite, which was soda-activated and milled until a particle size smaller  $100\text{ }\mu\text{m}$  could be achieved.

Namorit S(mectite) represents an Indian sodium bentonite, soda-activated, and milled down to a particle size of smaller  $63\text{ }\mu\text{m}$ . The material was distributed by *Stephan Schmidt KG* and *Hüttenus Albertus Chemische Werke GmbH*, respectively. Both companies produce and trade special clays, clay and other industrial minerals in terms of agronomy, geotechnical and foundry applications, and for other special uses.

## 2.2 Sample preparation and purification

### 2.2.1 Fractionation

In order to ensure, that mainly smectite-group minerals will be used for the following experiments a clay fraction  $<2\text{ }\mu\text{m}$  has to be separated from the raw bentonites or clays, respectively. Therefore, the raw material was dispersed in deionized water with a concentration of 5 wt.% by an ultrasonic treatment. Afterwards, the enrichment of clay- and/or smectite-group minerals was performed by separating the fraction  $<2\text{ }\mu\text{m}$  by Atterberg sedimentation under consideration of *Stoke's* law.

The clay-water-suspension was filled in graduated plastic cylinders, shaken, and then kept untouched for about 22 hours. Over an outlet the suspension above the outlet was removed, while bigger particles and aggregates ( $>2\text{ }\mu\text{m}$ ) settled down below the outlet and remained in the cylinders. In the following, the cylinders were filled up with deionized water and the procedure was repeated.

After 6-8 circulations the suspension above the outlet was approximately clear and the main part of the clay fraction separated from the raw material.

The clay-suspension was accumulated in 5l buckets and forced to sediment by the addition of salts: NaCl, KCl,  $\text{MgCl}_2$ , or  $\text{CaCl}_2$ , respectively. This procedure was also performed in order to achieve a first homoionic occupation of the interlayer of the smectite-group minerals.

### 2.2.2 Preparation of homoionic forms

The preparation of homoionic forms was performed by washing 10 g sample material under continuous stirring in 600 ml 3 M salt solution of NaCl, KCl,  $\text{MgCl}_2$ , or  $\text{CaCl}_2$ , respectively. After about 36 hours the stirrer was switched off, and the particles sedimented. The clear supernatant was removed and replaced by new 3 M salt solution.

This procedure was repeated six times. Bentonites C, D, E, H, and W were prepared in the four forms (Na, K, Mg, and Ca), Namorit S and Volclay only in the Mg- and Na-species respectively. The preparation of homoionic forms resulted in overall 22 different bentonite or smectite samples for the experiments. However, as mentioned above not all smectites were used for every experiment except BeC-Ca and BeW-Na, due to their natural occurrence as Ca- and Na-smectite respectively. All samples  $<2\text{ }\mu\text{m}$  were labeled in an uniform manner - first the name of the bentonite and then the type or species of interlayer cation i.e. BeD-Mg or Volclay-Na.

### 2.2.3 Dialysis and freeze-drying

In order to remove the remaining free salts from the clay dispersions after the atterberg sedimentation, but also after the preparation of homoionic forms, dialysis was performed.

Therefore, the suspensions were filled in Roth-Nadir dialysis tubings with a diameter of 50 mm and a pore size of 2.5-3 nm and immersed in plastic boxes with deionized water. The water was replaced several times and the dialysis was finished, when the electrical conductivity of the clay dispersion in the dialysis tubing was below  $20\text{ }\mu\text{S/cm}$ .

Afterwards the suspension was filled in one or two liter round-bottom flasks and freeze-dried by freezing in an ethanol-bath and drying under vacuum. Concluding, the sample material was stored in airtight PVC containers.



### 2.2.4 Steam treatment

The steam treatment was performed in Berghof digestic autoclaves (figure 9). Deionized water and sample material were filled in the PTFE insert. The sample insert was placed in the water insert and closed with a lid. Both inserts were placed in the steel body and closed. Steam treatments were performed at 200°C in an oven over six days. Of particular note is that the sample had no contact with liquid water during the steam process. For all experiments a smectite-to-water ratio of 1:20 was used. After the treatment the closed autoclaves were cooled down for 24 hours. Having reached room temperature, clear supernatant was removed for further analyses, solid was dried at 200°C for about one hour, held in a desiccator, and stored in airtight PVC containers.

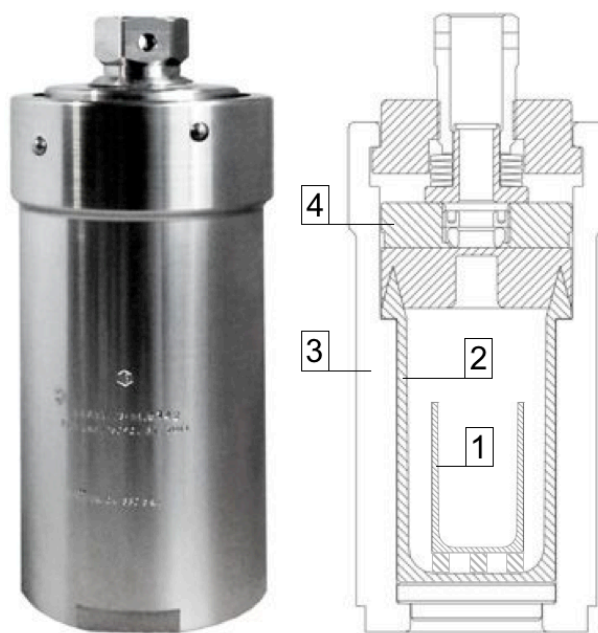


Figure 9: Pressure digestion vessel made of high alloy stainless steel SS 316 Ti, max. 200 bar, max. 250°C (Berghof autoclave DAB-3). Left: picture of the stainless steel body with lid, right: cross section (modified after Berghof (2012)). The autoclave consists of four main components: (1) 50 ml PTFE insert for the sample, (2) 250 ml PTFE insert for the water with lid, (3) high alloy stainless steel body with bayonet lock and (4) Rupture disc to reliably limit maximum pressure.

In order to examine differences between unprocessed and steam treated bentonite samples, laboratory tests were performed as listed below. For all experiments only the clay fraction  $<2\text{ }\mu\text{m}$  has been used. Most of the experiments were performed with BeC-Ca and BeW-Na, other samples were only used partially.

## 2.3 Colorimetry

The change in color in the course of steam treatment was quantified with colorimetry using a Chroma meter (CR-400, Konica Minolta, Germany). In the  $L^*a^*b^*$  color space (DIN 6174, 2007)  $L$  describes the brightness (luminance) of color, which ranges between 0 (black) and 100 (white). The parameter  $a^*$  can range between -150 and +100, where negative values indicate a green and positive ones a red color. The parameter  $b^*$  may vary between -100 (blue) and +150 (yellow). Relative uncertainty on  $L$ ,  $a^*$ , and  $b^*$  is according to the Chroma meter manual less than  $\pm 1\%$ .

## 2.4 Sedimentation experiments

### 2.4.1 Preliminary sedimentation experiments

For a preliminary test and to check the results regarding the sedimentation volume by Oscarson & Dixon (1989), 1 g sample material was dispersed in 30 ml deionized water. The suspensions were stored at room temperature (20°C) and photos were taken for qualitative observations regarding the sedimentation volume after 0, 5, 15, 30, 60 min, 2, 3, 5, 8, 26, 98, 172 hours, 11, and 169 days.

### 2.4.2 Sedimentation volume

One gram of sample material dispersed in 56 ml deionized water was filled in graduated cylinders. After adding 3 g  $\text{MgCl}_2 \times 6 \text{H}_2\text{O}$  (Merck, Germany) to the clay dispersion to facilitate flocculation, the cylinders were shaken and left for sedimentation for one day. The sedimentation volume is given in percent referring to the initial volume of 56 ml. The test procedure is described in Oscarson & Dixon (1989).

## 2.5 Solution chemistry

The ionic composition of supernatant water after steaming may provide a measure of possible dissolution processes due to the vapor treatment. Therefore, supernatant was analyzed by ion chromatography (IC 850 Professional, Metrohm Germany) for anions  $\text{F}^-$ ,  $\text{Br}^-$ ,  $\text{Cl}^-$ ,  $\text{NO}_2^-$ ,  $\text{NO}_3^-$ ,  $\text{SO}_4^{2-}$ ,  $\text{PO}_4^{3-}$ , and cations  $\text{Li}^+$ ,  $\text{NH}_4^+$ ,  $\text{K}^+$ ,  $\text{Na}^+$ ,  $\text{Cs}^+$ ,  $\text{Mg}^{2+}$ ,  $\text{Ca}^{2+}$ . The lower detection limit is 0.5 mg/l for all ions.

The deionized water was essentially free from any contamination. For the second test only water was filled in the autoclaves, whereas the standard test procedure remained unchanged. In order to quantify removable ions of the unprocessed sample, bentonite material was dispersed in deionized water (1:70) and kept in dispersion for five days. After sedimentation, clear supernatant was filtered (0.45  $\mu\text{m}$ ) and concentrations of common ions were determined. The last test represents the standard steam treatment, where the water in the autoclaves was analyzed after steaming. In order to show if water vapor affects tetrahedral or octahedral sheets, silicon and aluminium were measured in the supernatant. For checking whether the concentrations of *Al* and *Si* have to be ascribed to the steam treatment, blank experiments were performed. One gram of sample was dispersed in 20 ml deionized water and kept in dispersion for 5 days, the aluminium and silicon concentrations were determined in the clear supernatants. Background concentrations  $c_0$  of *Al* ( $c_{0,\text{Al}} = 0.4 \text{ mg/L}$ ) and *Si* ( $c_{0,\text{Si}} = 0.1 \text{ mg/L}$ ) were measured in deionized water and subtracted from sample concentrations.

Silicon was measured by the molybdenum blue method according to Köster (1979), pp. 39 at a wavelength of 650 nm. Aluminium was measured using the aluminon red method according to Köster (1979), pp.51 at a wavelength of 530 nm. Relative uncertainties on concentrations are 3 and 0.3 % for *Al* and *Si* respectively (Köster, 1979). An UV/VIS spectrophotometer (Specord 210 Plus, Analytik Jena, Germany) was used to perform photometric measurements.

## 2.6 Chemical characterization (XRF)

Major elements (Fe, Mn, Ti, Ca, K, S, P, Si, Al, Mg, and Na) were determined with an energy-dispersive XRF spectrometer (Spectro Xlab 2000) on fused pellets. The samples were dried at 105°C and the loss on ignition (LOI) was determined by calcining the sample at 1000°C for two hours. This calcined material was then fused into pellets using Fluxana FX-X65. The structural formulae of smectite were calculated according to Köster (1977) by using the results of XRD- and XRF-measurements.

## 2.7 Mineralogical characterization (XRD)

XRD patterns were measured with a Bruker D8 Advance  $\theta - \theta$  diffractometer (CuK $\alpha$  radiation generated at 40 mA and 40 kV) with a variable divergence slit width set to 12 mm sample length and a receiving slit width of 0.2 mm. The Rietveld program BGMN (Bergmann & Kleeberg, 1998) was used to determine the quantitative mineralogical composition of non-oriented powder samples ( $<2\ \mu\text{m}$ ). All samples were analyzed from 2 to 92  $^\circ 2\theta$  with a measuring time of 3 s per step.

## 2.8 Surface-near chemistry (XPS)

XPS was chosen in order to check for a possible change of the internal chemical structure after steam treatment. Specimens were prepared as films from a 1 wt.% dispersion of Volclay-Na, BeC-Ca, BeD-Mg, and BeH-K  $<2\ \mu\text{m}$  in deionized water. Aliquots of the dispersion were withdrawn with a pipette and carefully distributed over a petrographic microscope glass slide. After evaporation of residual water specimens were dried at 200  $^\circ\text{C}$  and kept in a desiccator until use. Angle-resolved XPS measurements of Volclay-Na were carried out on a THERMO Theta Probe spectrometer (Thermo Fisher Scientific, USA). The incident beam consisted of monochromatic AlK $\alpha$  radiation with a photon energy of  $E = 1486.6\ \text{eV}$ . Step width and spot size were defined as 0.1 eV and 400  $\mu\text{m}$ , respectively. In the case of Al $_{2p}$  and Si $_{2p}$  measurements dwell time was set to 200 ms and 400 scans were performed for each angle. The O $_{1s}$  line was recorded with a dwell time of 100 ms and 10 scans per angle.

Further angle-resolved XPS measurements of BeC-Ca, BeD-Mg, and BeH-K were carried out on a XPS/AES/UPS-system of PREVAC sp. z o.o. (Poland) with a Hemispherical Analyzer R4000 of VG Scienta Ltd. (UK). The incident beam consisted of non-monochromatic AlK $\alpha$  radiation. All lines of Al $_{2p}$ , Si $_{2p}$ , O $_{1s}$ , and C $_{1s}$  were recorded 5 scans per angle. Step width and dwell time per step were defined as 0.05 eV and 100 ms respectively; pass energy of the analyzer was fixed at 100 eV.

The angle of the incident beam was either 38  $^\circ$  or 68  $^\circ$ , measured against the vertical direction. During all experiments a flood-gun was used for charge compensation.

## 2.9 Particle size

In order to show whether the steam treatment leads either to particle growth or to particle dissolution, particle sizes or equivalent sphere diameters (ESD) respectively of unprocessed and treated smectites were calculated from turbidity measurements of dispersions having increasing concentrations of solid. Turbidity values can be related to equivalent sphere diameters using the Mie theory of light scattering (Lange (1968); Lange (1969); Melik & Fogler (1983); Lange (1995); Lagaly *et al.* (1997)). 150 mg sample material was dispersed in 150 mL deionized water by ultrasonic treatment (5 min). An aliquot of 0.1 mL was added to 50 mL deionized water and the dispersion homogenized by a peristaltic pump in a loop including a flow-through cuvette. After measuring absorption at 850 nm, the next aliquot of 0.1 mL was added to the dispersion. This procedure was repeated 20 times, resulting in a total of 20 measurements at increasing concentrations. An UV/VIS spectrophotometer (Specord 210 Plus, Analytik Jena, Germany) was used to measure the absorption. In order to calculate the particle size, the measured absorption has to be converted into turbidity according to equation (1), where  $L$  is the scattering length of the cuvette ( $L = 1\ \text{cm}$ ) and  $D$  the measured absorption (Lagaly *et al.*, 1997):

$$\tau = \left( \frac{2.303}{L} \right) \cdot D \quad (1)$$

A plot of the clay-water-solution concentration  $c$  vs. the calculated turbidity  $\tau$  should result in a linear function with a slope of  $\partial\tau/\partial c$ .

$$r_{particle} = \left( \frac{\left(\frac{\tau}{c}\right) \cdot \lambda^4 \cdot \rho}{32 \cdot \pi^4 \cdot n_{fluid}^4 \cdot \left(\frac{m^2-1}{m^2+2}\right)^2} \right)^{1/3} \cdot 10^7 \quad \text{with} \quad m = \frac{n_{solid}}{n_{fluid}} \quad (2)$$

Equivalent sphere radii ( $r_{particle}$  in nm) were obtained from averages of 20 measurements. Following this notation, parameters and constants used in equations (1 and 2) have to be inserted in cgs-units. The wavelength of the photometer is  $\lambda = 8.5 \times 10^{-5}$  cm,  $\rho = 2.6$  g mL<sup>-1</sup> is the density of the mineral,  $n_{fluid} = 1.33$  the refractive index of the fluid (deionized water), and  $n_{solid} = 1.59$  (Lagaly *et al.*, 1997) the refractive index of the solid phase. However, a slightly smaller  $n_{solid}$  was chosen because newer literature (Anthony *et al.*, 2013) provided values of  $n$  as low as 1.51 for montmorillonite. The absolute error of ESD measurements ranges between 0.5 and 9.0 nm.

## 2.10 Nitrogen Sorption

### 2.10.1 Adsorption and Desorption Isotherms and specific surface area

Nitrogen sorption experiments were performed at 77 K at a Micromeritics Gemini VII (Micromeritics Instrument Corporation, Norcross, USA). The samples were previously degassed at temperatures of 50, 70, 90, 110, 130, 150, 170, and 200°C for each 4-5 hours. The long time of degassing and heating was selected to ensure that the desorption part of the isotherm meets the adsorption one after the hysteresis loop ends.

Ad- and desorption isotherms with 42 and 29 data points respectively were recorded between  $p/p_0 = 0.007$  and 0.995. From the linear part of the adsorption isotherm, specific surface areas (SSA) were determined after the BET-theory (Brunauer *et al.*, 1938). The lower and upper limit for BET-SSA calculation was set to  $p/p_0 = 0.01$  (Rouquerol *et al.*, 1999) and the maximum of the Rouquerol plot, respectively. Raw data were evaluated using the Software MicroActive (Version 3.00, Micromeritics).

### 2.10.2 Surface roughness

Another point of interest with special regard to electrokinetics represents the surface roughness or surface fractality. The t-method or t-plot, which should only be applied for non-porous surfaces, provides a first check of surface porosity, if it is non-linear (Rouquerol *et al.*, 1999). For further quantitative investigations a thermodynamic method for the determination of surface fractality based on nitrogen sorption was applied (Neimark (1990); Neimark & Unger (1993)). The equations are related to the theory of capillary condensation in mesopores (size more than 1 nm) and include the relative pressure ( $p/p_0$ ) as only measured quantity. The method encloses the following three equations:

$$\log [S_{lg}(p/p_0)] = \text{const} - (D - 2) \log [a_c(p/p_0)] \quad (3)$$

where  $S_{lg}(p/p_0)$  represents the area of condensed nitrogen-vapor equilibrium at a relative pressure,  $a_c(p/p_0)$  is the mean radius of curvature, and  $D$  is the fractal dimension. According to the Kiselev equation,

$$S(p/p_0) = (RT/\sigma) \int_{N(p/p_0)}^{N_{max}} \ln(p_0/p) dN \quad (4)$$

$S(p/p_0)$  could be determined by integrating the adsorption isotherm from the actual value  $N(p/p_0)$  to the maximal value  $N_{max}$ . Here,  $R$  is the universal gas constant,  $T$  is the temperature, and  $\sigma$  is the surface tension of liquid nitrogen. The mean radius of curvature was then calculated using the Kelvin equation,

$$a_c(p/p_0) = 2\sigma\nu_m/RT \cdot \ln(p_0/p) \quad (5)$$

where  $v_m$  is the molar volume of liquid nitrogen. The results of equation 4 and 5 were inserted in equation 3, from which the surface fractal dimension was derived. Furthermore, the minimum  $r_{min}$  and maximum  $r_{max}$  fractals were calculated from the start and the end point of the linear fit to equation 5. On the basis of the above presented theory it is possible to determine surface fractals in the range between 1 and 100 nm (Neimark & Unger (1993); Neimark *et al.* (1993)).

## 2.11 Water adsorption

The water adsorption or water uptake capacity is widely used in quality control for industrial clay minerals and bentonites. The water adsorption of unprocessed and steamed bentonites was determined using method and instrumentation after Dieng (2005), a recent modification of the Enslin-Neff method (Neff, 1959). For the test 0.2 g dry sample material (oven-dried at 200 °C) were brought in direct contact with liquid water. The measurement lasted 24 h, a time period in which evaporation can be neglected. Relative uncertainty on the water adsorption is  $\pm 2.5\%$  (Dieng, 2005).

## 2.12 Cation exchange capacity (CEC)

In order to obtain information about charge conditions in the interlayer of smectite and their change due to steaming, cation exchange capacity (CEC) was determined with the copper(II)-triethylenetetramine (CuTrien) method after Meier & Kahr (1999). For the experiment 100 mg sample material was dispersed in 50 mL deionized water by shaking. Then 2 mL of a 0.1 mol/L Cu-Trien solution, made from  $\text{CuSO}_4 \times 5 \text{ H}_2\text{O}$  (Merck, Germany) and triethylene tetramine (purum >97 %, Sigma Aldrich, Germany) was added. After one hour, the dispersion was filtered (pore size of the filter  $0.45 \mu\text{m}$ ) and its absorption was measured with an UV/VIS spectrophotometer (Specord 210 Plus, Analytik Jena, Germany) at 577 nm (max. absorption of the CuTrien solution). Relative uncertainty on the CEC-measurements is  $\pm 3\%$ .

## 2.13 Methylene blue sorption (MBS)

The interaction of dye molecules like methyl orange or methylene blue with clay minerals has been studied extensively (Kahr & Madsen (1995); Bujdák *et al.* (2001); Jacobs & Schoonheydt (2001); Ma *et al.* (2004); Czimerová *et al.* (2004)). Furthermore, the determination of smectite content of bentonites by methylene blue absorption represents a standard method in quality control in foundry technology (Grefhorst (2006); VDG P35 (1999)).

For the test, 50 mg of sample material was dispersed in 70 ml of deionized water by ultrasonic treatment for 5 min. Subsequently 8 ml of a  $1.25 \times 10^{-4}$  mol/l methylene blue solution (Clin-Tech Ltd., United Kingdom) was added. Absorption spectra of clay-dye dispersions were measured between 400 and 800 nm using an UV/VIS spectral photometer (Specord 210 Plus, Analytik Jena, Germany). A single experiment lasted 20 hours, while spectra were recorded every 15 min.

## 2.14 Electrokinetics

### 2.14.1 Conductometric titrations

Conductometric titrations were performed to gain information about differences between the isoconductive point and aspect ratio of unprocessed and steam treated samples. Test procedure and data processing followed the instructions of Weber *et al.* (2013), which are based on the theoretical considerations of Dukhin & Derjaguin (1974).

Conductometric titrations were conducted in an 80 ml glass vessel, which was contained in a water bath (Julabo F12). All experiments were tempered to  $25.0 \pm 0.1^\circ\text{C}$  and permanent stirred (Metrohm propeller stirrer 722). A conductivity meter (WTW LF 3000, accuracy  $\pm 10 \mu\text{S/cm}$  in

the measurement range  $>3 \text{ mS/cm}$ ) was used to measure the conductivity of the clay dispersion. Background concentrations of 1 M NaCl or  $\text{CaCl}_2$  added in same steps as in experiments in 50 ml 30 mM NaCl or 20 mM  $\text{CaCl}_2$  respectively were subtracted from experimental data. If the isoconductive point of the dispersion is reached the difference between the conductivity of the electrolyte solution  $K_L$  and the dispersion  $K_{disp}$  is zero. Below the isoconductive point the difference  $\Delta K$  is negative and above it is positive. The aspect ratio (ratio between length and thickness) was determined by dispersing 0.8–1.5 g sample in 50 mL 30 mM NaCl or 20 mM  $\text{CaCl}_2$  respectively, depending on the interlayer occupation of the sample. Subsequent 1.5 ml of 1 M NaCl or  $\text{CaCl}_2$  in steps of  $100 \mu\text{L}$  was added. The pH was measured only at the end of every experiment to avoid unintended KCl input by pH probe; temperature was monitored during every experiment. The absolute error of the aspect ratio is  $\pm 1$  (Weber *et al.*, 2013).

### 2.14.2 Dynamic mobility

A DT 1200 acoustic and electroacoustic spectrometer (Dispersion Technology Inc., New York, USA) was used to gain information about the magnitude of the dynamic mobility  $Mag(u^*d)$  of unprocessed and steam treated smectite particles at a frequency of 3 MHz (Dukhin & Goetz, 2002). The sensor was calibrated against a standard silica (Silica Ludox, 10 %, Quantachrome GmbH & Co. KG, Odelzhausen, Germany).

For electrokinetics, 1.5 g BeW-Na or 4.0 g BeC-Ca were dispersed in 100 ml 5 mM NaCl or  $\text{CaCl}_2$ , respectively. Instead of deionized water the before mentioned electrolyte solution were used to prevent exchange reactions between smectite and dispersion agent. Afterwards, 1M NaCl or  $\text{CaCl}_2$  were added to the dispersions in steps of 0.1, 0.3, 0.5, 1.0, 3.5, and 6.0 ml. During the experiment the colloid vibration current (CVI signal) was measured four times after each addition of NaCl or  $\text{CaCl}_2$ .

Blank titrations were performed to obtain an IVI signal that was subsequent subtracted from the experimental CVI signal resulting in a signal independent of the dispersion agent.

### 2.14.3 Potentiometric titrations

In order to gain information about the charge conditions at the particle surface of smectites potentiometric titrations were performed. Therefore, 200 mg sample material was dispersed in the initial volume  $V_0$  of 100 mL of a 100 mmol/L NaCl or a 50 mmol/L  $\text{CaCl}_2$  solution.

During the experiment the dispersions were stirred, while the temperature was kept approximately constant at 21–23°C. As titrand 0.1 M HCl in 100 mmol/L NaCl or 50 mmol/L  $\text{CaCl}_2$  was used for its respective smectite-species. After each addition of 0.05, 0.1, or 0.2 mL HCl the stirrer was switched off and the pH measured in the clear supernatant after sedimentation of material.

The measurement of pH was performed by detection of a voltage difference between the measuring and the reference electrode. Before measurements the electrode bridge was calibrated against deionized water and the respective salt-solution of NaCl or  $\text{CaCl}_2$ , respectively. Intercept and slope were determined by fitting a linear function to the measured values of the calibration.

The titration occurred from a comparable high pH down to a pH between 2-3. A back-titration up to high pH and afterwards again down to low was not performed, because the measuring volume compared to the initial volume would be too high and dilution would occur. Hence, a statement about hysteresis could not be made.

The measurement of pH was performed with a salt bridge filled with 100 mmol/l NaCl or 50 mmol/l  $\text{CaCl}_2$ , depending on the smectite-species and equilibrated over night.

While every experiment the clay suspensions were flushed with nitrogen in order to degass  $\text{CO}_2$  and to avoid a drift of pH due to the interaction of the suspension with oxygen in the air.

The protonation of the solid or the particle surface, respectively was calculated after the following equations:

$$V_{tot} = V_{int} + V_{add} \quad (6)$$

where  $V_{tot}$  is the total volume (in mL),  $V_{int}$  is the initial volume and  $V_{add}$  represents the added titrant of HCl.

The voltage difference between measuring and reference electrode was measured and converted in a pH by using equation 7.

$$pH = \frac{U \cdot E_{Int}}{E_{Sl}} \quad (7)$$

where  $U$  represents the measured voltage difference in [V],  $E_{Int}$  is the intercept, and  $E_{Sl}$  the slope of the fitted linear function.

The protons in solution  $n_{Prot,solution}$  and the protons added  $n_{Prot,add}$  were calculated according to equations 8 and 9.

$$n_{Prot,solution} = 10^{-pH} \cdot V_{tot} \quad (8)$$

$$n_{Prot,add} = V_{acid} \cdot M_{acid} \cdot + \frac{10^{-7} - 10^{-pH}}{V_{int}} \quad (9)$$

where  $M_{acid}$  is the molarity in [mol/L] and  $V_{acid}$  the cumulative volume of the acid. The protons on the solid  $n_{Prot,solid}$  in [mol] were determined by using equation 10.

$$n_{Prot,solid} = n_{Prot,add} - n_{Prot,solution} \quad (10)$$

and the protons on solid in [mmol/g] by equation 11

$$c_{Prot,solid} = \frac{n_{Prot,solid} \cdot 10^3}{m_{solid,dry}} \quad (11)$$

where  $m_{solid,dry}$  is the dry mass of the solid or the sample material respectively. The presentation of the results occurs as a plot of  $c_{Prot,solid}$  against the calculated pH of the solution.

## 2.15 Rheology

The rheology or flow behavior respectively of bentonite dispersions was performed with a rotation viscometer Bohlin Gemini HR 200 Nano (Malvern Instruments, GB). For the determination of rheological parameters different measuring geometries are possible: coaxial cylinder, cone-plate, and plate-plate. Because only less amount of vapor treated sample was available a cone-plate-system with a diameter of 40 mm and an angle of 4° was used, for which 2 ml of suspension are sufficient. During the experiment the temperature was kept constant by a Peltier element at 25 °C with an accuracy of 0.1 °C. The thermal equilibration time was set to 30 s and preshearing was switched off. After filling the bentonite dispersion into the measurement chamber it was closed to avoid evaporation.

In a first test series the flow behavior of the bentonite dispersion was tried to characterize by recording a hysteresis curve in the shear rate range between  $1.4 \times 10^{-5}$  and  $1.0 \times 10^{-3} \text{ s}^{-1}$ . By applying this experimental conditions it is possible to determine changes in viscosity depending on increasing shear rates. Based on low shear rates and therefore low shear stresses the values of viscosity varied very strong. These variations of rheological properties could not be applied for a reasonable data evaluation. Hence, a direct measurement of viscosity at increasing shear rates could not be performed.

In a second test series the bentonite dispersions (2 wt-% in deionized water) were characterized at constant shear rates  $\dot{\gamma} [\text{s}^{-1}]$ : 0.001, 0.0025, 0.005, 0.0075, 0.01, 0.1, and 1.0. For each shear rate seven values of dynamic viscosity  $\eta [\text{Pa} \cdot \text{s}]$  were recorded, averaged, and the standard deviation was calculated. This test procedure resulted in much smaller variations in viscosity and was applied to all bentonite dispersions. As result from above mentioned measurements the averaged viscosity depending on the respective shear rate could be derived as well for untreated as for steamed samples.

Furthermore, the shear stress  $\tau [\text{Pa}]$  was measured during the experiments and could be related to the shear rate  $\dot{\gamma}$ . This relationship also called a consistency curve could be applied to characterize the flow behavior of clay mineral dispersions.

---

# Chapter 3

## Results



### 3 Results

#### 3.1 Foundry specific characterization (S&B)

The raw bentonites BeC, -D, -E, -H, and -W were provided by S&B industrial minerals. They are used in foundry technology for bentonite-bonded moulding sands. S&B characterized and analyzed the bentonites in terms of common foundry specific parameters and properties, which are presented in the following table 3. The other two clays in this study (Namorit S and Volclay) are applied for other uses, hence a similar characterization is not included. The particular testing procedure is not part of this study, only the measured values will be compared and discussed.

Table 3: Foundry specific properties and parameters of raw bentonites (Be - bentonite, results from S&B industrial minerals, Marl, status 06.08.2010).

Sample number (S&B)	FR-	08-0906	08-0907	08-0908	08-0909	08-0910
sample description		Be H	Be D	Be E	Be W	Be C
		Ca-bentonite soda-activated			Na-bentonite natural	Ca-bentonite unactivated
Mb consumption	[ml/g]	69.2	68.5	60.2	64.3	54.6
Mb adsorption	[mg/g]	400	386	339	362	307
smectite content (Mb-method after VDG*)	[%]	83.3	80.3	70.6	75.4	64.0
sulfur content	[%]	0	0.19	0.005	0.27	0.05
carbonate (method after Scheibler**)	[%]	4.67	8.0	5.1	5.5	1.1
soda content	[%]	3.2	4.1	3.0	2.8	0
swelling volume	[ml/g]	16.3	11	11.8	11	4.5
pH value (50 g/l)	[-]	10.4	10.2	10.3	9.8	9.0
conductivity (50 g/l)	[ $\mu$ S/cm]	1143	1193	1028	874	209
dry sieving residue ( $>90 \mu$ m)	[-]	20.2	10.7	7.2	10.3	5.8

\* VDG - Verein Deutscher Gießereifachleute, method after VDG P69 (1999)

\*\* determination of lime content, method after Scheibler DIN 18129 (2011)

From Mb consumption and adsorption the smectite content was determined after VDG P69 (1999), a similar method as the calculation of smectite content from other sorption methods, i.e. CEC with copper-trien (Meier & Kahr, 1999). The smectite content of the samples ranges between 64.0 % and 83.3 % corresponding to the assumption that activated bentonites for foundry applications show contents  $>70$  %. In the following the smectite contents derived from Mb-sorption could be compared with values from other experiments (i.e. CEC).

While sulfur content is not of interest for further considerations, the carbonate could be reduced to calcite and/or dolomite and probably proportional to added soda for activation. The degree of activation varied between 2.8 % and 4.1 %, while the unactivated Ca-bentonite is free from soda. With regard to the swelling volume the unactivated Ca-bentonite (BeC) shows the lowest value with 4.5 mL/g, while the activated Na-bentonites shows increased values up to 16.3 mL/g. However, the swelling volume of the natural Na-bentonite (BeW) is high compared to those of the activated Na-species (BeH, BeD, and BeE).

As expected the activated Na-bentonites offer high values of pH and electrical conductivity, which exceed the particular values of the unactivated bentonites BeW and BeC.

The dry sieving residue ranges between 5.8 % and 20.2 %. Considering that all samples were milled industrially to  $< 100 \mu\text{m}$  (table 1.2.3.2) a fraction between 90 and  $100 \mu\text{m}$  is presented by this value. However, due to dry sieving aggregation could not be avoided.

## 3.2 Chemical characterization

### 3.2.1 Raw material

The raw bentonites as well as the used fractionized samples ( $< 2 \mu\text{m}$ ) were characterized by XRF. The results of the chemical characterization of raw materials are presented in the following table 4. Volclay and Namorit S were not analyzed because both are only part of a few experiments and the characterization of raw materials is not of greater importance of further considerations.

Table 4: Chemical composition of raw bentonites (results from XRF corrected by loss of ignition).

sample	Oxide content [wt.%]										
	SiO <sub>2</sub>	Fe <sub>2</sub> O <sub>3</sub>	TiO <sub>2</sub>	Al <sub>2</sub> O <sub>3</sub>	MnO	MgO	CaO	Na <sub>2</sub> O	K <sub>2</sub> O	P <sub>2</sub> O <sub>5</sub>	SO <sub>3</sub>
BeC	60.83	3.72	0.32	26.61	0.02	2.63	1.74	0.44	0.47	0.18	0.18
BeD	59.52	6.41	0.87	18.92	0.07	4.03	4.59	3.12	0.85	0.12	0.76
BeE	62.44	4.80	0.43	19.95	0.05	3.96	2.41	2.72	1.62	0.15	0.14
BeH	54.21	12.93	2.64	20.42	0.05	2.56	2.35	2.46	0.99	0.36	0.15
BeW	63.15	3.66	0.33	20.52	0.05	2.83	3.92	2.64	0.68	0.19	0.87

Besides SiO<sub>2</sub> and Al<sub>2</sub>O<sub>3</sub>, which are as expected the main components of all samples with measured values between 54.21 wt.% and 63.15 wt.% as well as 18.92 wt.% and 26.61 wt.%, respectively, Fe<sub>2</sub>O<sub>3</sub>, MgO, CaO, and Na<sub>2</sub>O are of greater importance for the characterization.

The Fe<sub>2</sub>O<sub>3</sub>-contents show a great variation between 3.66 wt.% and 12.93 wt.% which could be reflected in terms of its color. While bentonites with low "impurities" are of a light white color, those with higher Fe<sub>2</sub>O<sub>3</sub>-contents are light brown or beige (see chapter 3.4).

The main cations of tetrahedral and octahedral sheets of a smectite are built up by Si, Al, Fe, and Mg, the interlayer could consists i.a. of Na, Ca, Mg, and/or K. Other potential sources for the aforementioned cations represent kaolinite and different feldspars.

The activation with soda leads to increased Na<sub>2</sub>O-contents (2.46 - 3.12 wt.%) of bentonite BeH, BeD, and BeE, while BeC (unactivated Ca-bentonite) shows the lowest Na<sub>2</sub>O-contents (0.44 wt.%). Bentonite W (unactivated Na-bentonite) shows a Na<sub>2</sub>O-content between the activated ones and the unactivated Ca-bentonite (BeC). The soda-contents (see table 3) correlate with Na<sub>2</sub>O-contents, while absolute values are in the same range.

TiO<sub>2</sub>-contents could be reduced to common Ti-bearing minerals like anatase, brookite, and/or rutile and are not structural part of typical bentonites or smectites, respectively. The other oxide contents (MnO, P<sub>2</sub>O<sub>5</sub>, and SO<sub>3</sub>) are not of greater importance for further considerations.

### 3.2.2 Clay fraction ( $< 2 \mu\text{m}$ )

The following two tables 5a and 5b show the results of an exemplary determination of the chemical composition of the separated clay fraction of bentonites BeC-Ca and BeW-Na, each sample in its unprocessed and steam treated form.

Table 5: (a, left) Chemical composition of bentonite samples, fraction  $<2\mu\text{m}$  (results from XRF corrected by loss of ignition) and (b, right) Structural formulae of bentonite samples, fraction  $<2\mu\text{m}$ .

Sample	Oxide content [wt. %]											[-]	
	SiO <sub>2</sub>	Fe <sub>2</sub> O <sub>3</sub>	TiO <sub>2</sub>	Al <sub>2</sub> O <sub>3</sub>	MnO	MgO	CaO	Na <sub>2</sub> O	K <sub>2</sub> O	P <sub>2</sub> O <sub>5</sub>	SO <sub>3</sub>		Cr <sub>2</sub> O <sub>3</sub>
BeC Ca unprocessed	61.68	5.15	0.28	25.79	0.02	2.38	2.72	0.35	0.25	0.11	0.39	<0.20	2.39
BeC Ca steam treated	60.98	4.90	0.27	25.66	0.02	2.43	2.63	0.30	0.25	0.10	0.36	<0.20	2.38
BeW Na unprocessed	65.90	4.26	0.30	22.15	0.01	2.63	0.31	2.43	0.28	0.20	0.40	<0.20	2.98
BeW Na steam treated	67.44	4.02	0.31	20.08	0.01	2.70	0.57	2.33	0.28	0.16	0.67	<0.20	3.36

Sample	Structural formula	
	Ca <sub>0.18</sub> Na <sub>0.04</sub> K <sub>0.02</sub> (Al <sub>1.58</sub> Fe <sub>0.23</sub> Mg <sub>0.19</sub> ) [(Si <sub>3.73</sub> Al <sub>0.27</sub> ) O <sub>10</sub> (OH) <sub>2</sub> ] * n H <sub>2</sub> O	
BeC Ca unprocessed	Ca <sub>0.18</sub> Na <sub>0.04</sub> K <sub>0.02</sub> (Al <sub>1.58</sub> Fe <sub>0.23</sub> Mg <sub>0.19</sub> ) [(Si <sub>3.73</sub> Al <sub>0.27</sub> ) O <sub>10</sub> (OH) <sub>2</sub> ] * n H <sub>2</sub> O	
BeC Ca steam treated	Ca <sub>0.17</sub> Na <sub>0.04</sub> K <sub>0.02</sub> (Al <sub>1.57</sub> Fe <sub>0.23</sub> Mg <sub>0.20</sub> ) [(Si <sub>3.73</sub> Al <sub>0.27</sub> ) O <sub>10</sub> (OH) <sub>2</sub> ] * n H <sub>2</sub> O	
BeW Na unprocessed	Na <sub>0.28</sub> Ca <sub>0.02</sub> K <sub>0.02</sub> (Al <sub>1.55</sub> Fe <sub>0.20</sub> Mg <sub>0.25</sub> ) [(Si <sub>3.97</sub> Al <sub>0.03</sub> ) O <sub>10</sub> (OH) <sub>2</sub> ] * n H <sub>2</sub> O	
BeW Na steam treated	Na <sub>0.27</sub> Ca <sub>0.04</sub> K <sub>0.02</sub> (Al <sub>1.50</sub> Fe <sub>0.19</sub> Mg <sub>0.31</sub> ) [(Si <sub>4</sub> ) O <sub>10</sub> (OH) <sub>2</sub> ] * n H <sub>2</sub> O	

Furthermore, the structural formulae of the four samples were calculated after Köster (1977). Hence, a change of the chemical composition of the samples after the steam treatment was not expected, only the presented four samples were measured by XRF and their structural formulae were calculated. This assumption was confirmed by the before listed results. The differences between unprocessed and steam treated samples are comparable low.

Although small differences could be observed, an in- or decrease of an oxide content of an unprocessed sample is not accompanied with a simultaneous in- or decrease of an oxide content of a treated sample. As already mentioned in chapter 1.2.3.2 the interlayer of smectite is not

predominantly occupied by one characteristic cation. The structural formulae presented in table 5b show, that the four samples are not characterized by an homoionic interlayer, but by an interlayer built up by Ca, Na, and K. The order of interlayer cations correlates with the previously performed preparation of homoionic forms presented in chapter 2.2.2.

### 3.3 Mineralogical characterization

#### 3.3.1 Raw Material

The mineralogical composition of the raw bentonites is presented in table 6, whereas for BeC, BeD, BeE, BeH, and BeW quantitative and for Volclay and Namorit S qualitative results are shown. The qualitative results were taken from Marchel (2008).

A special focus is placed on the smectite contents, which are in a range between 63.0 wt.% and >90 wt.%. BeC, BeH, and Namorit S show a medium to high content of kaolinite and approximately all bentonites consist to a smaller content of quartz and different feldspars. Accessory minerals contained in the raw bentonites are anatase, muscovite, calcite, goethite, and magnetite.

The smectite contents correlate with the amount of smectite calculated from methylene blue adsorption, performed by S&B (see chapter 3.1).

The used bentonites meet the definitions after Grim & Güven (1978), Murray (2007), and EUBA (2009), whereas after Grefhorst (2006) all bentonites except BeC would be preferred for foundry applications, because of their smectite-contents greater 70 %.

However, as described above, BeC offers a high content of kaolinite (29.2 %) leading to a high correlation between smectite content calculated from Mb-adsorption and XRD.

This comparison of methods determining smectite contents demonstrate, that adsorption methods sample not only swelling clay minerals (i.a. smectites), but also respond to non-swelling clay minerals (i.a. kaolinite), resulting in falsified results. Hence, it would be more practicable to determine bulk clay or clay mineral contents by adsorption methods and not of a specific mineral.

The seven presented raw minerals or bentonites repectively show a typical range of mineralogical compositions and could be based on their smectite contents, other minerals i.e. quartz, feldspars, and the parameters measured by S&B (chapter 3.1) be identified as bentonites (Grim & Güven, 1978).

Table 6: Mineralogical composition of raw bentonites (results from XRD).

\* Qualitative data of Volclay and Namorit S were taken from Marchel (2008).

Sample	Smectite	Mineral phase [wt.%]						
		Kaolinite	Quartz	Sum Feldspar	Anatase	Muscovite	Calcite	Goethite Magnetite
BeC	63.0	29.2	2.5	2.6	0	2.7	0	0 0
BeD	87.3	0	3.3	7.4	0	0	2.0	0 0
BeE	79.1	0	6.2	4.4	0	9.2	1.1	0 0
BeH	86.5	6.0	3.0	2.4	1.0	0	1.1	0 0
BeW	84.2	0	5.0	6.3	0	2.5	2.0	0 0
Volclay*	(>80)	0	+	+	0	0	+	0 0
Namorit S*	(>90)	+	+	0	0	0	+	+

### 3.3.2 Clay fraction ( $< 2 \mu\text{m}$ )

#### 3.3.2.1 Mineralogical composition

The fractionation (see chapter 2.2.1) resulted because of the settling time in a clay fraction with a particle size smaller  $2 \mu\text{m}$ . Hence, a pure smectite would be preferred for further experiments in order to avoid disruptive factors based on the mineralogical composition, a mineralogical characterization of the fraction smaller  $2 \mu\text{m}$  was performed.

Beside other minerals (i.e. kaolinite, quartz, calcite, Ti-oxides) a dioctahedral magnesium-, sodium- and/or calcium smectite structure (montmorillonite) was used for the quantitative characterization with the Rietveld method of all presented samples.

In the course of the enrichment of a clay fraction the clay minerals became more important while the other minerals turn into background, resulting in the following mineral contents.

The results of the XRD measurements including the fitted mineral phases and an enlarged section of the (001)-reflection of smectite are presented in the following figure 10 and figure 11; exemplary for BeD in the four homoionic forms, Volclay-Na, and Namorit S-Mg, for both unprocessed and steam treated samples.

The bentonites BeC-W (fraction  $< 2 \mu\text{m}$ ) in all its prepared homoionic forms are almost pure smectites with a very low amount of anatase ( $< 1\%$ ). Impurities and undefined or unfitted phases could not be observed.

Volclay consists of smectite (91 %), halite (7 %), and quartz (2 %). The amount of halite could be reduced to impurities resulting from an uncompleted dialysis or in an unlikely case to a real content of halite. Further experiments show, that this impurity has no or only a low influence on other measured or calculated parameters.

Namorit-S consists of smectite (93 %), kaolinite (6 %), and anatase ( $< 1\%$ ). Other accessory mineral phases, unfitted reflections, or impurities were not found.

In general, no changes in peak positions were observed for the smectites after steaming. Minor differences in peak intensities between unprocessed and treated samples were observed especially for the (001) and other (00 $l$ )-reflections of smectite (figure 11). These differences are assumed to result from sample preparation (texturing and aggregation) and are, therefore, considered to be insignificant. The other minerals included in Rietveld analysis did not show both neither a shift in peak position, nor differences in peak intensities.

The comparison of peak positions of different samples is possible, because humidity and storage time were the same for unprocessed and treated samples. After drying at  $200^\circ\text{C}$ , the samples were stored in PVC containers and measured with XRD after 1–2 weeks. The XRD measurements took about 8 hours, during which the samples were exposed to room temperature and humidity. However, this time period would be sufficient to create similar hydration states for unprocessed and treated samples.

#### 3.3.2.2 Lattice parameters

Changes on the unit cell scale were checked by X-ray diffraction on powder samples combined with Rietveld analysis. Both hydration state and kind of interlayer cation are known to shift not only the  $c$ -dimension, but also affect the  $a$ - and/or  $b$ - dimensions (Huang *et al.*, 1994). The lattice constant  $b$ , which is sensitive especially to iron contents of octahedral sites, did not change after the treatment within limits of tolerance calculated by the Rietveld analysing software (Heuser *et al.*, 2013). Furthermore, the lattice constant  $a$  did not offer any changes after steaming, which was also not expected. A change of the  $a$ -direction is actually not known to be strongly linked to, e.g., a special oxide content or special properties.

The XRD measurements show in general no differences and/or changes between unprocessed and steam treated samples.

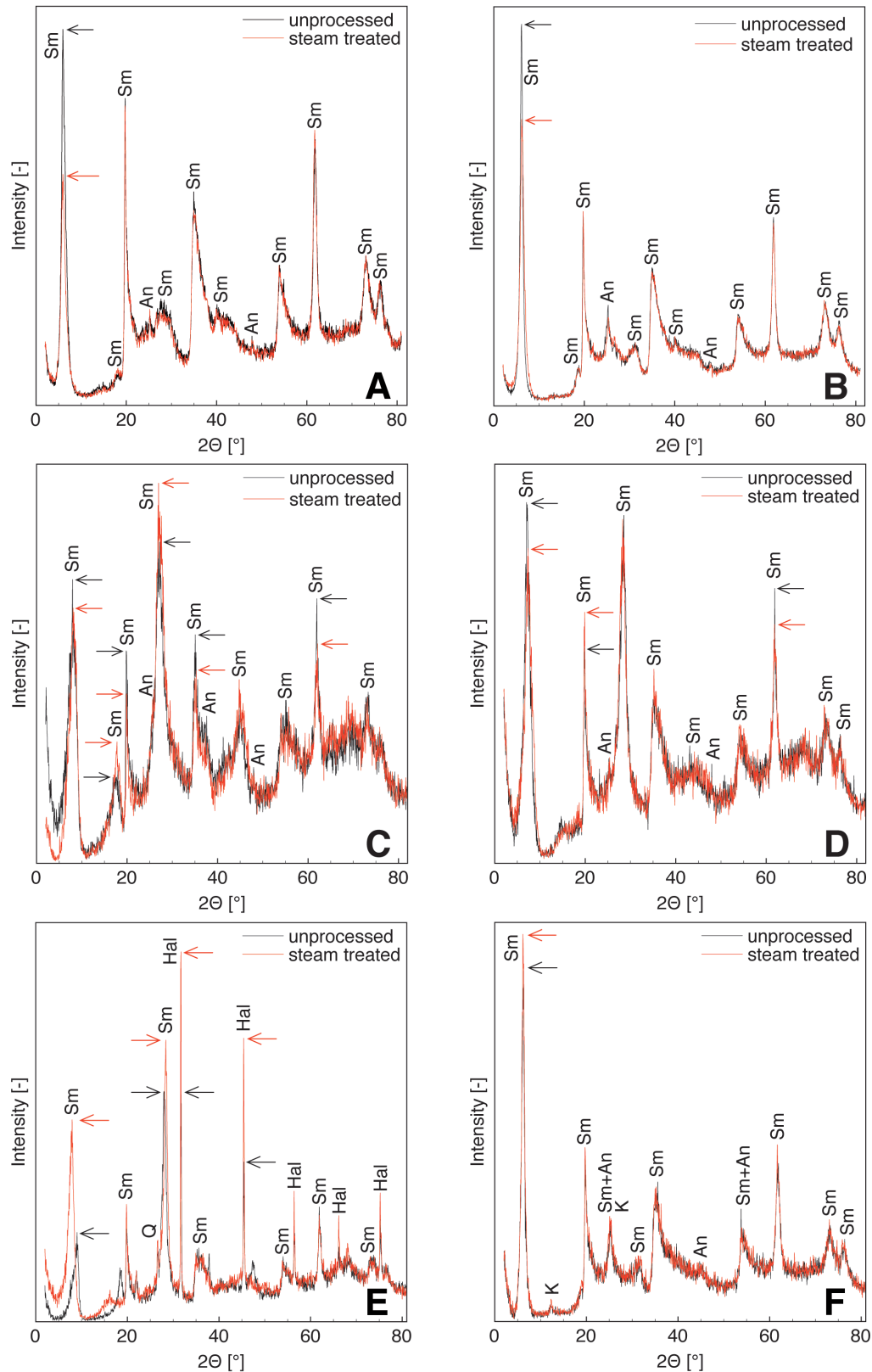


Figure 10: XRD patterns of samples  $< 2\mu\text{m}$ : A – Bentonite D-Ca, B – Bentonite D-Mg, C – Bentonite D-K, D – Bentonite D-Na and E-Volclay-Na, F-Namorit S-Mg. The black line represents the unprocessed sample, the red line the steam treated one.

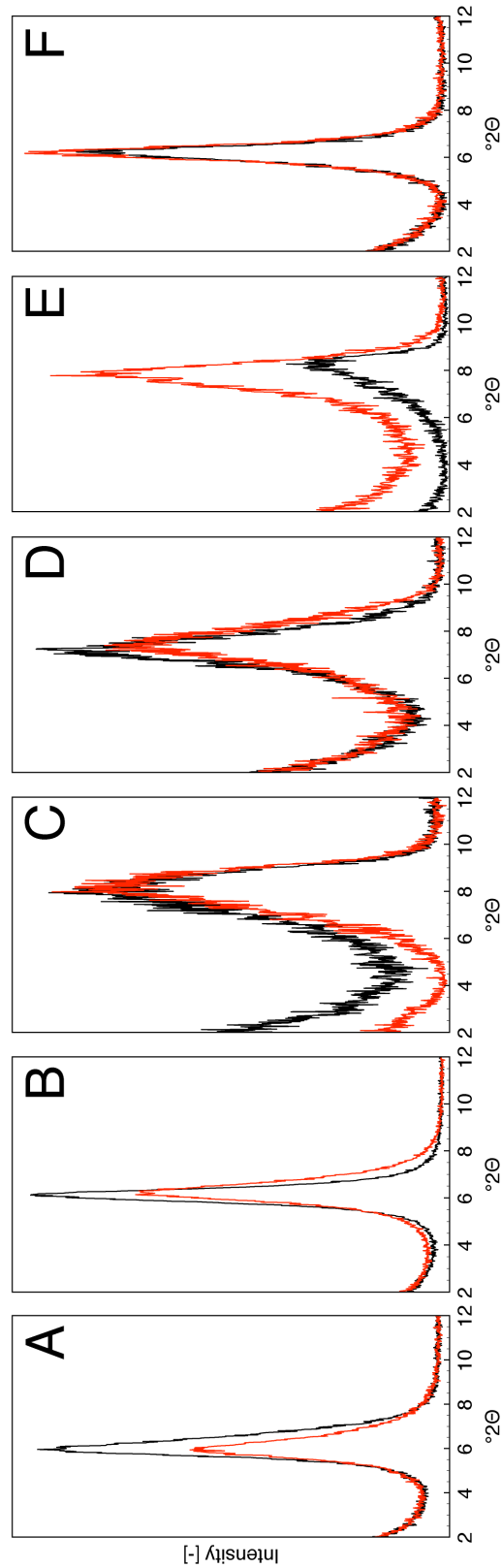


Figure 11: (001)-reflection of smectite: A – Bentonite D-Ca, B – Bentonite D-Mg, C – Bentonite D-K, D – Bentonite D-Na and E-Volclay-Na, F-Namorit S-Mg. The black line represents the unprocessed sample, the red line the steam treated one.

### 3.4 Colorimetry

The examined samples show qualitative, visual colors of white, beige, grey, light yellow, light brown, and light red to red-brown. The visual impression is, that the color did not change in the course of the steam treatment.

Figure 12 shows the results of the color measurements in the  $L^*a^*b^*$  color space.

The measured parameters  $L$ ,  $a^*$ , and especially  $b^*$  are known to be linked to oxide-contents and/or other special properties of minerals. The parameter  $b^*$  shows a direct relation to the iron-content ( $\text{Fe}_2\text{O}_3$ ) and therefore, to  $b$ -directions of smectites and its refractive indices (Heuser *et al.*, 2013).

$L$  describes the brightness (luminance) of color, which ranges for the examined samples between 65 and 95. The samples are therefore located in the white part of the  $L$  scale. A trend between unprocessed and steam treated samples could not be observed.

The parameter  $a^*$  ranges between -3 and +6, hence, a clear green or red color is not present within the samples. From figure 12 a small trend to higher values of  $a^*$  after the treatment is visible, but not of great importance.

The parameter  $b^*$  varies between 5 and 23, which describes a small yellow proportion of the color of samples.

A clear trend between unprocessed and steam treated samples could not be observed. Some samples show decreased values of  $b^*$  after steaming, some show increased ones. Except a few samples, which offer a great increase of  $b^*$  after the treatment, the others remain untouched. Based on the color measurements and the aforementioned relations between  $b^*$  and the iron-content (Heuser *et al.*, 2013), the examined samples should show similar iron-contents before and after steaming. This assumption seems to be valid in terms of the two examined samples BeW-Na and BeC-Ca (see table 5), although, a small decrease of the  $\text{Fe}_2\text{O}_3$ -content of both samples was observed after the treatment.

In general, it could be summarized, that the color measurements confirmed the visual impression, which did not reveal any differences between unprocessed and treated smectites (figure 12), also within the relative uncertainty on  $L$ ,  $a^*$ , and  $b^*$  of  $\pm 1\%$ .

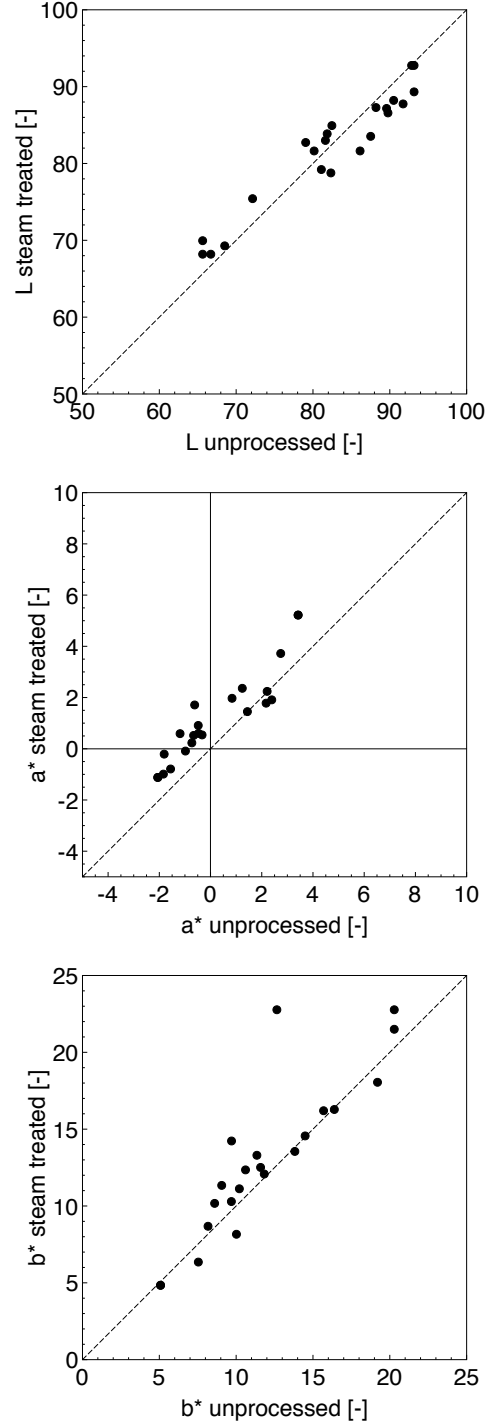


Figure 12: Results of colorimetry in the  $L^*a^*b^*$  color space of unprocessed and steam treated samples.



### 3.5 Sedimentation experiments

#### 3.5.1 Preliminary sedimentation experiments

The results of the preliminary determination of the sedimentation volume (SV) are displayed in figure 14 and 15. The solid lines in both figures indicate the suspension surface as well as the limit between clear supernatant and the sedimented material. In terms of the sodium smectite (BeW-Na, figure 14) the suspension of the unprocessed one remains stable without any sedimentation of material. In contrast, the suspension of the steam treated sodium smectite (BeW-Na) shows a first sedimentation after 5 hours with a comparable strong decrease until 11 days, whereas between 11 and 169 days the SV stays more or less constant.

Regarding the calcium smectite (BeC-Ca, figure 15) the suspensions as well of the unprocessed as of the steam treated sample show an instantaneous sedimentation. After 11 days both samples are completely settled, whereas the treated sample settled a little bit faster and the SV is smaller compared to that of the unprocessed sample.

The preliminary tests confirmed the observations made by Oscarson & Dixon (1989) and gave a first idea of differences between unprocessed and treated as well as between monovalent and divalent smectite samples.

#### 3.5.2 Sedimentation volume

The sedimentation volume (SV) represents the maximum volume captured by unconfined clay in suspension after a fixed time. Oscarson & Dixon (1989) described the influence of water vapor on the sedimentation volume of montmorillonite with regard to the temperature of the vapor and the moisture in the system. In order to verify these results the specific volume of selected unprocessed and steam treated samples was quantified. Sedimentation volumes of treated samples were always lower than those of unprocessed ones, which was ascribed to a change in swelling capacity of smectite (Oscarson & Dixon, 1989). A linear relationship between unprocessed and treated samples was found (figure 13), although with a low correlation factor of  $R^2=0.66$  (without Volclay  $R^2=0.92$ ).

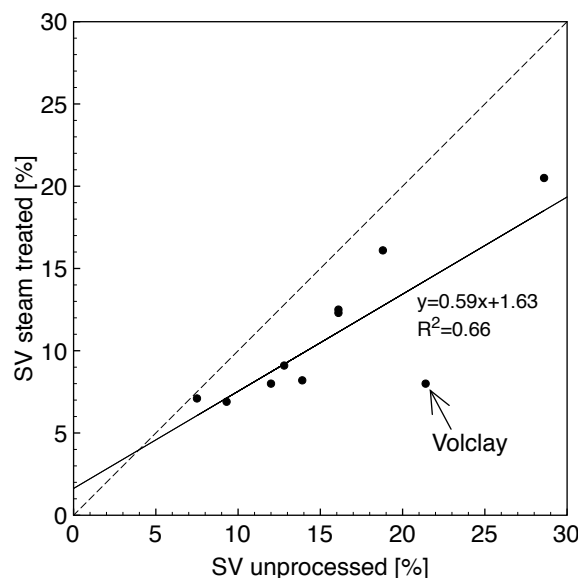


Figure 13: Sedimentation volume (SV) of selected samples after one day of sedimentation time. Results are presented as percentage of the initial volume (56 ml). Dotted line:  $y=x$ , full line: linear regression (see text for explanation).

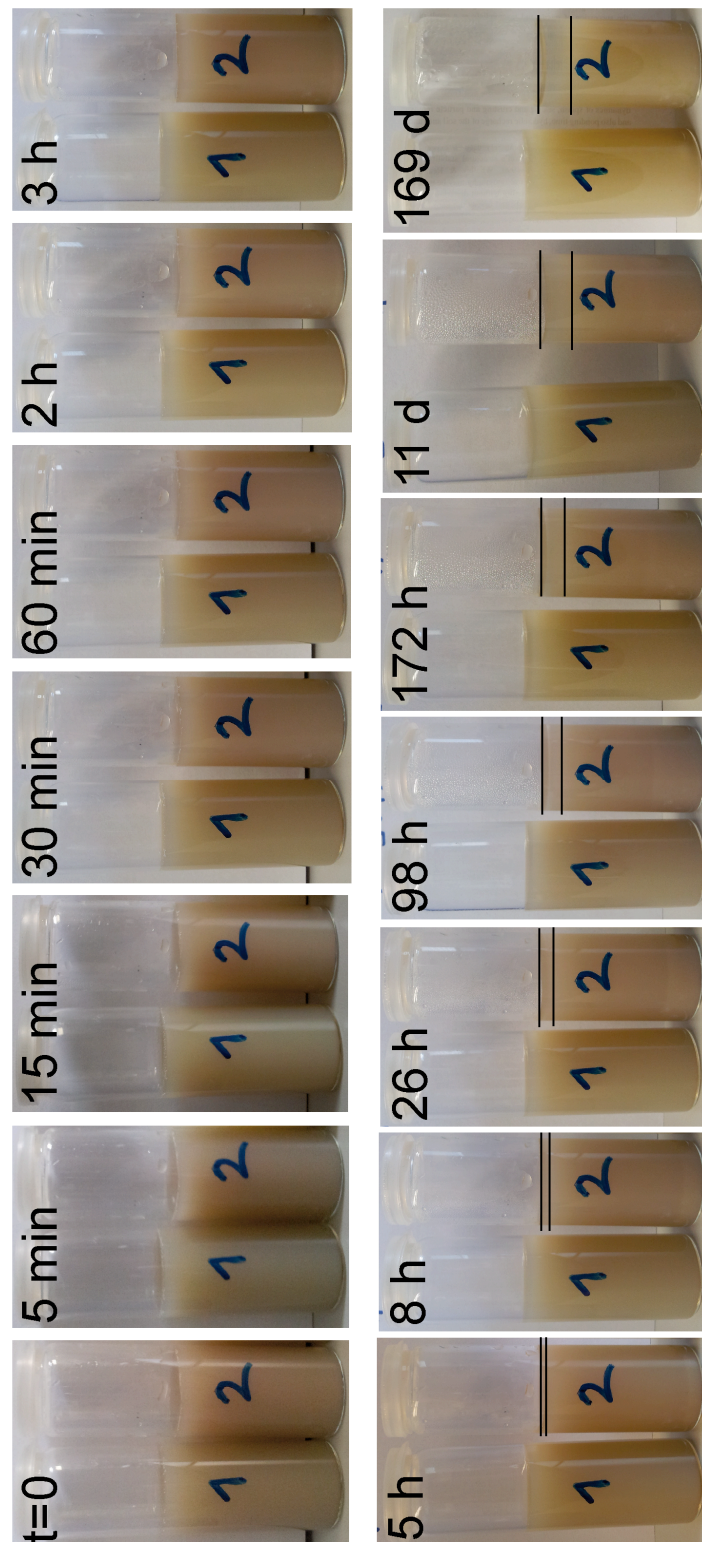


Figure 14: Preliminary sedimentation experiments of BeW-Na: 1. unprocessed and 2. steam treated sample. The solid line indicates the limit between clear supernatant and the sedimented material in terms of the treated sample.

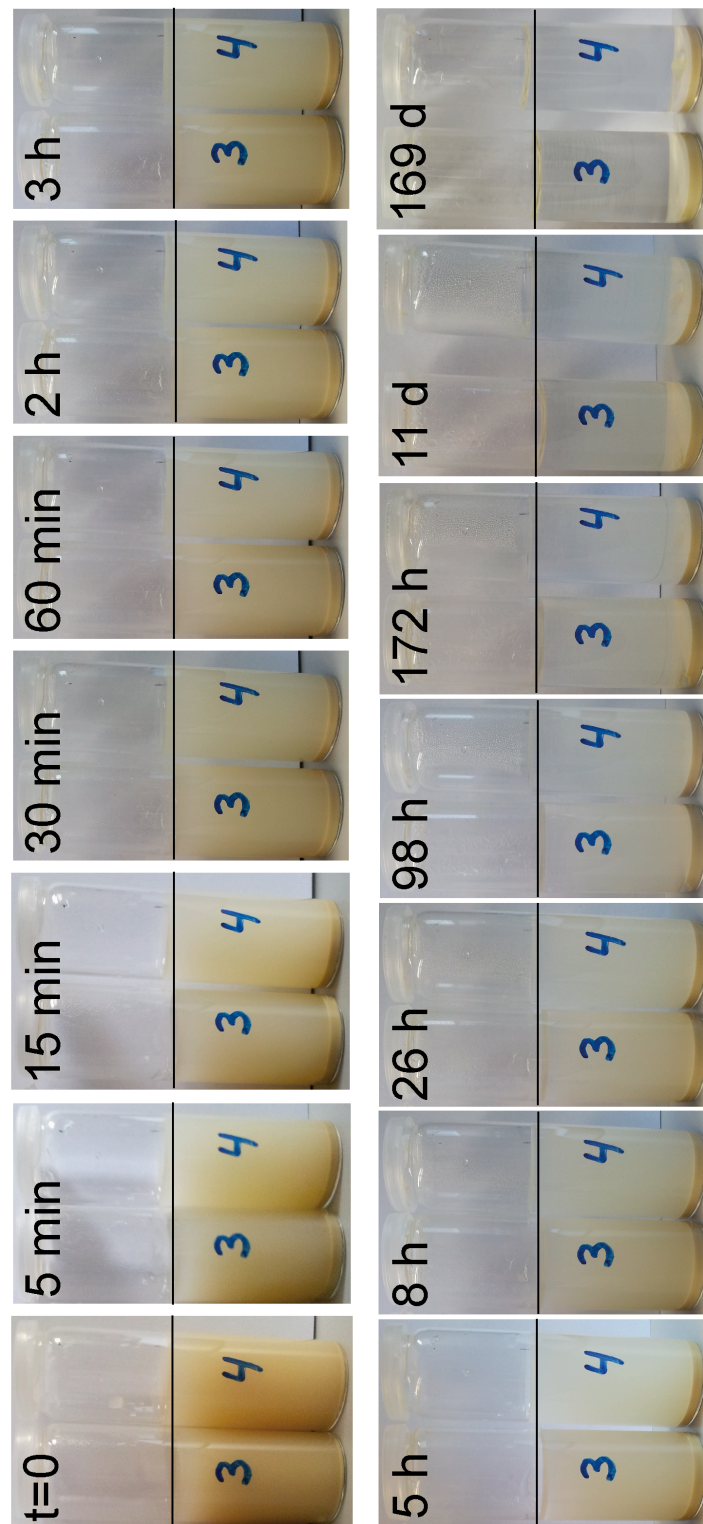


Figure 15: Preliminary sedimentation experiments of BeC-Ca: 3. unprocessed and 4. steam treated sample. The solid line indicates the suspension surface.

### 3.6 Solution chemistry

#### 3.6.1 Ionic inventory

In all samples, lithium, cesium, and calcium, as well as bromide, nitrite, and phosphate, were below detection limit (0.5 mg/l) of ion chromatography. In general, all concentrations were in the lower [mg/l]-range. Differences between the four samples can be assigned to measurement uncertainties and a low contamination by PTFE inlets of the autoclaves as shown by test no. 2 (table 7), respectively.

#### 3.6.2 Silicon and Aluminum

Aluminum concentrations of the blank samples and the steam treated supernatant did not exceed the concentrations found in untreated deionized water. For silicon, the steam treatment consistently lowered the concentrations relative to those of the dispersions made from untreated samples (table 7).

Table 7: Concentration of silicon and aluminum in the supernatant water after the treatment, in 1 g sample material dispensed in 20 ml deionized water after filtration (0.45  $\mu$ m filter), and in deionized water used for analyses.

<b>Si [mg/l]</b>		
Sample	supernatant water after treatment	1 g untreated material dispersed in 20 ml deionized water
Namorit S	4.742	31.26
BeH Ca	0.492	9.704
Volclay	5.766	35.42

<b>Al [mg/l]</b>		
Sample	supernatant water after treatment	1 g untreated material dispersed in 20 ml deionized water
Namorit S	0	0.38
BeH Ca	0	0.41
Volclay	0	0.36

	Si	Al
	[mg/l]	[mg/l]
Deionized water	0.085	0.44

#### 3.6.3 Electric conductivity and pH

The electric conductivity measured at unprocessed and steam treated samples did not show any differences between both. Conspicuous high or low values were also not observed. Hence, it may be expected that the steam treatment did not change or influence the electric conductivity to a noticeable extent.

The pH of some unprocessed and steam treated samples is presented in figure 16, whereas exemplary only a few samples were measured. The differences between unprocessed and treated samples are not equal or similar for the tested samples. A few samples show increased, some show decreased values of pH after steaming. After graphics were arranged divided for smectites with monovalent and divalent interlayer cations it seems to be obvious, that smectites with a monovalent interlayer cation show increased, those with a divalent interlayer cation decreased values of pH after the steam treatment. This observation indicates, that the surface of the smectites is affected by water vapor to some extent. Thereby, the surface near structure or adsorbed cations maybe changed by steam.

A more detailed view is provided in the next chapter 3.7 and chapter 3.13 - *Electrokinetics*.

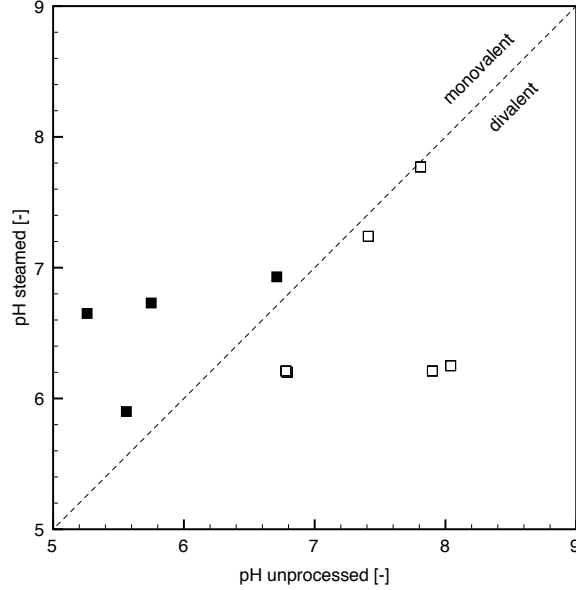


Figure 16: pH of unprocessed and treated samples.

### 3.7 Surface-near chemistry

XPS peaks of Volclay-Na were fitted, after a linear background subtraction, by Gaussian peak-profiles using *Fityk* (Wojdyr, 2010). Unfortunately, no reference line was measured which renders the quantification and a direct comparison of binding energies impossible. Nonetheless, qualitative information regarding differences between samples can be obtained by comparing distances between peak centers of species *A* and *B*,  $\Delta(AB)$  according to equation (12). As well  $\Delta(AB)$  as  $center_A$  and  $center_B$  represent binding energies, however both are labeled as geometric points.

$$\Delta(AB) = (center_A - center_B)_{treated} - (center_A - center_B)_{untreated} \quad (12)$$

Differences  $\Delta(AB)$  in binding energies, as calculated from eq. (12), are in all cases smaller than 0.07 eV. After a linear subtraction of a Shirley background, XPS peaks of BeC-Ca, BeD-Mg, and BeH-K were fitted by Gaussian/Lorentz peak-profiles using *CasaXPS* (Fairley, 2009) and the characteristic peak parameters obtained from all fits were listed (table 8). For these measurements carbon  $C_{1s}$  at 284.6 eV was used as a reference for a direct comparison of binding energies. After calibration of all binding energies in relation to this reference the deviation of binding energies were not more than  $\pm 0.1$  eV.

Since the precision of binding energy determination is generally estimated to be 0.1 eV (Canesson, 1982; Paterson & Swaffield, 1994), the rather small shifts in peak positions are not interpreted to be significant. From these results it is concluded that the steam treatment did not alter the binding energy of the investigated species.

Table 8: Characteristic peak parameters of fitted  $Al_{2p}$ ,  $Si_{2p}$  and  $O_{1s}$  XPS peaks at working angles of 38° and 68° for steam treated and unprocessed smectite samples (fraction  $<2\mu m$ ) and the four examined interlayer cations.

<b>Volclay Na</b>						
Untreated	38°			68°		
	$Al_{2p}$	$Si_{2p}$	$O_{1s}$	$Al_{2p}$	$Si_{2p}$	$O_{1s}$
Center [eV]	74.20	102.37	531.66	74.16	102.31	531.63
Height [cps]	120.17	455.12	2718.16	58.63	232.72	1585.25
FWHM [eV]	1.65	1.78	1.94	1.68	1.81	1.97
Treated	38°			68°		
	$Al_{2p}$	$Si_{2p}$	$O_{1s}$	$Al_{2p}$	$Si_{2p}$	$O_{1s}$
Center [eV]	74.44	102.59	531.95	74.39	102.52	531.91
Height [cps]	107.89	417.95	2507.06	54.44	218.93	1504.50
FWHM [eV]	1.94	2.02	2.18	1.96	2.04	2.22
<b>BeH K</b>						
Untreated	38°			68°		
	$Al_{2p}$	$Si_{2p}$	$O_{1s}$	$Al_{2p}$	$Si_{2p}$	$O_{1s}$
Center [eV]	74.2	102.4	531.5	74.0	102.3	531.4
Height [cps]	75735	218156	1246495	46541	122185	522195
FWHM [eV]	2.02	2.13	2.37	2.22	2.46	2.67
Treated	38°			68°		
	$Al_{2p}$	$Si_{2p}$	$O_{1s}$	$Al_{2p}$	$Si_{2p}$	$O_{1s}$
Center [eV]	74.2	102.5	531.5	74.1	102.3	531.4
Height [cps]	64896	148288	730853	60044	166322	794525
FWHM [eV]	2.02	2.12	2.43	2.05	2.33	2.48
<b>BeC Ca</b>						
Untreated	38°			68°		
	$Al_{2p}$	$Si_{2p}$	$O_{1s}$	$Al_{2p}$	$Si_{2p}$	$O_{1s}$
Center [eV]	74.4	102.5	531.7	74.3	102.4	531.6
Height [cps]	69721	191144	922851	63722	172170	775608
FWHM [eV]	1.98	2.21	2.39	1.94	2.11	2.38
Treated	38°			68°		
	$Al_{2p}$	$Si_{2p}$	$O_{1s}$	$Al_{2p}$	$Si_{2p}$	$O_{1s}$
Center [eV]	74.4	102.6	531.7	74.4	102.6	531.6
Height [cps]	64580	156029	688327	54307	130362	569123
FWHM [eV]	2.26	2.57	3.05	2.67	2.77	3.06
<b>BeD Mg</b>						
Untreated	38°			68°		
	$Al_{2p}$	$Si_{2p}$	$O_{1s}$	$Al_{2p}$	$Si_{2p}$	$O_{1s}$
Center [eV]	74.4	102.5	531.6	74.3	102.4	531.5
Height [cps]	65972	178281	812361	54070	137681	585774
FWHM [eV]	2.07	2.26	2.53	2.35	2.46	2.73
Treated	38°			68°		
	$Al_{2p}$	$Si_{2p}$	$O_{1s}$	$Al_{2p}$	$Si_{2p}$	$O_{1s}$
Center [eV]	74.2	102.3	531.5	74.2	102.3	531.3
Height [cps]	68431	181651	844522	58304	147363	625588
FWHM [eV]	2.30	2.52	2.79	2.66	2.58	3.08

### 3.8 Particle size

Sodium-exchanged smectites show comparable smaller equivalent sphere diameters (ESD) than smectites exchanged with other cations. Aggregation during oven drying after steaming and destruction of aggregates during sonication of particles in water could explain the scattering of ESD measurements above and below the 1:1 line. The treatment itself, however, did not lead to any systematic trend. Neither the kind of interlayer cation (figure 17B) nor the kind of smectite provided a distinction (figure 17A).

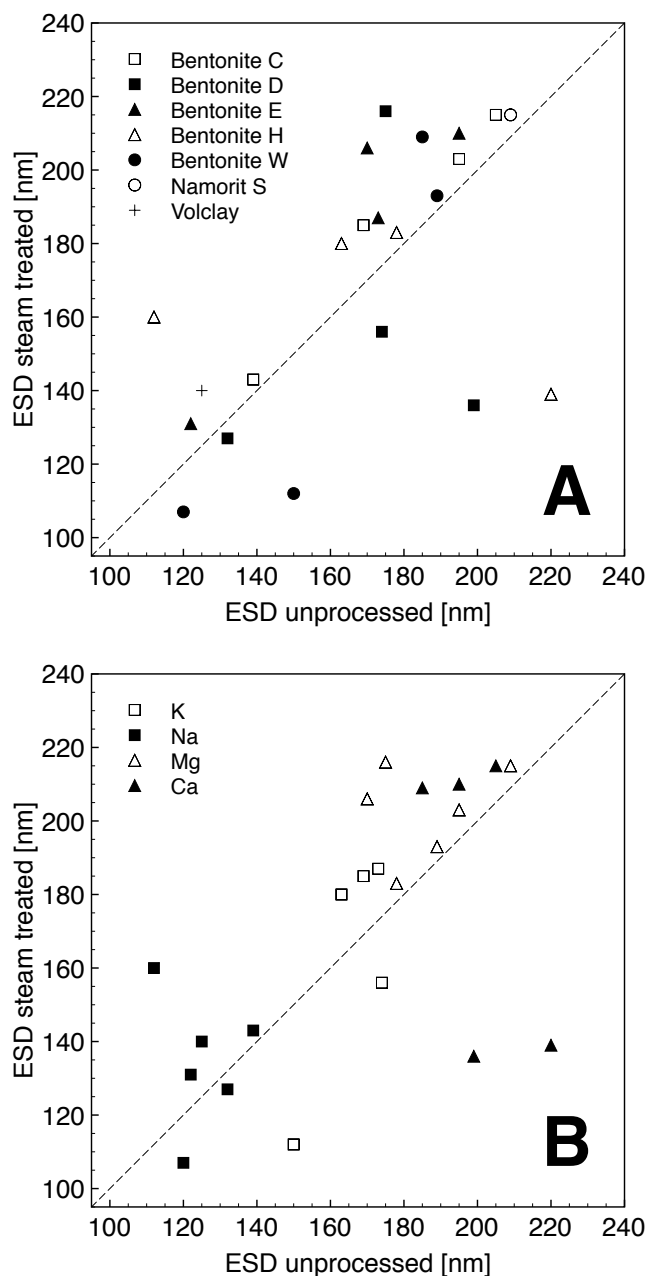


Figure 17: Comparison between equivalent sphere diameters (ESD) of steam-treated and unprocessed smectites. Sorted by bentonite species (A) and by interlayer cation (B).

### 3.9 Nitrogen sorption

#### 3.9.1 Adsorption and desorption isotherms and specific surface area

The ad- and desorption isotherms (figure 18) of the four samples are characterized as type IV that is typical for many mesoporous industrial adsorbents (Sing *et al.*, 1985). Furthermore, mono- and multilayer adsorption takes place as indicated by the beginning part of the isotherm. A hysteresis loop of type H3/4 was observed, which could be reduced to capillary condensation in mesopores. These types (H3/4) are characteristic for aggregates of platy particles and slit-shaped or narrow slit-like pores, respectively (Sing *et al.*, 1985).

In terms of BeC-Ca the differences between the unprocessed and steam treated sample are comparable low. The treated sample shows a higher adsorbed volume at a pressure of  $p/p_0=1$ . Regarding BeW-Na the isotherm of the treated sample shows a shift of the complete ad- and desorption isotherm to lower values of  $Q$ . The curve shape is similar for both, the unprocessed and the treated sample.

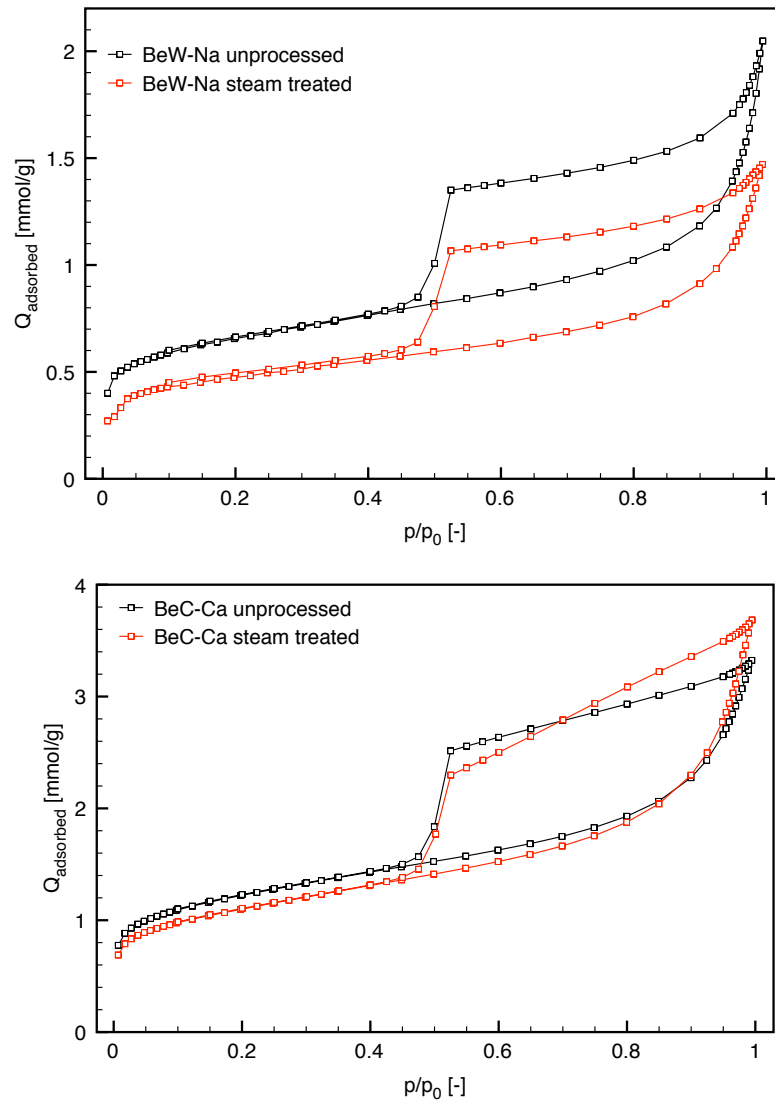


Figure 18: Ad-/desorption isotherms of unprocessed and steam treated samples (Nitrogen sorption).



From the linear part of the adsorption isotherm specific surface areas (SSA) were calculated after the BET theory (table 9). Due to the size of the adsorbate only external surface areas could be determined by  $N_2$ -sorption. For both samples the SSA decreased after the steam treatment, whereas the surface area of the calcium smectite is twice that of the sodium one. The error on the BET-SSA determination resulted in  $<1.1\%$ .

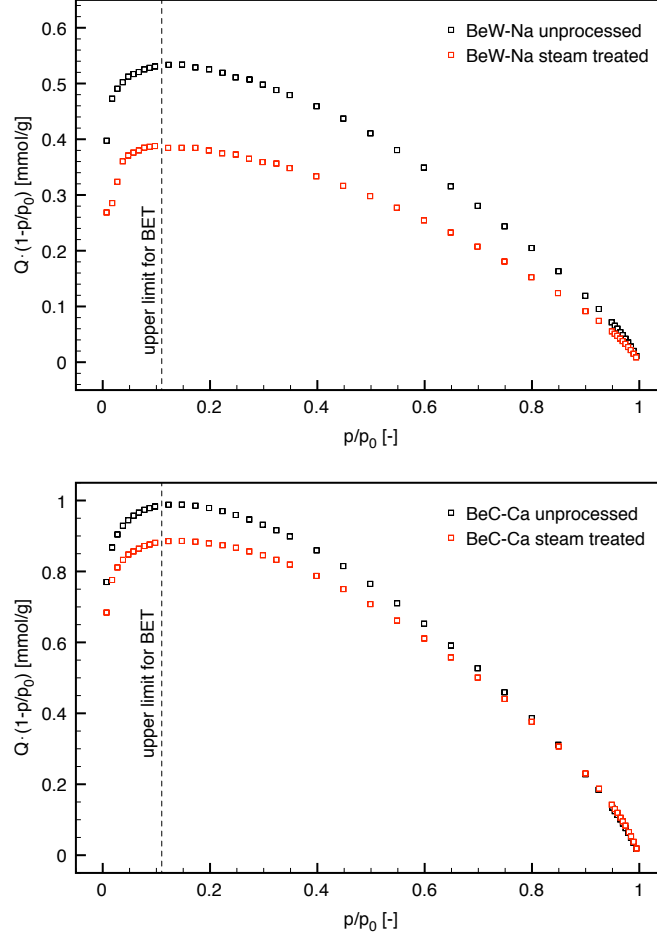


Figure 19: Rouquerol plots of unprocessed and steam treated samples.

The *Rouquerol*-transform-plots (figure 19, Rouquerol *et al.* (1999), Thommes (2010)) should show increased values for  $Q \cdot (1 - p/p_0)$  with increasing  $p/p_0$  until a maximum is reached and values for  $Q \cdot (1 - p/p_0)$  decrease with increasing  $p/p_0$ . The left part of the *Rouquerol*-transform-plots could be used for the calculation of BET-surface-areas (figure 19, dashed line), which was performed analog. For the calculation values up to a  $p/p_0=1.0$  were used. BeW-Na shows maximum values  $Q \cdot (1 - p/p_0)$  of 0.54 mmol/g and 0.38 mmol/g for the unprocessed and treated sample, respectively. In terms of BeC-Ca, the unprocessed and treated samples reached values  $Q \cdot (1 - p/p_0)$  of 1.00 mmol/g and 0.88 mmol/g, respectively. The curve shape of both plots BeW-Na and BeC-Ca show differences between unprocessed and steam treated samples, as already shown by figure 18.

The BET surface area plots (figure 20) show a linear presentation of the adsorption data up to  $p/p_0=1.0$ , which was used for the calculation of surface areas. Both diagrams offer similar differences of unprocessed and treated samples, as already indicated by the ad- and desorption isotherms (figure 18) and the *Rouquerol*-transform-plots (figure 19). The linear regression fitted to measured values resulted in  $R^2$  of approximately 1, that verify the quality of the determination of BET surface areas.

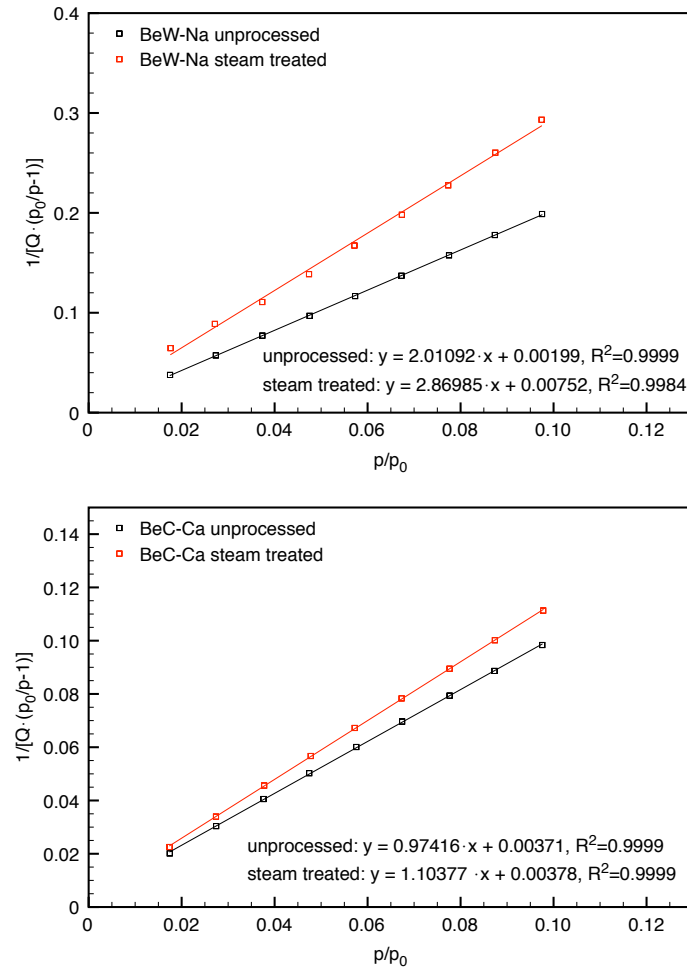


Figure 20: BET surface area plots of unprocessed and steam treated samples.

Table 9: Specific surface areas (SSA) calculated after BET-theory from Nitrogen sorption.

Sample	SSA [m <sup>2</sup> /g]	
	unprocessed	steam treated
BeW-Na	53.17 ± 0.11	40.66 ± 0.45
BeC-Ca	98.70 ± 0.25	88.34 ± 0.21

### 3.9.2 Surface roughness

The surface roughness was studied by the application of a thermodynamic method to determine surface fractal dimensions from physisorption (Neimark & Unger, 1993). Previously, the non-linearity of the t-plot (figure 21, type c, Lippens & de Boer (1965)) indicated surface- and/or mesoporosity. While the t-plots of BeC-Ca are similar, those of BeW-Na show clear differences between unprocessed and treated sample. However, for the calculation of surface fractals the t-plots represent only a first indication for further considerations and calculation.

These results could be confirmed by the calculation of surface fractals (figure 22, table 10). The fractal dimension  $D$  is approximately the same for both samples and for unprocessed and steam treated ones. A value of  $D$  near 2 indicates an almost planar/smooth surface with fractals,

which are in the range between  $\sim 2$  ( $r_{min}$ ) and  $\sim 12$  nm ( $r_{max}$ ). Generally, the surfaces of the four samples have a similar fractal character regarding both the fractal dimension and the minimal and maximal fractals. Differences between unprocessed and steam treated samples were not observed.

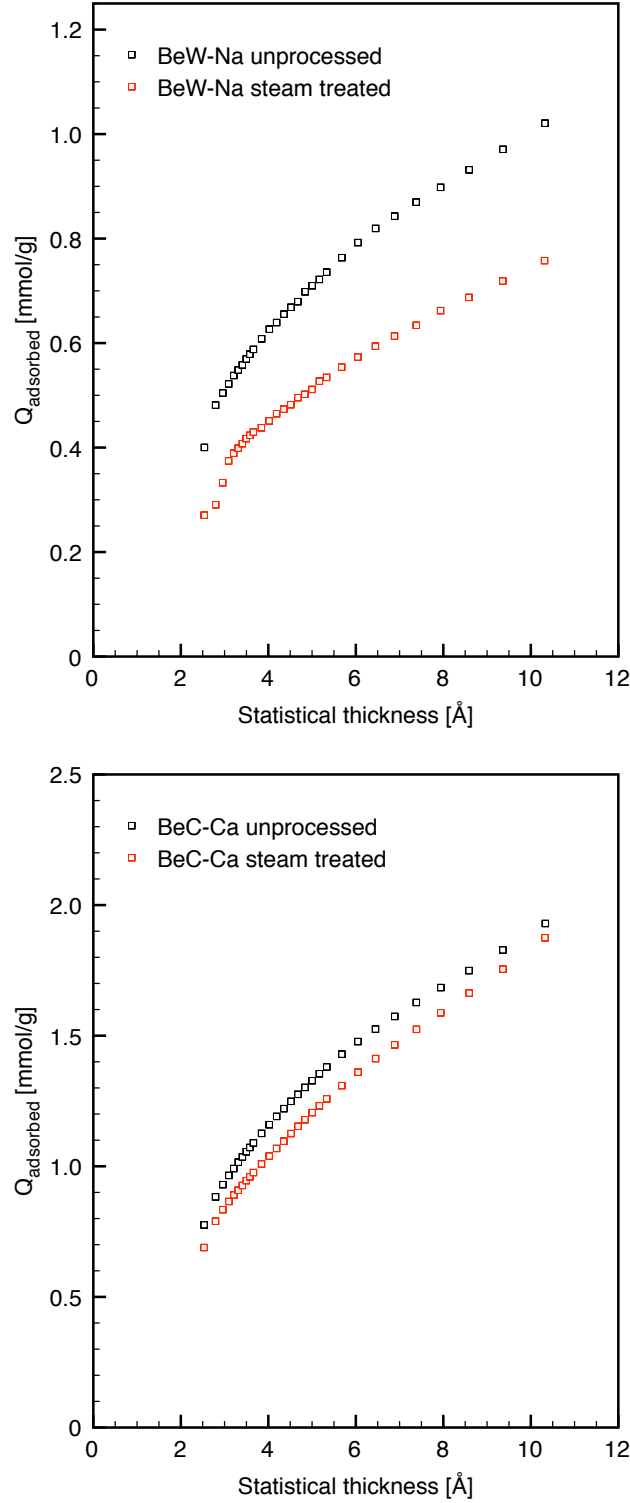


Figure 21: T-plots of unprocessed and steam treated samples.

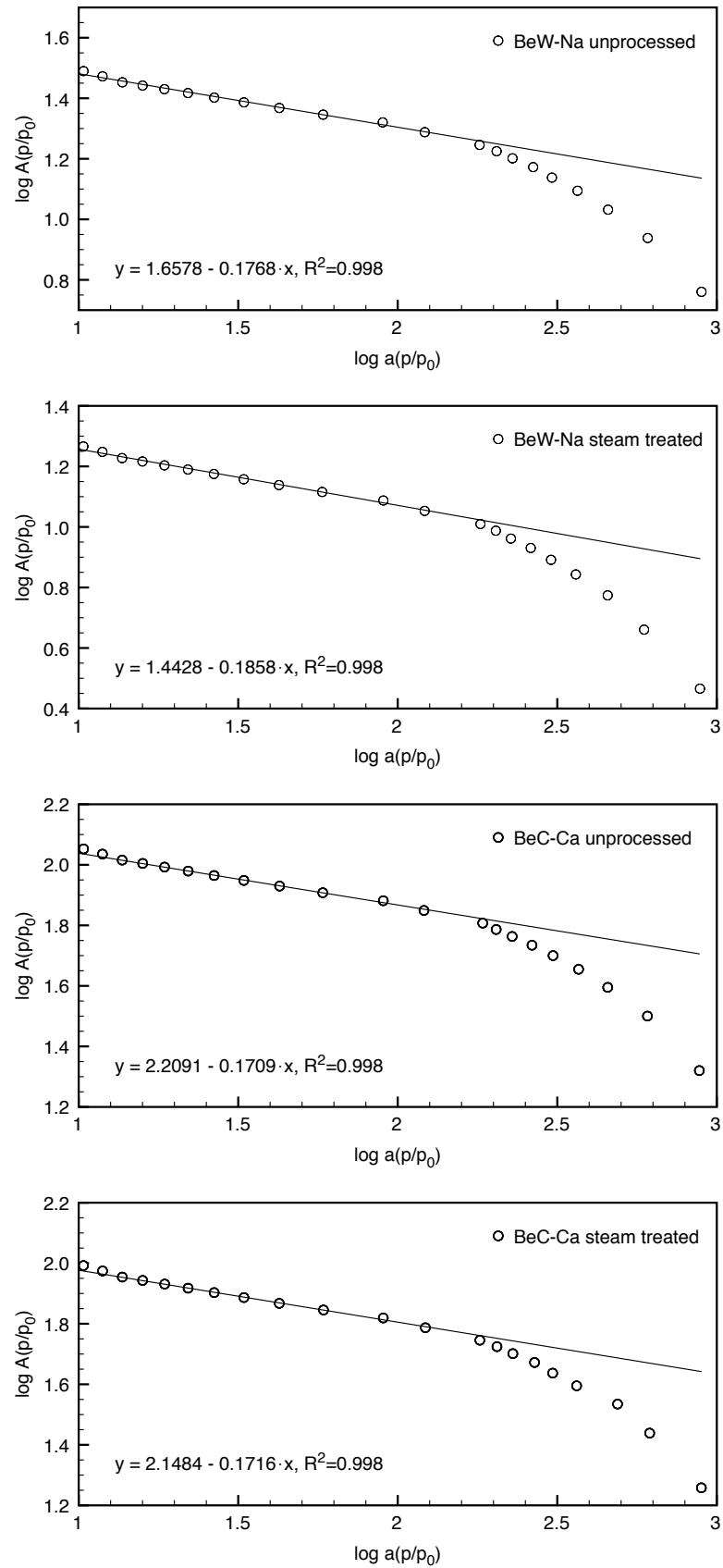


Figure 22: Determination of fractal dimensions. The solid line represents the linear fit.

Table 10: Fractality of unprocessed and treated samples:  $D$  fractal dimension,  $r_{min}$  and  $r_{max}$  are the minimal and maximal fractals respectively, and the correlation coefficient  $R^2$  for the calculation of fractals.

Sample		D [-]	$r_{min}$ [nm]	$r_{max}$ [nm]	$R^2$ [-]
BeW-Na	unprocessed	2.169	1.4	12.2	0.998
	steam treated	2.179	1.4	12.1	0.998
BeC-Ca	unprocessed	2.171	1.4	12.1	0.998
	steam treated	2.172	1.4	12.2	0.998

### 3.10 Water adsorption

Water adsorption varies substantially as a function of the interlayer cations of smectite (e.g. Montes-H. *et al.* (2003); Montes-H. & Geraud (2004)). Moreover, a clear distinction between monovalent and divalent interlayer cations was observed.

Due to changes in the width of the filling area on the filter plate of the experimental equipment and the dependence of water adsorption on the interlayer cation of smectite, samples adsorbed different amounts of water at the beginning of the experiments (figure 23). With increasing time, the water adsorption of treated and unprocessed samples differed by more than the experimental error of 2.5 % (Dieng, 2005). Therefore, differences in water adsorption between unprocessed and treated samples (figure 23, values in brackets) are significant.

In contrast, water adsorption rates showed differences only at the beginning of the test. After 30-60 min, rates of unprocessed and treated samples were identical within the uncertainty and rapidly converged towards zero.

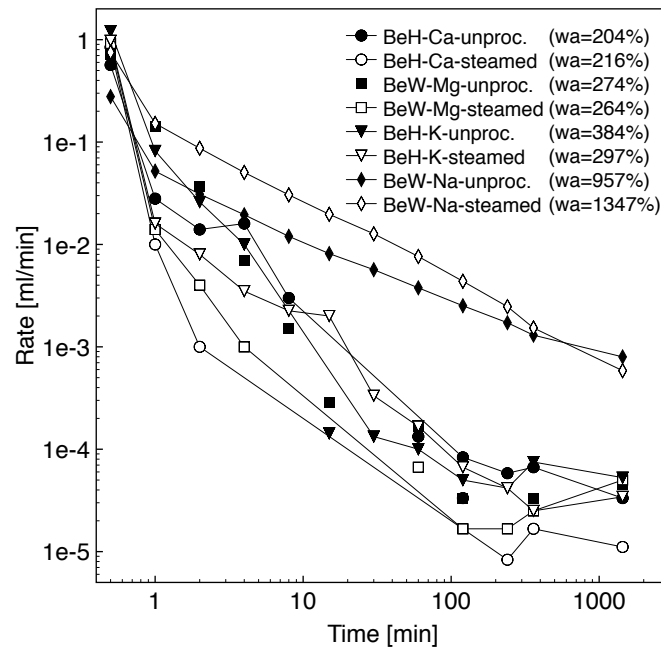


Figure 23: Rates of water adsorption versus time of selected samples and interlayer cations. The values in brackets represent the water adsorption (wa) after 24 h in percent.

### 3.11 Cation exchange capacity

The CEC of some samples decreased, for others it remained unchanged after the steam treatment. CEC of unprocessed and treated samples did not correlate (figure 24A/B) with each other.

Furthermore, the kind of smectite had no influence on the CEC, but the interlayer cation of smectite had (figure 24A/B). Samples saturated with divalent cations showed no or minor changes in CEC, whereas samples with monovalent cations reacted due to steaming. For most of the samples, CEC of K-smectites plot below CEC of Na-smectites (figure 24B).

The pH of clay dispersions for the CuTrien-method was approximately equal for all unprocessed and treated samples and ranged between pH 6-7.

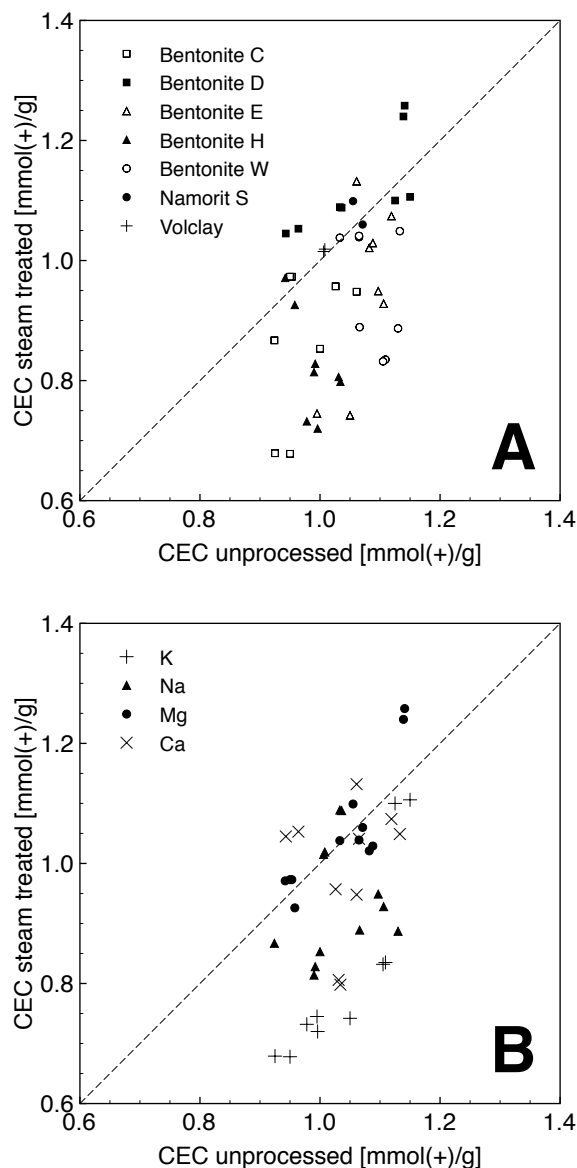


Figure 24: Comparison between the cation exchange capacity of steam-treated and unprocessed smectites. Sorted by bentonite species (A) and interlayer cation (B).

## 3.12 Methylene blue sorption

### 3.12.1 Vis-spectra of dye dispersions

The spectra of methylene blue sorption (MBS) experiments showed band positions at  $577\pm 4$  nm,  $614\pm 9$  nm,  $675\pm 6$  nm, and  $768\pm 4$  nm, respectively (figure 25), which changed both with time and kind of interlayer cation. However, MBS-kinetics were performed with different bentonites or smectites respectively, showing, that the smectite type (BeC-W, Volclay, Namorit S) has no noticeable influence on the spectra.

The observed bands could be assigned to agglomerates (576 nm), dimers (614 nm), monomers (671 nm), and J-aggregates (770 nm). Further detailed information about the position of bands and its interpretation could be read at i.e. Bujdák *et al.* (1998), Bujdák *et al.* (2001), Bujdák *et al.* (2002), Czímerová *et al.* (2003), and Czimerová *et al.* (2004).

Table 11 below summarizes measured and theoretical band positions, as well as a theoretical assignment or indication of bands to properties of smectites.

Table 11: Measured and theoretical band positions, after Bujdák *et al.* (2001) and Bujdák *et al.* (2002).

band name		position		assigned property
		measured [nm]	theoretical [nm]	
agglomerates/ H-aggregates	$(\text{MB}^+)_n$	$577\pm 4$	576	charge density
dimers	$(\text{MB}^+)_2$	$614\pm 9$	614	-
monomers	$(\text{MB}^+)$	$675\pm 6$	671	layer charge
J-aggregates / protonated form	$\text{MBH}^{2+}$	$768\pm 4$	770	layer charge

The assigned property will be part of the discussion in chapter 4 and is only presented in table 11 for the sake of completeness.

The steam treatment had no noticeable effect on band positions. The intensity, however, depended strongly on the kind of interlayer cation (Czimerová *et al.*, 2004), especially on the number of bands and their positions. Samples with a divalent cation in the interlayer (figure 25A, B, F) showed only one characteristic band at  $577\pm 4$  nm. On the other hand, samples with a monovalent interlayer cation (figure 25C, D, E) showed minor differences in intensities after steaming, but no shift in position.

The pure methylene blue solution showed two characteristic bands in the visible spectrum at 616 nm and 668 nm.

Both bands are clearly visible within the spectra of monovalent interlayer cations after 30 min as well as after 1200 min. The spectra of samples with a divalent interlayer cations only show remains of both bands of the pure methylene blue solution.

However, both bands (616 nm and 668 nm) are in the approximately same range of the position of dimers (614 nm) and monomers (671 nm) and therefore, not in all cases clearly distinguishable from one another.

In contrast, spectra of samples with a divalent cation in the interlayer only show remains of the two characteristic methylene blue bands, which are not differentiable from measured values.

Sorption rates of methylene blue for monovalent cations were almost instantaneous, whereas for divalent ones it took 5-10 min before equilibrium was reached. The results of MBS for the unprocessed smectites regarding the type of interlayer cation, valence, and sorption time are comparable to the results from other authors, which were already mentioned above.

Therefore, in the following chapter 3.12.2 a more detailed view on the four single bands (see table 11) is presented.

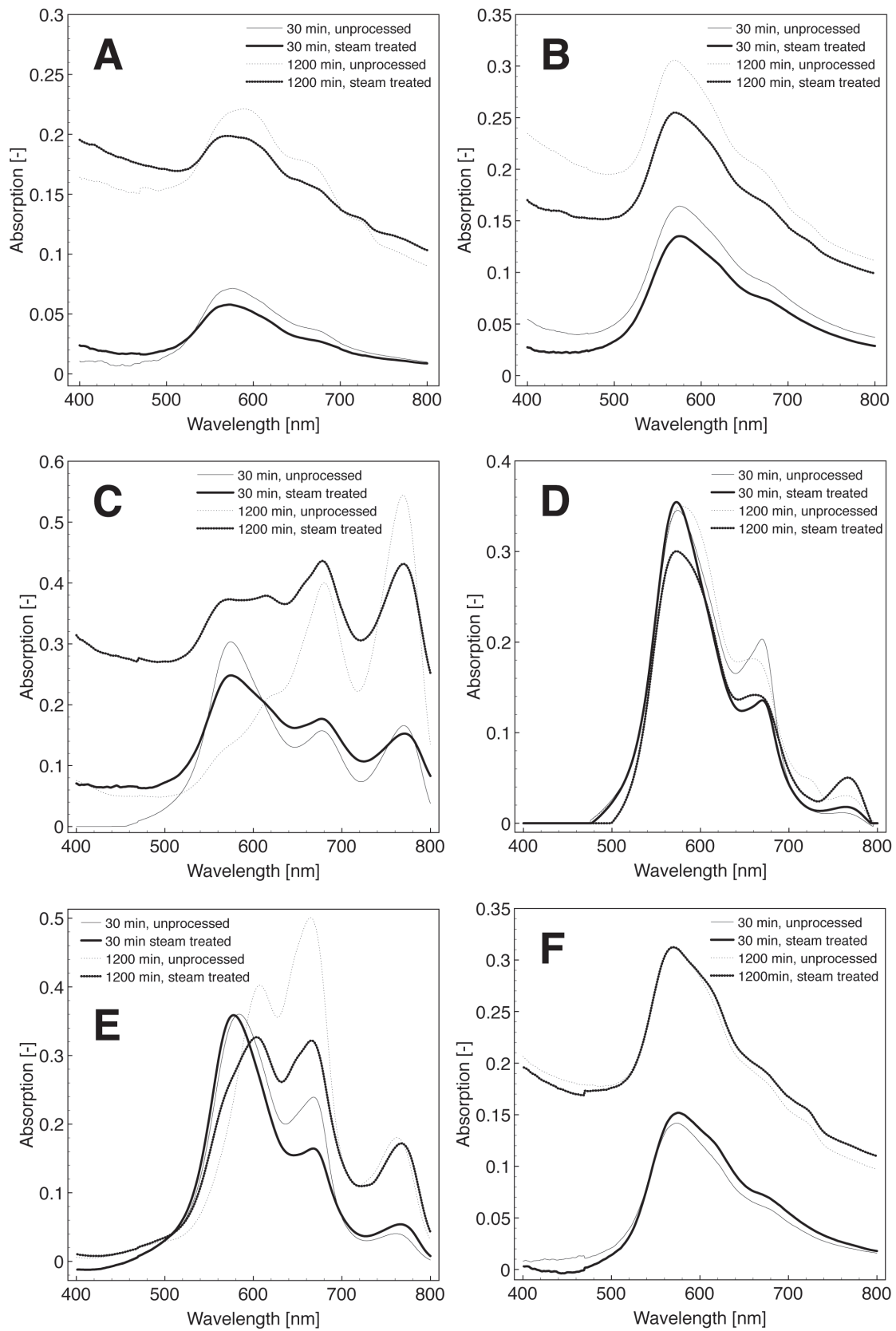


Figure 25: Methyleneblue spectra of bentonite D A-Ca, B-Mg, C-K, D-Na and E-Volclay-Na, F-Namorit S-Mg, 30 min and 1200 min after start of the experiment.



### 3.12.2 Time dependent band intensity

The afterwards presented figures 26, 27, and 28 show the progress of the characteristic bands of the examined samples over time for unprocessed and steam treated ones.

BeD-Na (figure 26, above) shows three characteristic bands at 576 nm, 671 nm, and 768 nm, which remained approximately unaffected over time and less affected by the steam treatment. The agglomerates of the unprocessed sample as well as the monomers show decreased values of absorption after steaming, the J-aggregates were slightly increased by water vapor.

The situation regarding BeD-K (figure 26, down) is different compared to BeD-Na. All four characteristic band positions could be observed, which are affected by both time and the steam treatment. A clear development of the band positions over time could not be observed.

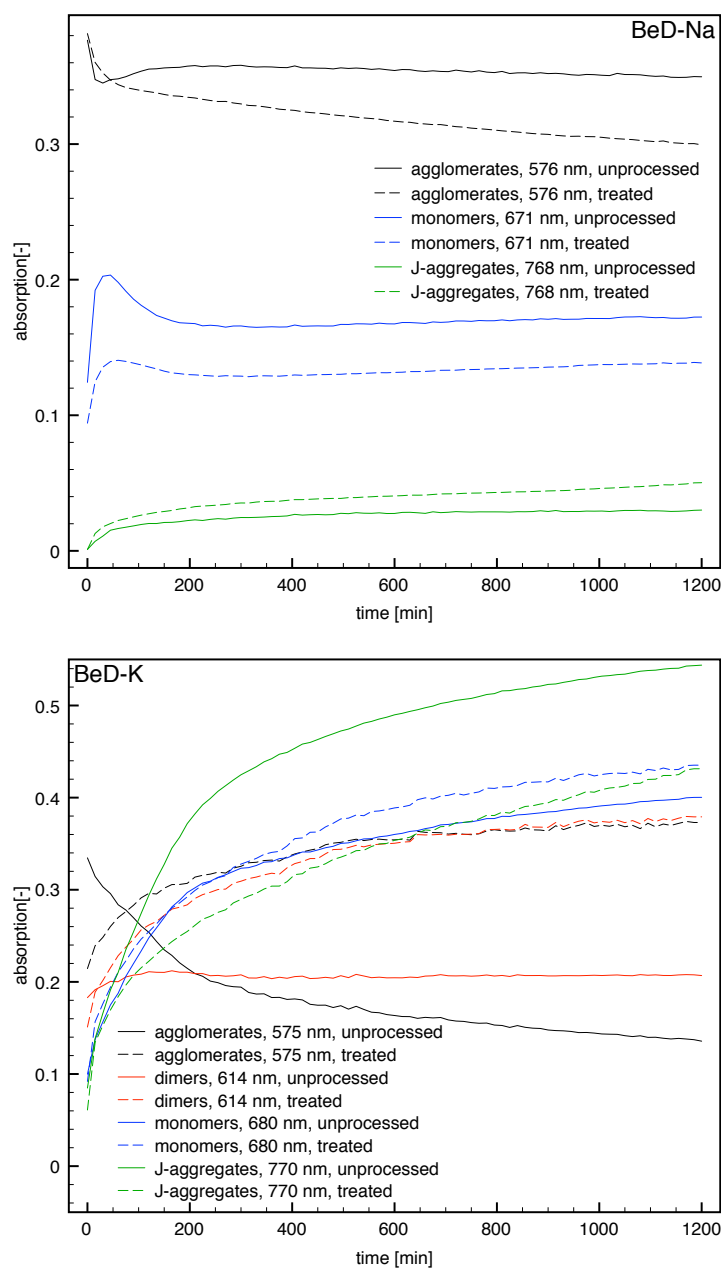


Figure 26: Time dependent changes of Methyleneblue spectra of BeD-Na (above) and BeD-K (down) each for the unprocessed and treated sample.

The development of spectra and band positions regarding the samples BeD-Ca and BeD-Mg are similar for the unprocessed one. Both samples show three characteristic bands at 575 nm, 614 nm, and 674 nm, that increase with increasing time. The respective steam treated samples show a similar curve shape, whereas the absorption of BeD-Ca increases first slightly and beginning at 700 min faster until at 1000 min the measured values came close to those of the unprocessed sample.

The number of bands remains unaffected over time and / or by steam. Also the order of bands (agglomerates - dimers - monomers) over time shows no changes before and after steam treatment. Uncommon measured values could not be observed. The differences between unprocessed and steam treated samples are comparable low.

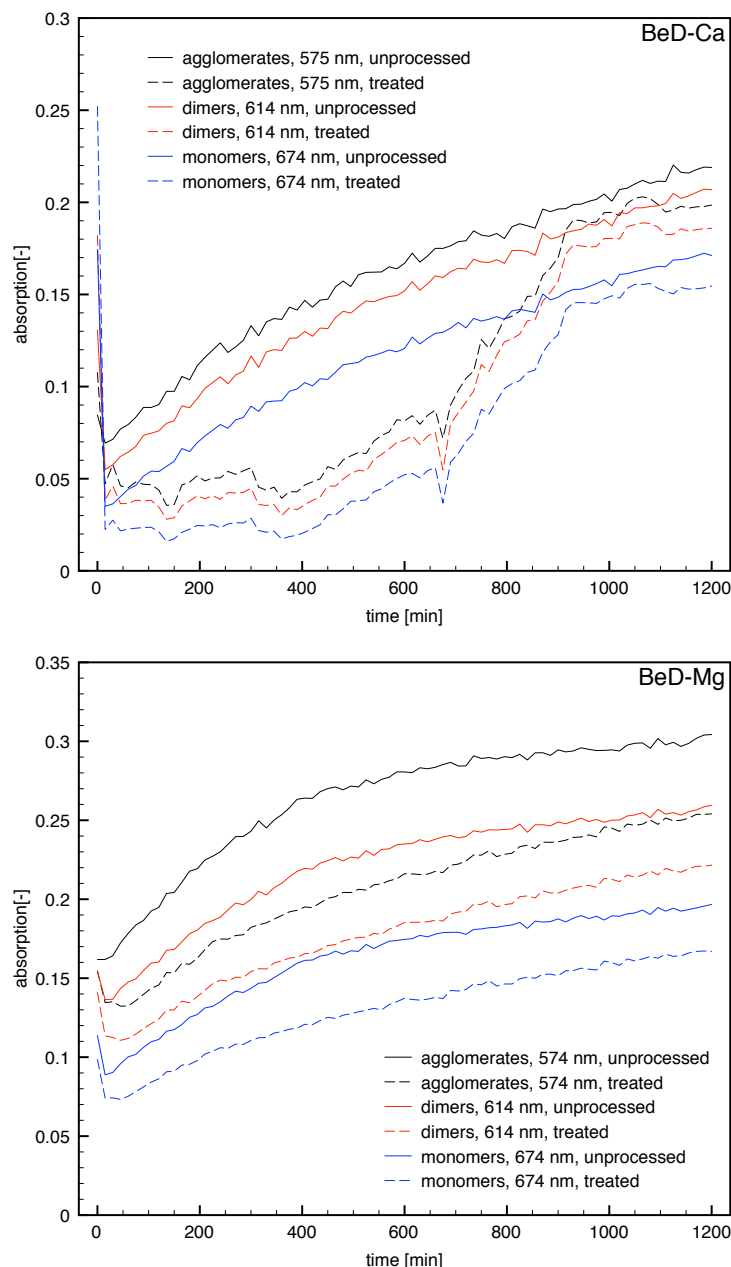


Figure 27: Time dependent changes of Methyleneblue spectra of BeD-Ca (above) and BeD-Mg (down) each for the unprocessed and treated sample.

The sample Namorit S-Mg (figure 28, above) shows an increase of band intensities over time for both unprocessed and treated sample. Between neither the number of bands nor band intensities of unprocessed and water vapor treated samples differences exist.

Regarding Volclay-Na all four band positions are visible 576 nm, 605 nm, 667 nm, and 765 nm. The J-aggregates remain unaffected by steam. Dimers and monomers show lower, agglomerates higher values of absorption after the treatment. Compared to BeD-Na the development of the number of bands and its positions and intensities is not equal.

As already mentioned in table 11 the respective band positions could be assigned to properties of smectites. Based on the measured bands as well the charge density as the layer charge were affected by the steam treatment.

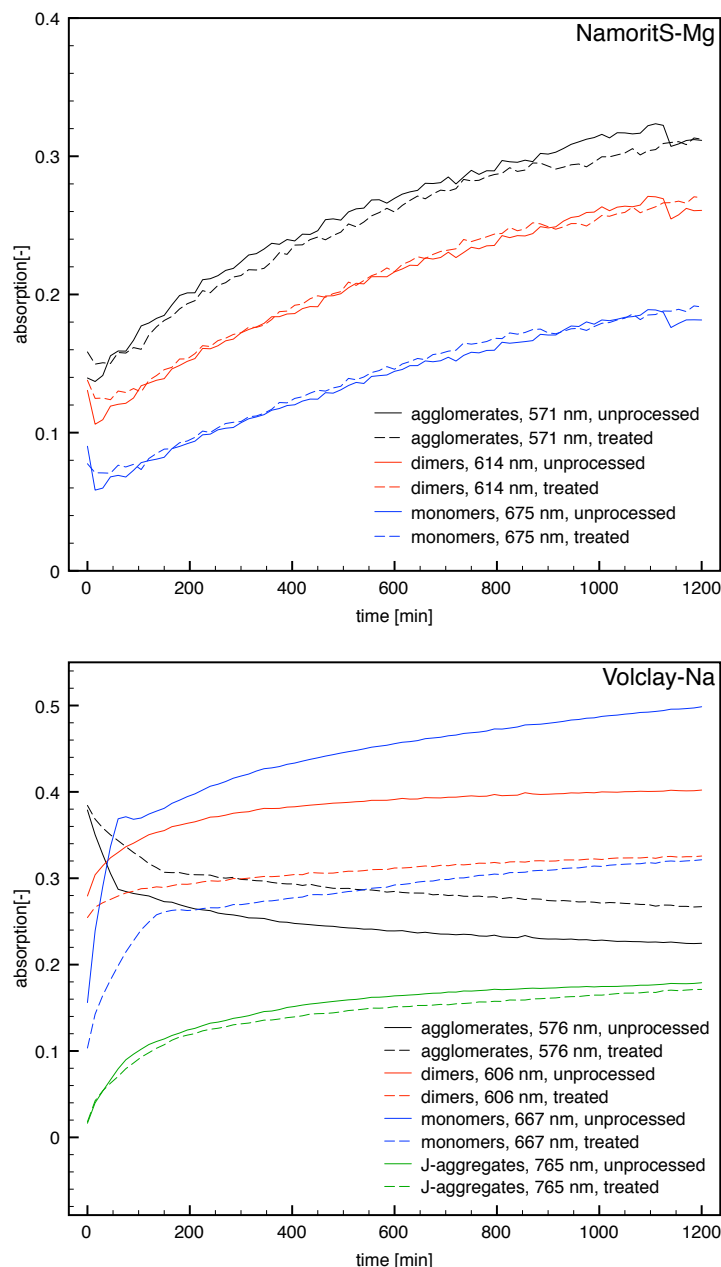


Figure 28: Time dependent changes of Methyleneblue spectra of Namorit S-Mg (above) and Volclay-Na (down) each for the unprocessed and treated sample.

In general it could be summarized, that except Namorit S-Mg all other samples show a reaction to the steam treatment. The band intensities change after the treatment and also with time, but a clear development of band positions and intensities over time that is valid for all samples could not be observed.

### 3.12.3 Time dependent MB area

A last point of view regarding MBS-kinetics represents the time-dependent MB area. Therefore, the area under the curves (see figure 25) was calculated by using the curve fitting software *Fityk* (Wojdyr, 2010). The calculated area was set in relation to the maximal area over time, resulting in values of  $A/A_{max}$ , that were plotted against the squareroot of time.

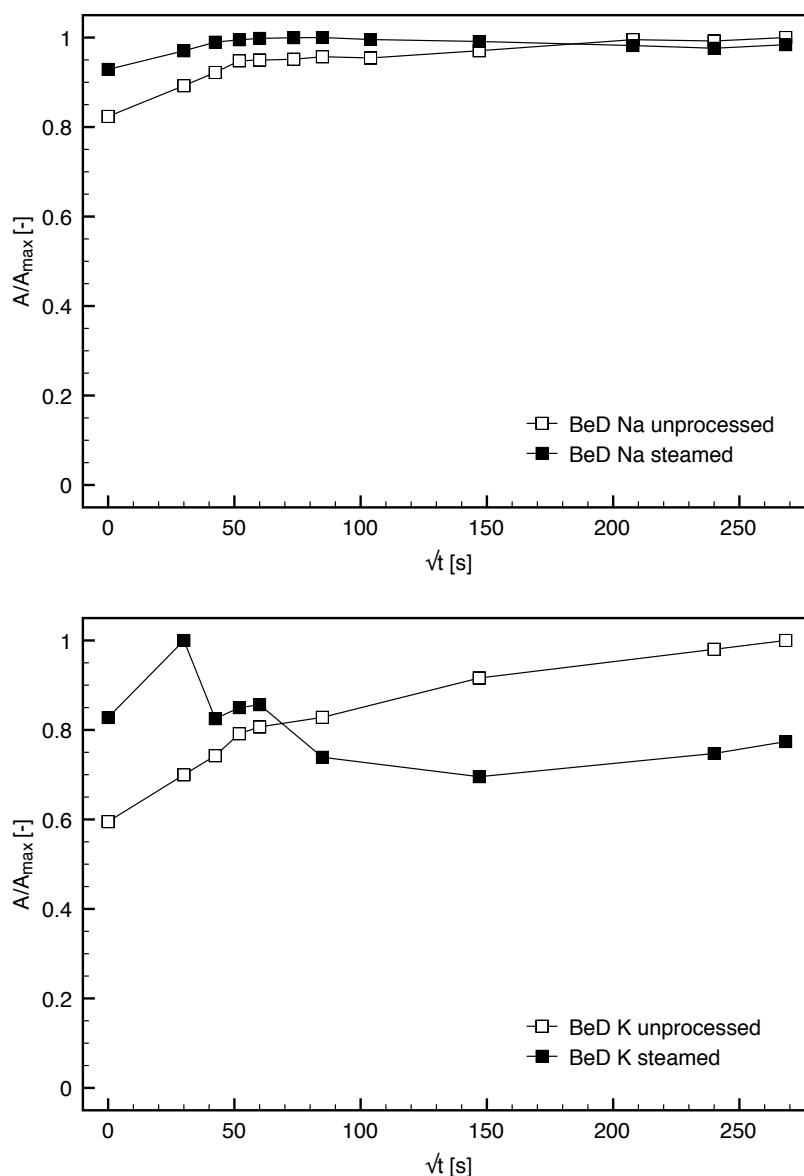


Figure 29: Time dependent changes of Methyleneblue spectra. Development of the area below the sorption curves for BeD-Na and BeD-K.

The area under the curves is assumed to be directly related to the volume of MB, that is adsorbed or could be adsorbed by the smectite. In terms of figure 29, 30, and 31 as well the maximal volume of MB-solution adsorbed on smectite, as the reallocation of adsorbed MB from the surface into the structure or reverse could be observed. This reallocation would result in a change of band positions and its intensities, as observed in figure 26, 27, and 28. While the maximum value of the MB-area represents a quantitative, the reallocation only provide a qualitative statement.

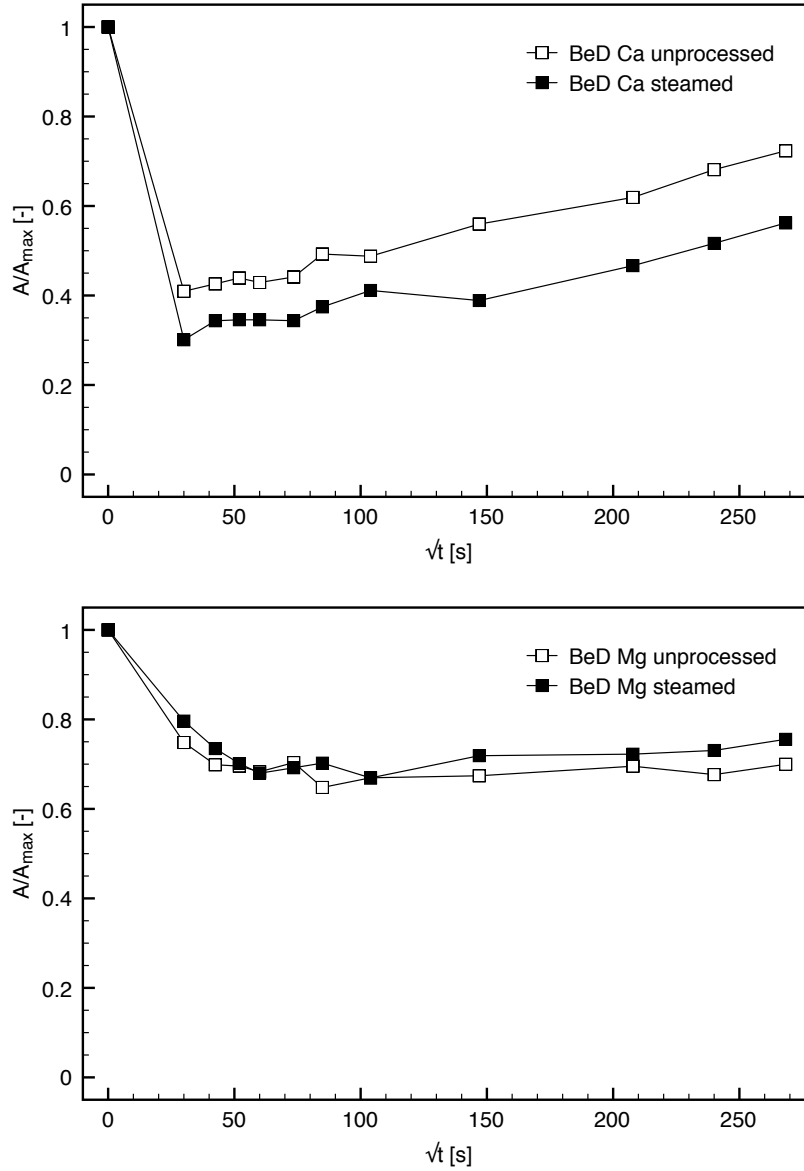


Figure 30: Time dependent changes of Methyleneblue spectra. Development of the area below the sorption curves for BeD-Ca and BeD-Mg.

The samples BeD-Na, BeD-Mg, Namorit S-Mg, and Volclay-Na show no differences between the unprocessed and the steam treated smectite. Only low differences were observed at the beginning of the sorption process, but after about 6400s the curves of unprocessed and steam treated samples are approximately equal. This observation indicates, that as well the volume of MB-solution adsorbed as the distribution and/or reallocation of already adsorbed MB-solution is the same for both the unprocessed and the treated sample.

The other both examined samples BeD-K and BeD-Ca show differences between the unprocessed and the treated one. Regarding both ones, the steam treated samples offer lower values of time-dependent MB-area, which means, that the treated samples adsorbed a lower absolute amount of MB-solution over time.

Most of the samples remain unaffected by steam. The other ones only show comparable low differences between unprocessed and steam treated samples, resulting in the assumption, that absolute values of adsorbed MB-solution seems to be not very different. However, as indicated by the time-dependent band intensity a reallocation of MB-solution from the surface to structural parts of the smectite maybe occurred.

A clear trend regarding interlayer cation or valence is not visible. It is noticeable, that some samples show the highest value of  $A/A_{max}$  not at the end of the experiment, but at the beginning or in the middle. This observation indicates, that during the experiment the respective sample is subjected to a desorption process from the smectite into the free MB-solution.

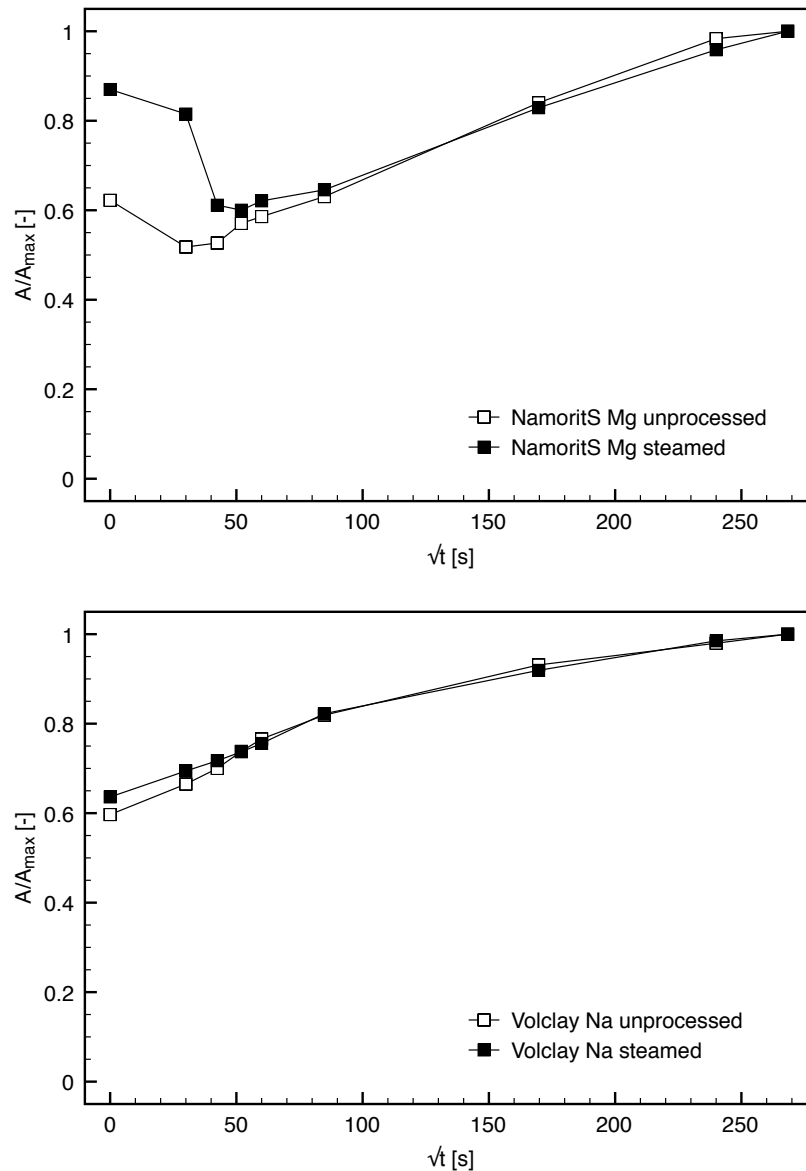


Figure 31: Time dependent changes of Methyleneblue spectra. Development of the area below the sorption curves for Namorit S-Mg and Volclay-Na.

### 3.13 Electrokinetics

#### 3.13.1 Conductometric titrations

From the implementation of conductometric titrations two general informations were available: the curve shape and hence the isoconductive point  $K_{iso}$  (figure 32A/B) and furthermore the aspect ratio  $n$  (figure 33). With regard to the curve shape of the conductometric titrations a clear difference between unprocessed and treated sample could be observed for the sodium smectite (figure 32A). Both curves plot approximately parallel. The isoconductive point of the unprocessed sample was  $\sim 2600 \mu\text{S}/\text{cm}$ , whereas  $K_{iso}$  of the vapor treated one was  $\sim 4000 \mu\text{S}/\text{cm}$ .

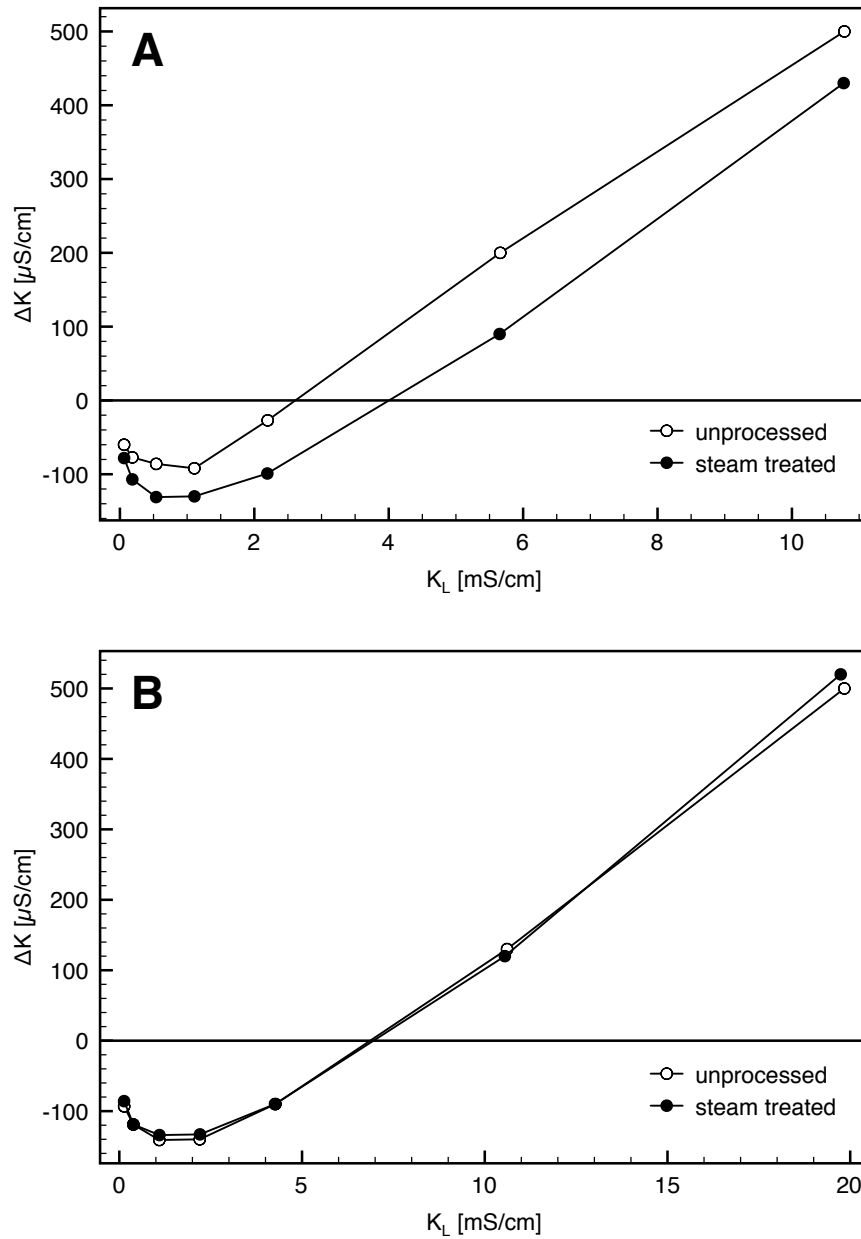


Figure 32: Differential conductivity  $\Delta K$  depending on the electric conductivity of the liquid  $K_L$  or bulk electrical conductivity respectively, A: BeW-Na, B: BeC-Ca.

In the case of the calcium smectite the titration curves of untreated and treated sample were almost identical considering the error of the conductivity measurement (figure 32B), resulting in an identical isoconductive points of both calcium samples.

The aspect ratio  $n$  was modified due to the vapor treatment, although the equivalent spherical diameter of the clay particles remained unaffected (Heuser *et al.*, 2014). The aspect ratio  $n_{Na}$  of the sodium smectite decreased after the vapor treatment from 57 to 41 contrary to the calcium smectite  $n_{Ca}$  where increased from 10 to 24. The steamed, redispersed and dried samples showed an aspect ratio in between the untreated and treated ones with  $n_{Na}=46$  and  $n_{Ca}=18$ .

Besides the before presented samples BeW-Na and BeC-Ca the aspect ratios of some further unprocessed and steam treated samples were measured, calculated, and presented in figure 33. It seems to be obvious, that no clear distinction based on smectite species or interlayer cation and valence is possible - a trend does therefore not exist, but approximately all samples show an affection by steam. The aspect ratio changes due to the treatment.

According to the error of  $n$  of the measurements of  $\pm 1$  the differences between unprocessed and steam treated samples could be safely considered.

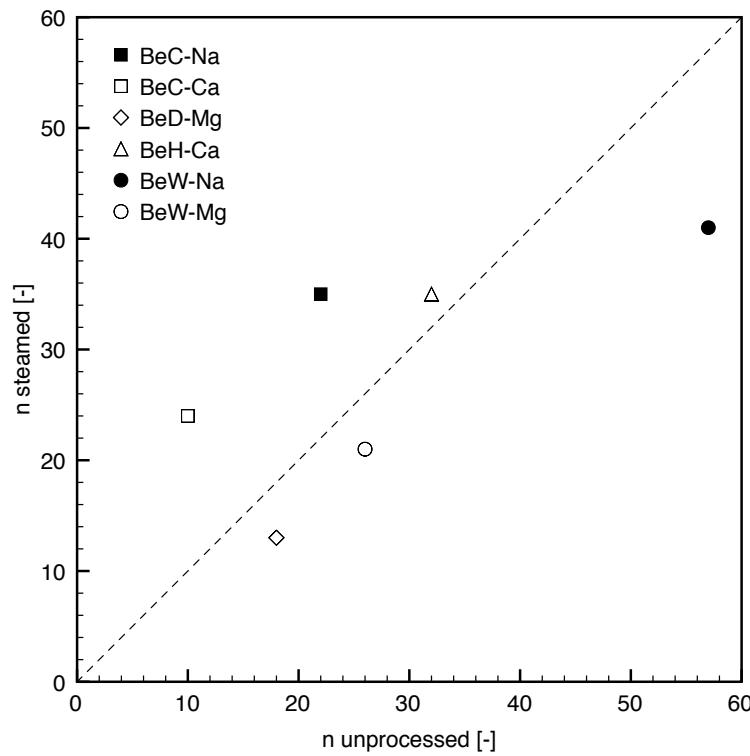


Figure 33: Particle shape  $n$  of unprocessed and vapor treated smectites

### 3.13.2 Dynamic mobility

The magnitude of the dynamic mobility  $Mag(u^*d)$  of sodium and calcium smectite samples increased with increasing electrolyte concentration (NaCl or CaCl<sub>2</sub>), reached a maximum, and decreased (figure 34A/B). The sodium-loaded samples showed clear differences between unprocessed and vapor treated. The maximum value for the unprocessed sodium-smectite was reached at 0.0094 mol/l NaCl with  $5.68 \times 10^{-8} \text{ m}^2/\text{V}\cdot\text{s}$ , whereas the vapor treated sample showed a maximum at 0.0191 mol/l NaCl with  $5.33 \times 10^{-8} \text{ m}^2/\text{V}\cdot\text{s}$ . The shift of mobility maxima in the course of the vapor treatment also appeared for the calcium-smectite. The mobility maximum of the unprocessed sample was reached at 0.0191 mol/l CaCl<sub>2</sub> with  $0.44 \times 10^{-8} \text{ m}^2/\text{V}\cdot\text{s}$ , whereas the vapor treated sample showed its maximum at 0.0517 mol/l CaCl<sub>2</sub> with  $0.33 \times 10^{-8} \text{ m}^2/\text{V}\cdot\text{s}$ . Clear differences between the untreated and treated calcium-smectite were observed.



Although the mobility curves offered no special features, the first data point of the unprocessed sodium-smectite is still somewhat confusing. It should plot above  $5.2 \times 10^{-8} \text{ m}^2/\text{V}\cdot\text{s}$  instead of  $5.5 \times 10^{-8} \text{ m}^2/\text{V}\cdot\text{s}$ . Comparing both curve pairs of untreated and treated samples the curve shape was much lower for the calcium-smectite as for the sodium-smectite.

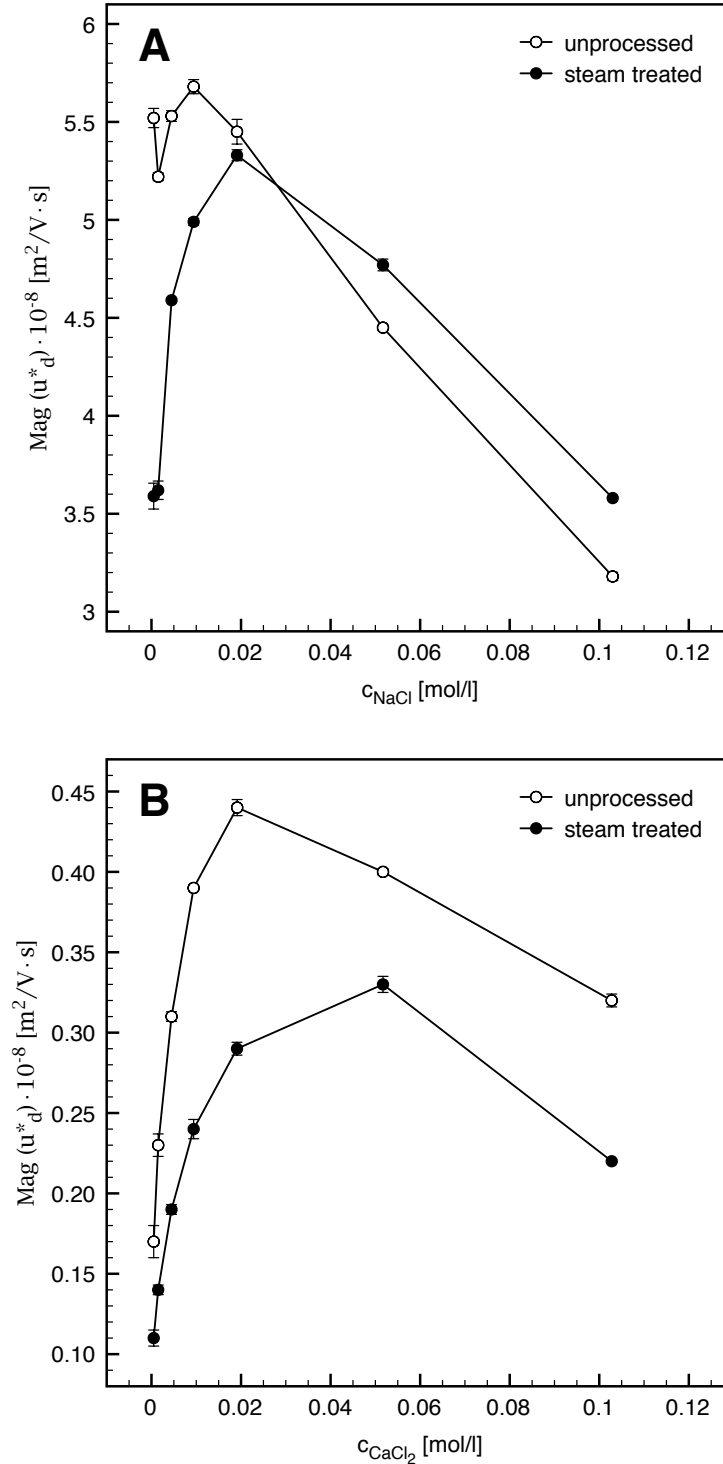


Figure 34: Magnitude of the dynamic mobility  $u^*_d$  depending on electrolyte concentration  $c$  of NaCl or CaCl<sub>2</sub> respectively, A: BeW-Na, B: BeC-Ca.

### 3.13.3 Potentiometric titrations

Potentiometric titrations were performed with the samples BeW-Na and BeC-Ca both in its unprocessed and steam treated form. Figure 35 shows the results of the calculated protons on solid (smectite) based on the addition of acid depending on the measured pH of the bulk solution. Clear differences in curve shape and the range of values between both samples are visible. Differences between unprocessed and treated samples are only obvious in terms of BeW-Na (figure 35A). Regarding BeC-Ca the curve shape of the unprocessed species is similar to that of the treated one, but with slightly decreased values of protons on solid of the steam treated sample (figure 35B).

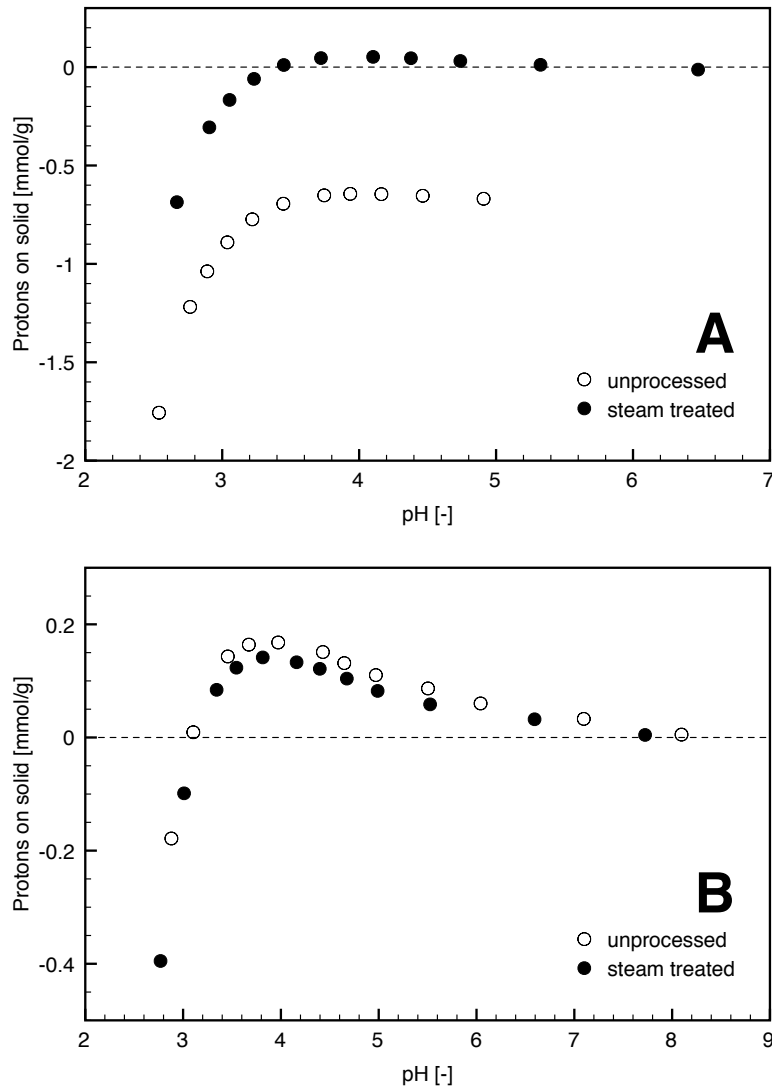


Figure 35: Potentiometric titrations of A: BeW-Na and B: BeC-Ca.

The pH of the suspensions of BeW-Na ranges between 2.4 and 6.6, with an amount of protons on solid between  $-1.8$  mmol/g and  $+0.2$  mmol/g. The suspensions of BeC-Ca shows a pH in the range of 2.6 and 8.2. Thereby, values of protons on solid between  $-0.4$  mmol/g and  $+0.2$  mmol/g were measured.

However, the protonation of the smectite surface of both samples (BeW-Na and BeC-Ca) reached a maximum at a pH of about 4.0 for the respective unprocessed and steam treated species.

### 3.14 Rheology

#### 3.14.1 Viscosity

The dynamic viscosity ( $\eta$ ) of the bentonite dispersions was comparably low for both pairs of unprocessed and vapor treated samples (figure 36A/B). However,  $\eta$  of all four samples was in the same order of magnitude and varied between  $2.3 \times 10^{-3}$  and  $2.8 \text{ Pa} \cdot \text{s}$  for the calcium smectite and between  $3.9 \times 10^{-3}$  and  $2.8 \text{ Pa} \cdot \text{s}$  for the sodium smectite. With increasing shear rates ( $\gamma$ )  $\eta$  decreased asymptotic (figure 36A/B). For the each eight single measurements of viscosity at one shear rate it was valid that the higher the shear rate the more constant and simultaneously lower the viscosity was.

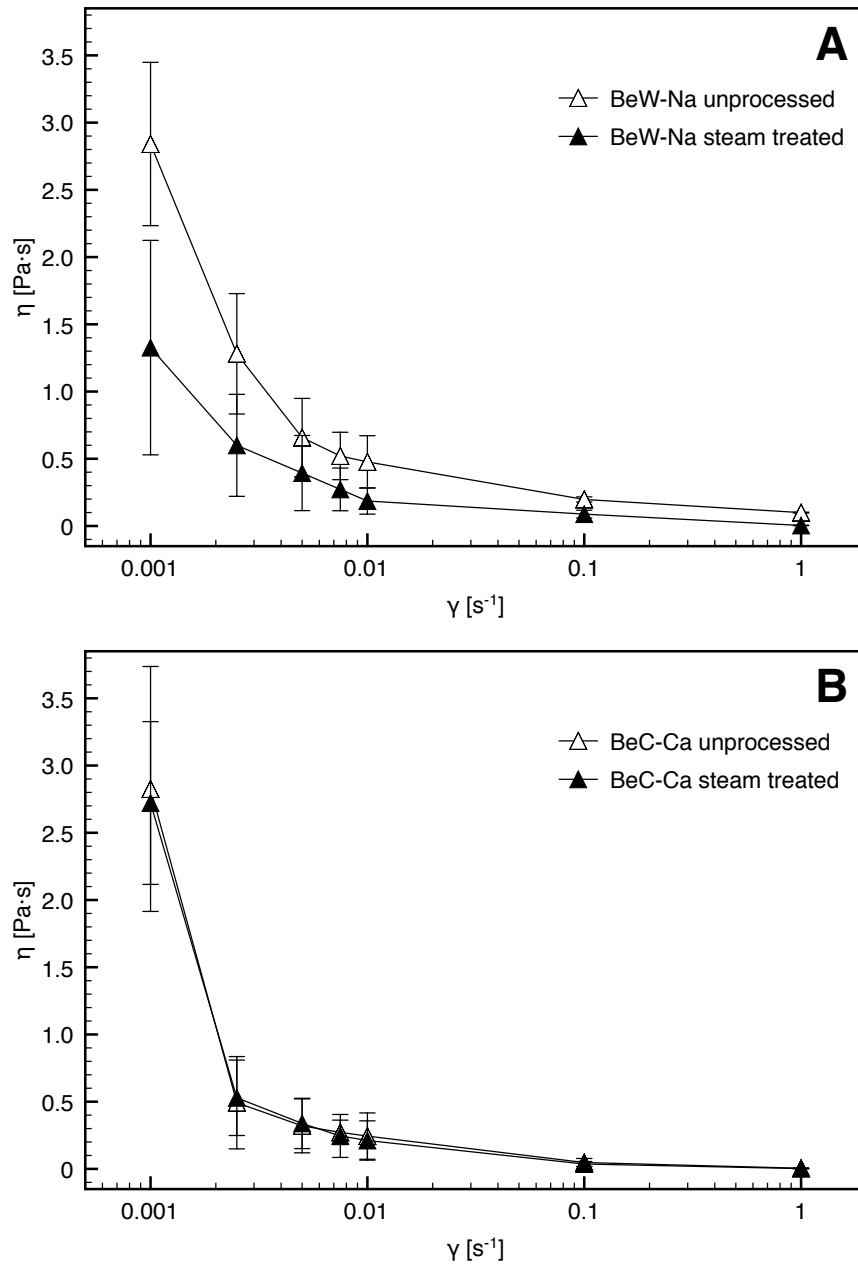


Figure 36: Dynamic viscosity of the bentonite dispersion (2 wt.%) depending on the shear rate, A: BeW-Na, B: BeC-Ca.

Although the relative error of the viscosity measurement was comparably high, especially for the three first shear rates a clear distinction between the sodium and the calcium smectites is possible. A difference between untreated and steamed sample could only be observed for the sodium smectite (figure 36A), the viscosity of the calcium one remained almost unaffected (figure 36B).

### 3.14.2 Shear stress

Another important relationship for the characterization of the rheological behavior of mineral dispersions represents the connection between shear stress  $\tau$  and shear rate  $\dot{\gamma}$ . These results could be used to define the type of flow (Luckham & Rossi, 1999).

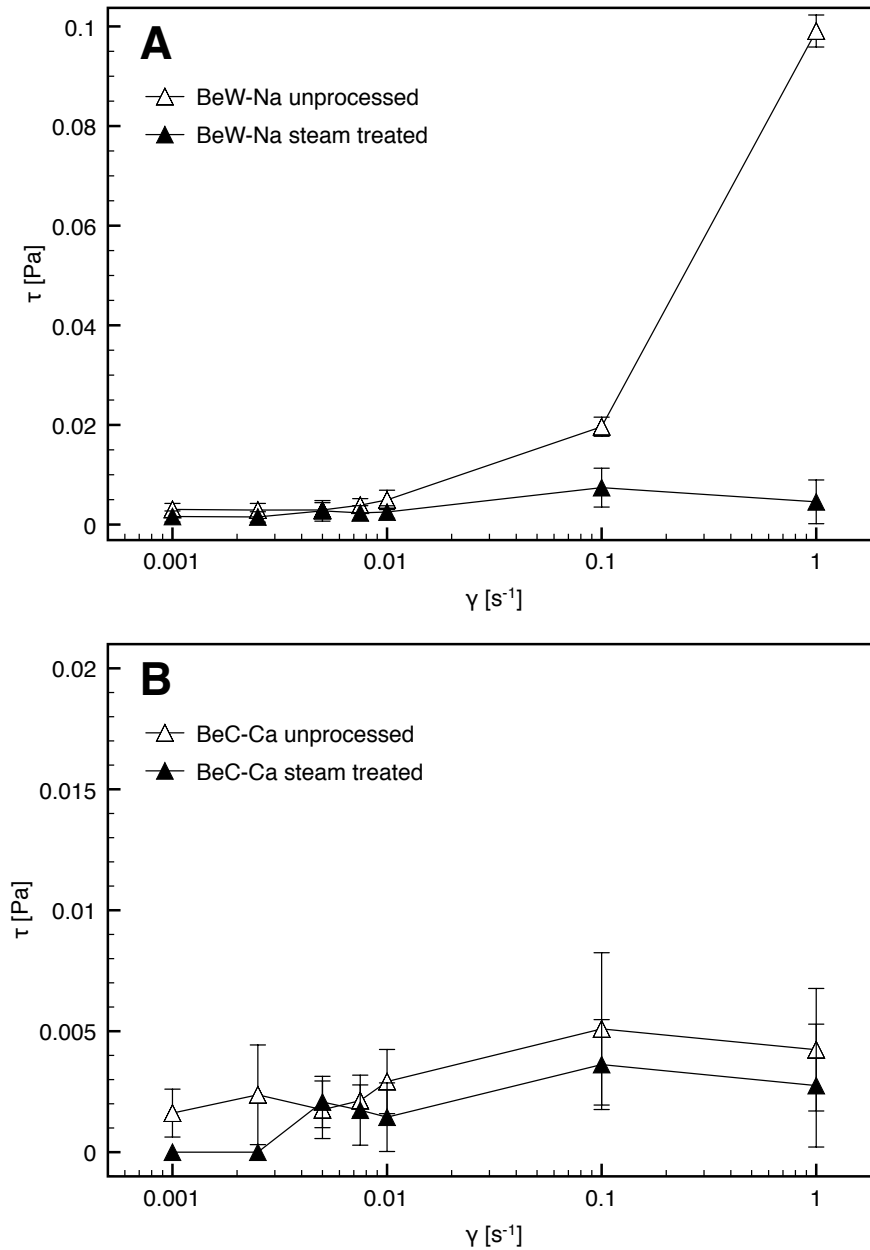


Figure 37: Shear stress of the bentonite dispersion (2 wt.%) depending on the shear rate, A: BeW-Na, B: BeC-Ca.

As mentioned above the error in the range of smaller shear rates was comparable high, which is also true in terms of shear stress (figure 37A/B). With increasing shear rates the stress increases while its error decreased. At the last shear step the stress decreased except for the unprocessed sodium smectite.

A clear distinction between untreated and vapor treated samples could only be observed for the sodium-loaded sample (figure 37A), the calcium one remained almost unaffected within the calculated error (figure 37B).

Luckham & Rossi (1999) distinguished four different types of flow: Newtonian, pseudoplastic, Bingham plastic, and dilatant. If shear stress and shear rate were direct proportional to one another, the dispersion was characterized as Newtonian fluid, resulting in a constant viscosity. The other flow types (pseudoplastic, Bingham plastic, and dilatant) showed a variation of viscosity with the shear rate. Those were described as non-Newtonian fluids.

Because shear stress and shear rate were not directly proportional to one another and the viscosity was not constant within the shear range, the four dispersions could be characterized as non-Newtonian fluids. With regard to the curve shape, the smectite dispersions showed a pseudoplastic flow behavior.

This statement is in a good agreement with the findings of Luckham & Rossi (1999), observing that very dilute clay dispersions behave as pseudoplastic fluids.

---

# Chapter 4

## Discussion

## 4 Discussion

### 4.1 Steam Treatment

The results of the experiments will be discussed in the next subsection, however, the parameters of the steam treatment are of great interest for all experiments performed after. Therefore, a critical and detailed view on the steaming process seems to be essential for the further assessment of the results of the laboratory investigations.

#### 4.1.1 Temperature

The temperature of the steam treatment was set to 200°C. The first consideration regarding the temperature of steaming referred to the field of application namely casting in foundry technology. As mentioned in the introduction section (see chapter 1.3.1, figure 7), the temperature in the mould was at the beginning of the casting always above 200°C. Temperatures much higher than 200°C, for example at the wall of the casting, lead to a irreversible destruction of the smectite structure. This burnt-out material cannot be repatriated to the sand cycle and should be replaced by fresh moulding sand. Based on the casting tests and the temperature distribution monitored with thermocouples a value of 200°C seemed to be appropriate for the steam treatment in the autoclaves.

The second aspect regarding the temperature chosen for the treatment were previously performed studies. The treatment temperature of earlier work is summarized in table 12. Based on this results a temperature of 200°C is in the medium range compared to older work, which was mostly related to nuclear waste repositories.

Table 12: Temperature of steam treatments of previous work and this study.

Couture (1985a)	25–260°C
Couture (1985b)	150 & 250°C
Oscarson & Dixon (1989)	110–260°C
Güven (1990)	260°C
Pusch (2000)	90–110°C
This study	200°C

A third point of interest represents the influence of temperature on the results of the steam treatment. A meaningful result regarding this case was worked out by Oscarson & Dixon (1989). Figure 38 shows the specific volume or sedimentation volume respectively of 5 g clay steamed at some different temperatures for 11 days in a closed system. It is clearly visible that with increasing temperature the sedimentation volume decreases compared to the unsteamed sample. This result was reduced to an affection of the swelling capacity of montmorillonite by steam at temperatures down to 110°C. An alteration of the mineralogical composition and physical aggregation were not excluded, but deliver no full explanation for the changes after steaming (Oscarson & Dixon, 1989).

The fourth and last aspect for the chosen temperature were the autoclaves and especially their inlets. Both parts of the steaming equipment could resist only 200°C. A further the temperature limiting factor was the oven in which the treatment was performed.

Based on the four aforementioned aspects a temperature of 200°C seems to be high enough to detect differences between unprocessed and steam treated samples (see figure 38). Furthermore, the transfer of results from laboratory investigations to casting problems and errors in foundry industry is also possible with the chosen temperature. At last, the steaming equipment could

resist the temperature without destroying the PTFE inlets of the autoclaves. Hence, the temperature of the treatment should not lead to concerns for the further investigation of treated samples.

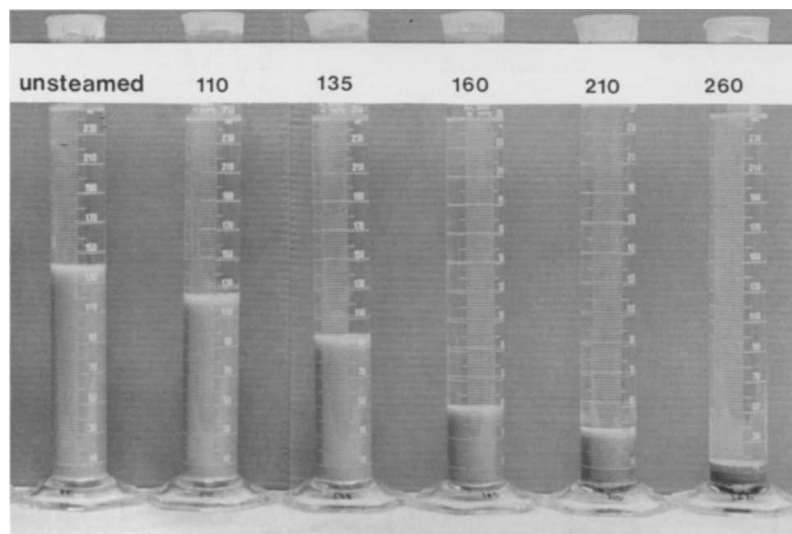


Figure 38: Specific volumes of 5 g of the clay after heating at the indicated temperatures (in °C) for 11 days at a moisture content of 0.20 g/g in a closed system. Extract from Oscarson & Dixon (1989).

#### 4.1.2 Duration

As well as the temperature of the steam treatment the duration plays an important role regarding the results of later laboratory experiments. The duration of steam treatments of older work and this one is summarized in table 13. The period of time varied significantly between the individual studies from one day to one year. Therefore, it was difficult to decide one time span for the steam treatment performed in this study.

Table 13: Duration of steam treatments of previous work and this study.

Couture (1985b)	7 days
Oscarson & Dixon (1989)	1, 11 & 21 days
Güven (1990)	1 day - 1 year
Pusch (2000)	30 days
This study	6 days

Most of the earlier studies were related mainly to the disposal of nuclear waste in underground repositories. In that case the clay barrier is exposed to steam at temperatures from sixty up to a few hundred degrees, which is fairly common under repository conditions (Güven, 1990). The influence of steam on smectite particles in foundry industry is significantly shorter compared to clay barriers for nuclear waste disposal. When the casting was finished and the condensation zone in the mould spreaded the bentonite or smectite is no longer affected by steam, but by dry heating originating from the hot casting (figure 7).

In order to get a first idea of the influence of duration of steaming cation exchange capacity (CEC, see chapter 2.12) and methylene blue sorption kinetics (MBS, see chapter 2.13) were measured at the sample Namorit S unprocessed and Namorit S treated for 5 and 10 days. The results of both measurements (CEC and MBS) did not offer great differences between the tested



samples, leading to the conclusion that the duration of steaming is less important compared to the temperature of steaming. Together with the knowledge of earlier studies a duration of the steam treatment of 6 days seemed to be sufficient to detect changes between unprocessed and treated samples. Also with regard to feasibility and efficiency at laboratory scale a time period of 6 days was set.

#### 4.1.3 Solid to liquid ratio

The solid to liquid ratio was set to 1:20 resulting in 1 g sample material and 20 g deionized water during all steam treatments. Comparing the solid to liquid ratio of this study with other work (see table 14) leads to the result that a broad spectrum of ratios exists. Although, in most of the older studies much larger ratios were used, also a value of 1:20 could be observed. The only limiting factor represents the amount of water, which should be high enough to generate a water vapor saturated atmosphere in the autoclave during the whole treatment. Caused by the used amount of water and the resulting pressure at 200°C the air in the autoclave could be assumed to be water vapor saturated.

Table 14: Solid to liquid ratio of steam treatments performed in previous work and this study.

Couture (1985a)	1:20, 5:1, and 15:1
Oscarson & Dixon (1989)	1:20, 1:5, and 1:3
Pusch (2000)	>1:20*
This study	1:20

\*The amount of water was 20 g, the amount of sample was not specified, but evidently greater than 1 g.

#### 4.1.4 Cooling down

Upon ending of the treatment the autoclaves were removed from the oven and cooled down to room temperature. After half a day they were opened and the inner PMMA inlets (figure 9, 1) including the samples put in a desiccator. During the cooling process the water vapor in the autoclave condenses to liquid water and accumulates in the outer inlets (figure 9, 2). While condensing it cannot be excluded that a drop of liquid water falls into the inner inlet and could wet the clay sample to an unknown extent. However, after the autoclaves were opened an uncontrolled wetting of the treated samples could not be observed in the course of all performed treatments. Therefore, the cooling process should not have influenced the previously treated samples in any negative way.

#### 4.1.5 Drying

After steaming and cooling down, the samples were dried at 200°C for 1-2 hours. The temperature was chosen according to the procedure during the casting (see chapter 1.3.1). At 200°C and below loss of adsorbed water or dehydration respectively occurs, dehydroxylation is expected only for temperatures above 450-500°C (Guggenheim & van Groos, 2001). Furthermore, no structural changes and hence, no changes in cation exchange capacity should appear below 220°C (Emmerich *et al.*, 1999). Based on the aforementioned results a drying temperature of 200°C should not have any (negative) effects on the steam treated samples.

## 4.2 Discussion of measured parameters

Several laboratory tests have been performed in order to show and quantify the influence of hot water vapor on smectite. Some of the experiments showed no systematic trend between vapor treated and unprocessed samples. In contrast, water adsorption, cation exchange capacity, sedimentation volume, methylene blue sorption, nitrogen-sorption, and conductometric as well as potentiometric titrations respond to the treatment.

The effects of steaming were generally not or only little influenced by the bentonite or clay species, whereas the interlayer cation of smectite exerted an obvious factor in the case of hot water vapor. Moreover, a distinction between monovalent and divalent cations seems to be clearly visible in most of the tests.

As suggested and previously shown by Bish *et al.* (1997) and Madsen (1998), the XRD measurements revealed no differences between unprocessed and treated samples. The peak positions of different mineral phases remained unaffected due to the vapor treatment; minor changes in peak intensity can easily be explained by slight changes in particle orientation, packing density and instrumental conditions affecting absolute intensities. The mineralogical composition of samples (XRD) and also the chemical environment of the investigated species (XPS) did not change due to the steam treatment.

Based on  $^{27}\text{Al}$ -NMR results, Bish *et al.* (1997) speculated about an attack of the octahedral sheet, resulting in a reduced proportion of octahedral Al after a steam treatment. Regarding the disposition of octahedral Al, the author assumed it to relocate at the surface of the smectite particles. A relocation of the octahedral species seems unlikely in view of the XPS results. Such an attack-relocation mechanism would be well detectable by XPS because the chemical environment of the element differs from the initial one and will shift the band energies. The latter was not observed here.

However, it is interesting to note that most of the peaks of the unprocessed sample show a smaller FWHM than peaks of treated sample (table 8). Ebina *et al.* (1997) interpreted FWHM's in terms of crystallinity. They reported a decreasing FWHM with increasing crystallinity. Also Mosser *et al.* (1992) predicted a dependence of the FWHM of the  $O_{1s}$  and  $Al_{2p}$  peaks on the crystallinity of a given sample. Translating these findings to the present situation would imply that the treated sample has a lower crystallinity than the unprocessed one.

Based on the result that chemistry and crystal structure of samples remained unchanged, only surface characteristics of the particle could explain the observed differences. Phase transitions or structural transformations of the present minerals are therefore unlikely.

Oscarson & Dixon (1989) reported that the decreased sedimentation volume depended on temperature and minor on moisture and related this effect to a decreased swelling capacity after steaming. The modification of SV and swelling capacity appeared already at temperatures of 110°C and increased with increasing temperature.

However, the SV in this study was only measured after a 200°C vapor treatment, but resulted in a decrease of SV, too. As known, changes in SV are related to different electrokinetic charge properties at the particle surface.

In contrast to the findings of Oscarson & Dixon (1989) but according to the results of Madsen (1998), the cation exchange capacities of K- and Na-smectites decreased up to 30% after the steam treatment, whereas the Mg- and Ca-smectites were within a 10% error range (according to the findings of Dohrmann *et al.* (2012)) identical.

Theoretically, an isochemical growth of smectite particles should change the proportion of exchange sites stemming from the permanent layer charge relative to the variable charge sites on the  $hk0$  faces. Hence, samples, which show no particle growth, should also show no changes in CEC. But no systematic trend between change of CEC and change of ESD was found (see figure 43A). Also the direct comparison between ESD and CEC leads to no correlation (see figure 43F).

The concentrations of the clay-water-dispersion for the methylene blue (MB) spectra were identical for unprocessed and treated samples. Assuming that density and diameter of clay particles remained unchanged due to the treatment, the absolute clay surface available for methylene blue sorption is approximately equal for both unprocessed and treated samples.

For this reason, the sorption kinetics of unprocessed and treated samples should be similar (figure 25), which is true in terms of band positions, but not with regard to absorption intensities. The kind of interlayer cation could be derived from the number of peaks and their positions and agreed with the results of Czimerová *et al.* (2004).

The four observed band positions are related to the four different forms of MB in clay dispersion: larger or higher agglomerates:  $(MB^+)_n$  -  $577 \pm 4$  nm, dimers:  $(MB^+)_2$  -  $614 \pm 9$  nm, monomers:  $MB^+$  -  $675 \pm 6$  nm, and the protonated form:  $MBH^{2+}$  or J-aggregates -  $768 \pm 4$  nm (Bujdák *et al.*, 2001). Changes in absorption intensity could be probably reduced to variations of layer charge for bands near  $675 \pm 6$  and  $768 \pm 4$  nm and charge density for the band near  $577 \pm 4$  nm (Bujdák *et al.* (1998); Bujdák *et al.* (2001)).

Figure 39 below demonstrates the orientation of methylene blue on smectite surfaces (Bujdák *et al.*, 2002). It seems to be obvious, that an increase of H- (agglomerates) and/or J-aggregates, expressed by a change of the bands (MBS-kinetic) near 576 nm and 770 nm, respectively, lead to an increase of the disordering at the smectite surface or probably in between its interlayer space. This observation could be made for approximately all examined samples of MBS-kinetics.

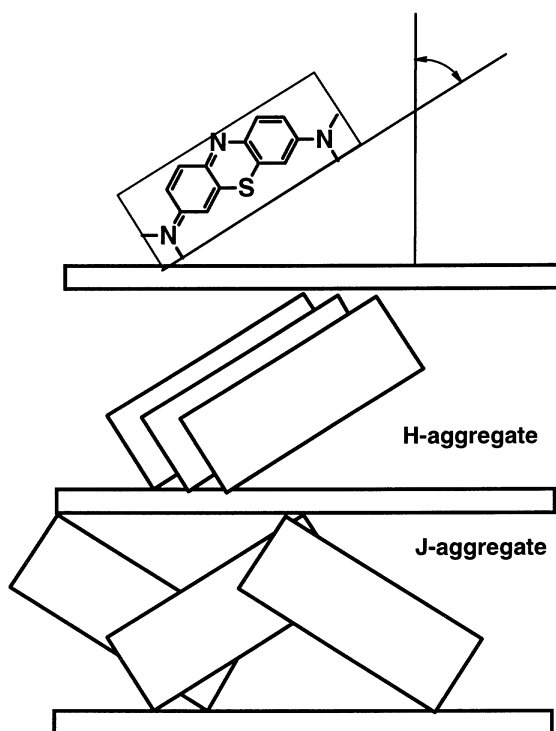


Figure 39: Orientation of methylene blue complex and arrangement of agglomerates / H- and J- aggregates / protonated form. The angle depends on the type of surface. Extract from Bujdák *et al.* (2002).

As previously indicated by CEC measurements and confirmed by MB-spectra, the charge conditions of samples with a divalent interlayer cation remained unaffected, whereas samples with a monovalent showed a decrease of CEC and also a change of MB-spectra. These qualitative differences between mono- and divalent loaded smectites are indicated by results of time depended VIS spectra of methylene blue clay interaction.

The equivalent sphere diameter ( $d_{ESD}$ ) was expected to increase after the steam treatment. Dissolution and recrystallisation processes in terms of Ostwald ripening (Eberl *et al.*, 1990) could occur due to enhanced temperature and pressure conditions in the autoclaves. Pusch & Kasbohm (2002) found that the hydrothermal alteration of bentonite as buffer material in nuclear waste repositories led to a particle growth of clay particles.

A further process that also leads to a change in particle size is aggregation. Oscarson & Dixon (1989) reported physical particle aggregation in terms of partially saturated and heated clays, which might be one contributing factor to the decrease in swelling capacity.

In contrast to the findings of Pusch & Kasbohm (2002) and Oscarson & Dixon (1989), a systematic increase of the ESD upon the hot vapor treatment has not been found. This might have been caused by too short times of treatment and too low temperatures. The effects of particle growth and particle aggregation could therefore not be confirmed under the experimental conditions in this study.

From the measurement of water adsorption two different results are available – an absolute value after 24 hours and rates for the water adsorption (figure 23). For the transfer of laboratory results into application in foundry technology and casting, almost only rates of water adsorption are important. Absolute values after 24 hours are only of lower interest with regard to moulding sand preparation and regeneration, because the time necessary for one casting cycle in serial production in a foundry is usually much smaller than 24 hours (Grefhorst *et al.*, 2005).

The absolute water adsorption or water uptake capacity as well as the rate of water adsorption showed no clear difference between unprocessed and treated samples. The water adsorption process depends after Montes-H. & Geraud (2004) strongly on relative humidity, interlayer cation, and amount of sample. Mechanical compaction of the sample plays a minor role and the drying temperature is not of interest regarding water adsorption. Relative humidity, amount of sample, drying temperature, and mechanical compaction were equal for both unprocessed and treated samples.

However, the influence of different interlayer cations on water adsorption was of great interest. As expected from Montes-H. *et al.* (2003), Montes-H. & Geraud (2004), and Kaufhold *et al.* (2010), the sodium-loaded samples showed very high water uptake capacities compared to those with a divalent interlayer cation. Samples saturated with  $Mg^{2+}$  and  $Ca^{2+}$  showed approximately equal amounts and rates, which agrees with results of Montes-H. & Geraud (2004). As shown by Dontsova *et al.* (2004), the smaller and even more hydrated cations ( $Na^+$  and  $Mg^{2+}$ ) lead to a higher water sorption of the smectite than those one with larger cations ( $K^+$  and  $Ca^{2+}$ ). The amount of adsorbed water as well as rates of adsorption were influenced by the interlayer cation with the order of:  $Na^+ > K^+ > Mg^{2+} > Ca^{2+}$  (figure 23).

The order of adsorption depending on interlayer cation largely varies from study to study (i.e. Montes-H. & Geraud (2004); Dontsova *et al.* (2004)). A comparison of values from this work with those of other studies is therefore only difficult to implement. The correlation between CEC and water adsorption as shown by Kaufhold *et al.* (2010) could not be observed (see figure 43B). After 30-60 min, however, the rates of water adsorption were equal and converged to zero (figure 23) independent of sample, interlayer cation, and unprocessed or steam treated.

This means that most of the adsorbed water had been taken up in the first minutes of the experiment, which leads to the conclusion that the water adsorption has no, or at least only little influence on the moulding sand regeneration process and the moulding sand quality, respectively. However, a finished adsorption did not mean, that the adsorbed water could not be redistributed within the smectite, between surface and structure.

In contrast to aluminium, increased silicon concentrations in samples after the vapor treatment were measured. Pusch (2000) observed similar results due to a hydrothermal treatment on MX-80 bentonite. During cooling down the samples subsequent to a hydrothermal treatment, silica from the surface of clay particles precipitated. This process caused superficial dissolution of smectite and accessory silicates and led to cementation and particle aggregation, respectively (Pusch, 2000). This observation made by Pusch (2000) might be one explanation for increased silicon concentrations.

However, in comparison to the *Si*-concentrations measured in the blank experiments (1 g sample immersed in 20 ml water for five days), the concentrations of *Si* after the steam treatment were rather low (see table 7). This can be explained by noting that the transport of ionic species is more effective in a liquid medium than in a gaseous phase.

In order to check if the measured *Si*-concentrations in the blank experiments can be ascribed to the dissolution of smectite, the blank experiment of BeH-Ca was modeled with *PhreeqC* (Parkhurst & Appelo, 1994) at pH 7. The calculated *Si*-concentration is lower than the measured one by a factor of six. Changing the pH to five does not affect this factor. These results suggest that the measured aqueous silicon concentrations cannot solely be ascribed to the dissolution of smectite.

Similar conclusions have been reached by Baeyens & Bradbury (1997) who concluded that aqueous *Si*-concentrations were controlled by the dissolution of quartz at circumneutral pH. Another potential source of *Si* are volcanic glasses stemming from the alteration of the bentonites (Hauser & Reynolds (1939); Delano *et al.* (1994); Klinkenberg *et al.* (2009)). As volcanic glasses are amorphous, the recalculation of low amounts based on XRD analyses may not be possible. The idea that measured aqueous *Si*-concentrations are not due to the dissolution of smectite are well in line with the observation that no structural changes take place due to the steam treatment.

The measurement of electrokinetics, rheological phenomena, and surface properties delivers entirely useful results regarding the interaction of smectite with hot water vapor. Based on the experience of Heuser *et al.* (2014) the interlayer cation of the smectite was of great interest. As expected the sodium smectite shows a stronger reaction due to the exposure to hot water vapor compared with the calcium smectite.

The aspect ratio provides an exact description of particle geometry, which is of great interest regarding rheological measurements. Requiring that particle geometry and rheology are directly linked together (Yuan & Murray (1997); Pabst (2004); Pabst *et al.* (2006)) a connection between viscosity and particle shape should exist.

Considering a constant particle shape during viscosity measurements the shear rate has a large influence on the relationship between aspect ratio and viscosity (figure 40). With increasing shear rates the viscosity is more and more independent of the aspect ratio and decreases to comparable very low values near zero. For the smallest shear rate the viscosity is high with huge variations depending on the aspect ratio.

For other shear rates the relationship between viscosity and aspect ratio (see figure 40) shows a more equally curve shape, mostly with an increase of viscosity with increasing aspect ratio. Although a relation between viscosity and aspect ratio is visible, a statement about the influence of hot water vapor on the relationship between viscosity and aspect ratio at different shear rates is not possible.

Another topic of interest was the influence of water vapor on the cation exchange capacity (CEC). For the monovalent samples the CEC showed changes of about 30 %, whereas the CEC of divalent smectites remained almost unaffected by steam. Hence, the ESD represents no suitable parameter to compare small changes of particle size the aspect ratio calculated in this work could be used to decide if changes of CEC only depend on particle geometry (Cadene *et al.*, 2005).

Previously, the equivalent spherical diameter ( $d_{ESD}$ ) was converted according to equation (13) into a disc diameter  $d_{disc}$  considering the aspect ratio (Weber *et al.*, 2013) and summarized with other parameters (table 15).

$$d_{disc} = \left( \frac{n}{1.5} \right)^{1/3} \cdot d_{ESD} \quad (13)$$

Regarding the sodium smectite a consistent trend between change of aspect ratio, change of disc diameter, change of CEC, and change of SSA can be observed. In contrast, the calcium-loaded sample shows a decrease of CEC and SSA, but a great increase of the aspect ratio and disc diameter. In terms of BeW-Na the change of CEC after steaming can be explained by a decrease of the aspect ratio.

Regarding BeC-Ca the small decrease of CEC cannot be reduced to the change of particle geometry, on contrary, based on the aspect ratio a great increase of CEC is expected. Hence, a further consideration should be involved.

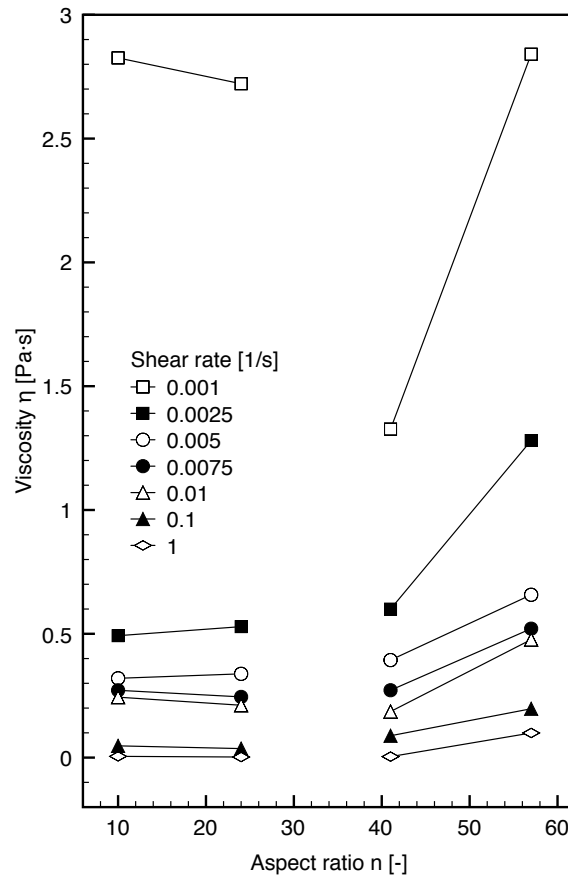


Figure 40: Viscosity in relation to the particle shape  $n$  for various shear rates;  $n=10$  – BeC-Ca unprocessed,  $n=24$  – BeC-Ca treated,  $n=41$  – BeW-Na treated, and  $n=57$  – BeW-Na unprocessed.

Table 15: Comparison of aspect ratio ( $n$ ), equivalent sphere diameter ( $d_{ESD}$ ), disc diameter ( $d_{disc}$ ), CEC, and SSA.

Sample		$n$ [-]	$d_{ESD}$ [nm]	$d_{disc}$ [nm]	CEC [mmol/g]	SSA [m <sup>2</sup> /g]
BeW-Na	unprocessed	57	120	403	1.098	53.2
	steamed	41	107	322	0.888	40.7
BeC-Ca	unprocessed	10	205	386	1.044	98.7
	steamed	24	215	542	0.953	88.3

Already in Heuser *et al.* (2014) it is assumed based on ESD measurements that no particle growth or dissolution respectively appeared. Nadeau (1985) presented three different types of growth of clay particles: unequal crystallization by a preferential growth on 110 and  $1\bar{1}0$  faces, a two-dimensional crystallization on the particle edges, and growing primarily on 001 surface.

Regarding the last process, the primarily growing on 001 surface, the ESD would show no changes comparing unprocessed with treated samples, contrary to the particle shape showing great variations. A similar, however, opposite process could be suggested for dissolution of clay particles. Although in Heuser *et al.* (2014) Ostwald ripening was excluded to change particle sizes, it could again be a driving force even in one direction. With regard to  $d_{disc}$  of Na-/Ca-smectites a stronger de-/increase of the particle size was observed after the steam treatment. This process could also be related to Ostwald ripening, but needs no preferential growth in one direction. In general, a change of particle dimensions due to steaming could be noticed.

The dynamic mobility  $u_d^*$  is the high frequency equivalent of the electrophoretic mobility  $u$  in a direct current (d.c.) electric field. The electrophoretic mobility is proportional to the zeta-potential  $\zeta$  and independent of particle geometry (size and shape) (Penner & Lagaly, 2001). Due to the frequency of electrokinetic measurements (3 MHz) only the dynamic mobility or its magnitude respectively can be derived. O'Brien *et al.* (1985) and O'Brien *et al.* (2003) showed that for variable solid contents particle size and zeta potential could be derived from mobility measurements. Simultaneously the dynamic mobility depends strongly on the zeta potential (Arroyo *et al.*, 2004). A qualitative interpretation of the measured mobilities is still possible regarding the surface modification by water vapor.

Rasmusson *et al.* (1997) calculated the surface conduction parameter  $\lambda$  (defined by Rowlands & O'Brien (1995)) and the zeta potential  $\zeta$  of Na-bentonite dispersions resulting in a linear relationship between both parameters. The zeta potential is therefore not the only parameter influencing the mobility but also the surface conductivity of a particle plays an important role. Van der Linde & Bijsterbosch (1990) measured electrokinetic potentials of sulfated polystyrene particles, obtained from streaming potentials in plugs, depending on the salt concentration. As part of their investigations the calculations were performed with and without inclusion of surface conduction (figure 41).

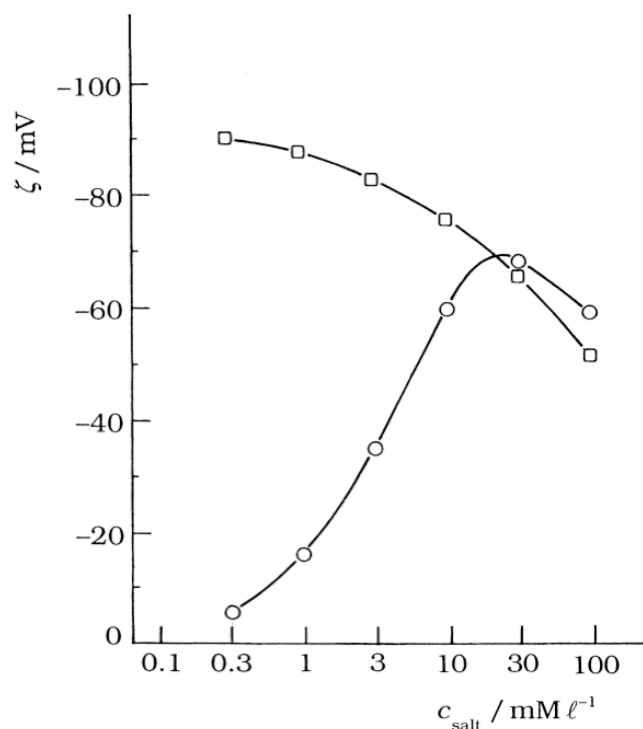


Figure 41: Electrokinetic potentials of sulfated polystyrene particles, obtained from streaming potentials in plugs: (circle) without and (square) with inclusion of surface conduction. (Extract from Lyklema and Minor, 1998 a redraw from van der Linde and Bijsterbosch, 1990).

Including surface conduction the zeta potential decreased continuously but non-linear with increasing salt concentration. Without surface conduction the potential reached a maximum with increasing salt concentration and decreased subsequent.

Although the above mentioned results were obtained at thermoplastics it seemed to be possible to transfer these observations to mobility measurements in this study. Regarding the calcium smectite comparable lower differences between unprocessed and steam treated sample exist. In terms of the sodium smectite a very similar curve shape compared to that displayed in figure 41 is visible. From this point of view the differences of mobility between unprocessed and treated sodium smectite are related to changes of surface conduction. Hence, the treated sample shows almost no surface conduction, in contrast the unprocessed one does. This suggestion might also be true in terms of the calcium smectite, but to a lesser extent.

The curve shape of the conductometric titrations is approximately identical comparing unprocessed and treated samples of calcium smectite. Regarding the sodium smectite the situation is somewhat different. The curve of the treated sample shows a horizontal shift compared to the unprocessed one resulting in a higher isoconductive point. The relationship between surface conductivity and electrolyte concentration was also reported by Lyklema (2001). Comparing the results of conductometric titrations with those of mobility measurements both indicate that due to the steam treatment the surface conductivity of the sodium smectite decreases rapidly.

Besides the relationship between aspect ratio and viscosity the rheological behavior of clay dispersions depends strongly on the internal structure of the clay-water-system. Dispersions with low and slightly increased solid concentrations (2-5 wt.%) show three different types of particle interaction: face-to-face, edge-to-edge, and face-to-edge, depending on ionic strength and pH (Durán *et al.* (2000); Penner & Lagaly (2001)). In the acid pH range face-to-edge attraction is the predominant interaction, whereas at basic pH the attraction between surfaces decreases resulting in a more relaxed internal structure (Durán *et al.*, 2000).

The pH of the dispersions prepared for rheological measurements (2 wt.%) was 5.75 and 6.73 for the unprocessed and vapor treated sodium smectite and 7.41 and 7.24 for the unprocessed and vapor treated calcium smectite (BeC-Ca). The change of pH due to the steam treatment of 0.17 pH units can be neglected regarding the calcium-loaded sample. However, the sodium smectite (BeW-Na) shows an increase of 0.98 pH units. While the pH of the calcium sample remains in the weakly basic pH range for both unprocessed and treated the unprocessed sodium one shows an acidic pH that increases towards neutral pH after steaming.

The development of pH can also be reflected by differences of viscosity comparing unprocessed with treated samples. The dispersion of the calcium-loaded sample shows almost low differences of pH accompany by approximately identical curve shapes in the viscosity-shear rate and the shear stress-shear rate diagram. The dispersion of the unprocessed sodium smectite shows an acidic pH resulting in a face-to-edge attraction (Durán *et al.*, 2000) and further resulting in higher viscosity values compared to the dispersion of the treated sample that shows nearly neutral pH leading to a more weakly internal structure. Furthermore, a sharp decrease of shear stress from acid to basic or rather unprocessed to vapor treated pH can be observed in terms of the sodium smectite, which is in good agreement with predictions regarding face-edge attraction energy of Durán *et al.* (2000).

Similar results regarding the relationship between rheological measurements or internal structure of dispersions and pH were observed by Arroyo *et al.* (2000) analyzing sodium montmorillonite dispersions using experimental data on dielectric dispersion.

The relationship between different pH resulting from the vapor treatment and rheological behavior agrees with the pH dependent interaction of edges and faces of clay particles leading to a change from edge-to-face attraction at acidic pH to a more weakly internal structure determined by face-to-face attraction at basic pH.

The change from acid to basic pH accompanies with a sharp decrease of shear stress observed at the sodium smectite comparing unprocessed with treated sample. Although, a correlation between aspect ratio and viscosity is found, a distinction between unprocessed and vapor treated samples is not possible neither for the sodium nor for the calcium smectite. The shear rate has a great influence as well on viscosity and shear stress as on the relationship between aspect ratio



and viscosity. The higher the shear rate the lower is the influence of particle shape on viscosity. Due to increasing shear rates the attraction between edges and faces of the clay particles is broken and the card house structure collapsed (Galindo-Rosales & Rubio-Hernández, 2006). This observation is in good agreement with the development of pH that decreases with increasing particle shape and changes from basic to acidic between the treated calcium and the treated sodium smectite (figure 40 and 42). A further description of the so-called card house structure and several influences on this built up can be found at Lagaly (1989) also concluding that pH has a great influence on the type of attraction (edge/face or face/face) of smectite particles.

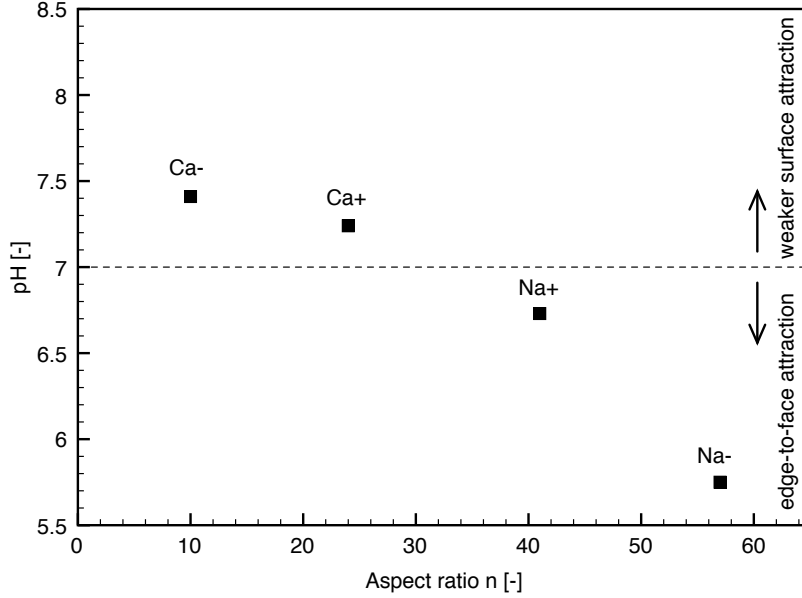


Figure 42: Particle shape  $n$  depending on pH of the sodium and calcium smectite dispersions (2 wt.%); "-" indicates an unprocessed, "+" a treated sample.

The conclusion is that the more acidic the pH the stronger the card house structure built up on edge-to-face attraction (Benna *et al.* (1999); Arroyo *et al.* (2000); Durán *et al.* (2000)), the higher the aspect ratio, and the higher the viscosity. At pH values above 7 edge-to-face coexists with face-to-face attraction leading to a more weakly internal structure (Durán *et al.* (2000); Galindo-Rosales & Rubio-Hernández (2006)). This connection between pH, particle shape, and viscosity decreases with increasing shear rates resulting in an almost constant viscosity at high shear rates for every aspect ratio (figure 40).

As mentioned before the shear rheology of clay mineral dispersions depends strongly on the aspect ratio  $n$  and the volume fraction  $\phi$ . While  $\phi$  was kept constant for all samples,  $n$  changed. Kitano *et al.* (1981) and Genovese (2012) examined and summarized the influence of several parameters on the viscosity of dispersions of non-spherical particles. Applying the equations of both works (after Barnes equation 14, Simha equation 15 and Kitano equation 17) on the data of this study it is obvious that a trend between aspect ratio and viscosity for one shear rate exists. The intrinsic viscosity could be calculated after:

$$[\eta]_{Barnes} = 0.3 \cdot n \quad (14)$$

and

$$[\eta]_{Simha} = \frac{16}{15} \cdot \frac{n}{\tan^{-1}n} \quad (15)$$

where  $[\eta]_{Barnes}$  and  $[\eta]_{Simha}$  is the intrinsic viscosity after Barnes and Simha, respectively (Genovese, 2012) and  $n$  is the aspect ratio. In order to compare calculated values of intrinsic

viscosity after *Barnes* and *Simha* with calculated values of relative viscosity (*Kitano et al.*, 1981) and measured values of relative viscosity in this work, the intrinsic viscosity has to be converted in the relative viscosity applying the following equation:

$$\eta_r = 1 + [\eta] \cdot \phi \quad (16)$$

where  $\phi$  represents the volume fraction of particles in dispersion. Furthermore, the relative viscosity after *Kitano et al.* (1981) could be calculated after:

$$\eta_{r,Kitano} = \left(1 - \frac{\phi}{0.54 - 0.0125 \cdot n}\right)^2. \quad (17)$$

The relative viscosity calculated after the three presented equations 14, 15, and 17 plot in the same range of measured viscosities in this work for shear rates between 0.001 and 0.005 1/s (see table 16). This means, that the aspect ratio contributes to measured viscosities in this work, nonetheless, it provides not a full explanation and therefore, other parameters exert also an influence on the viscosity of the studied clay mineral dispersions.

Table 16: Comparison of calculated and measured relative viscosity of unprocessed and treated smectites.

Sample		aspect ratio n [-]	relative viscosity			
			$\eta_{r,Barnes}$ [Pa·s]	$\eta_{r,Simha}$ [Pa·s]	$\eta_{r,Kitano}$ [Pa·s]	$\eta_{r,this\ work}$ [Pa·s]
BeW-Na	unprocessed	57	1.13	1.30	1.09	0.66-2.84
	steamed	41	1.09	1.22	0.52	0.40-1.33
BeC-Ca	unprocessed	10	1.02	1.06	0.96	0.32-2.83
	steamed	24	1.06	1.13	0.94	0.34-2.72

The dynamic mobility of clay mineral particles is influenced by many factors: particle shape, different charges at edges and faces, salt concentration, and surface conductance (*Penner & Lagaly*, 2001). Although the so-called card house structure built up on different charges at edges and faces of clay particles leads to significant changes of viscosity, the mobility cannot directly connected to rheological behavior depending also on different forms of particle attraction (*Penner & Lagaly*, 2001).

In terms of the calcium smectite the particle shape increased due to steaming from 10 to 24 accompanied by low differences of mobility. In contrast, the sodium loaded sample shows a decrease of particle shape from 57 to 41 leading to great changes of mobility comparing unprocessed and treated smectites. This observation indicates that the aspect ratio or its change represents not the major factor influencing the mobility. The conclusion is that not only the aspect ratio but also the modification of surface conduction due to steaming leads to differences between the dynamic mobility of unprocessed and steam treated samples (figure 41; *Van der Linde & Bijsterbosch* (1990)). Although the dynamic mobility is related to the zeta potential, a direct connection to the surface charge density cannot be formulated (*Lyklema*, 1995). It is therefore not possible to derive a maximum (minimum) of surface charge density from a maximum (minimum) of mobility for any electrolyte concentration (*Penner & Lagaly*, 2001).

From the measurement of nitrogen sorption specific surface areas (SSA) and surface fractal dimensions were derived. The SSA of this work plots in a similar range compared to the results of *Dogan et al.* (2006) and *Kaufhold et al.* (2010). Since only external surface areas could be determined with nitrogen sorption, SSA values between 20 and 150 m<sup>2</sup>/g are common for smectites. The ad- and desorption isotherms of the Na- and Ca-smectite show a very similar curve shape compared to the samples of *Kaufhold et al.* (2010)(figure 4b). The arrangement

of clay particles differs from an edge-to-face or card house structure regarding the calcium smectite to a dense laminar structure of the sodium smectite. An explanation for the larger SSA of Ca-smectites compared to Na-smectites can be given by the larger space between the charges in terms of the presence of divalent cations. This process leads to an increase of the nitrogen-accessible interlayer area (Kaufhold *et al.*, 2010).

The differences between unprocessed and steam treated samples might be reduced to aggregation of clay particles after steaming leading to partially N<sub>2</sub>-non-accessible interparticle space. Another potential explanation for the decrease of SSA of both samples could be the arrangement of clay particles. The development from disturbed to a more laminar structure after the steam treatment would also decrease the SSA because less particle surface would again be accessible for nitrogen.

The fractal analysis of examined smectites shows approximately equal values as well in terms of the fractal dimension  $D$  as regarding the fractals  $r$ . Comparing the results of this study with others comes to the conclusion that values of  $D=2.17$  and  $1.4 < r < 12.2$  are common for smectites (table 17).

However, the fractal dimension plots at the lower limit of found  $D$ -values, whereas a value of  $D=2$  accompanies with an Euclidean surface of perfect smoothness and planarity (Damme & Fripiat, 1985). Contrary, an upper limit of  $D$  up to 3 accompanies with a space filling and microporous surface of high irregularity, like silica gel or porous alumina (Damme & Fripiat, 1985).

Nonetheless, after Avnir *et al.* (1983) a smooth surface need not to be flat, but may be spherical or sievelike, provided that the radii of curvature ( $r$ ) are much greater than the size of the adsorbate molecule.

Table 17: Values of  $D$  and  $r$  from this work compared with others.

Sample	D [-]	r [nm]	Reference
pillard smectite	1.90-2.00	-	Damme & Fripiat (1985)
Ca-montmorillonite	2.80	-	Malekani <i>et al.</i> (1996)
Ca-/Mn-/Cu-mont.	2.87-2.97	$0.35 < r < 10.4$	Lee <i>et al.</i> (1999)
Ca-montmorillonite	2.74	-	Wang <i>et al.</i> (2004)
acid activated bentonite	1.94-2.11	-	Rožić <i>et al.</i> (2008)
Na-/Ca-smectite	2.17	$1.4 < r < 12.2$	This work

A further possible process behind the steam treatment and responsible for the observed surface charge modification should be discussed. The surface of the four studied samples shows a very similar non-planar and smooth fractal character.

The general assumption is that in the space between surface fractals amorphous silica is located (Jones & Uehara, 1973), which was removed by dissolution due to the steam treatment (Pusch, 2000). This assumption was confirmed by the measured silicon concentrations in the supernatant water after steaming (Heuser *et al.*, 2014).

Furthermore, XRD and XPS would remain unaffected by such a process because small amounts of amorphous material would be not detectable by XRD and the dissolved silicon is present in an equal form as studied by XPS and therefore indistinguishable.

It is conceivable that the surface charge properties (e.g. CEC) could also be affected by dissolution of amorphous silica. This process would lead to a change or shift respectively of the diffuse double layer closer to the smectite surface contributing to modifications in electrokinetics and probably to dynamic mobilities and surface conduction.

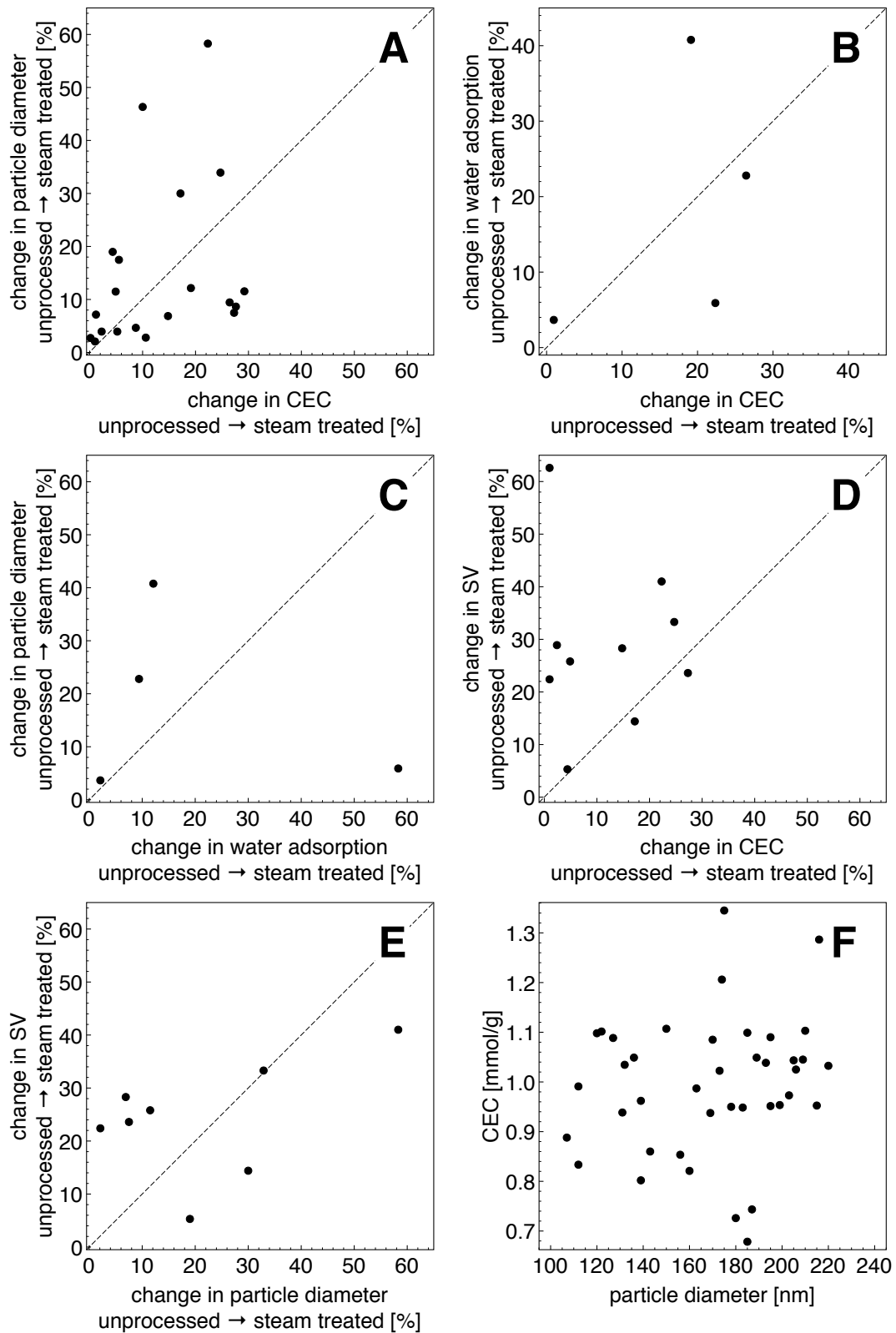


Figure 43: Scatter plots of measured parameters. A: change in particle diameter vs. change in CEC; B: change in water adsorption vs. change in CEC; C: change in particle diameter vs. change in water adsorption; D: change in sedimentation volume vs. change in CEC; E: change in sedimentation volume vs. change in particle diameter; F: CEC vs. particle diameter.

However, the author only speculate about such a dissolution process, which was not verified by performed experiments. An explanation for differences between monovalent and divalent smectites is at the moment not available.

Finally, some parameters were plotted against one another and presented in the following scatter plots (figure 43A-F). Figure 43A-E shows percentage changes of parameters, figure 43F a comparison of absolute values. The six presented plots demonstrate, that no correlation between the measured parameters exist, neither regarding relative changes, nor in the course of absolute values.

### 4.3 Impact on foundry technology

This study was performed in the course of an industrial application especially in foundry technology, but also regarding other divisions, like nuclear waste sealing. Hence, finally the question occurs which conclusions could be drawn from the results of this study or, respectively, how could they be transferred to industrial applications.

The water vapor or steam treatment affects the swelling volume, the permeability, and the surface structure and its charge conditions to a variable extent, depending on the examined parameter. Parameter and/or properties, that could be affected by steam, have to be searched in the field of electrokinetics and surface structure.

The observed parameters and properties, which show a reaction after the steam treatment, could to a large extent only be modified under laboratory conditions. In the area of an industrial environment the aforementioned aspects (see chapter 4.2) could not directly be influenced, because the variation of an industrial process, like a moulding, seems to be too high to transfer the results of the performed experiments to a concrete change of a procedure.

In general, it could be summarized, that the observed effects were most pronounced in the course of smectites with a monovalent interlayer cation. These smectites, primary sodium-montmorillonites or sodium bentonites respectively, represent the most common ones used in foundry technology. The homoionic occupation with sodium contributes to a significant improvement of foundry-relevant properties, but also lead to an increase of the noticeable affection by water vapor.

The circulation of moulding sands between a mould and the regenerating process, including the resting time in the sand-bunker takes some hours up to one day and could therefore not necessarily be long enough to ensure that distribution processes as indicated by MBS-kinetics are finished. Hence, a first step to reduce the affection of smectites by water vapor maybe a longer resting time in the sand-bunker.

Another potential is hidden behind the mixing process of used and fresh sand, bentonite, additives, and water. The amount of water is compared to the amount of the other parts low. Therefore, it should be considered how the water could be added to the other parts of the moulding sand, in order to reach an optimal mixed sand. It is conceivable, to add the water as a fine mist at room temperature or as water vapor at an enhanced temperature. In the course of an addition as water vapor the effects examined in this study will most probably occur, entailing an aforementioned increase of resting time of the moulding sand, in order to finish possible distribution processes.

The next step of the transmission of the results to an industrial process encloses the interaction of scientists from the fields of mineralogy and foundry technology. Thereby, an optimization of resting time and mixing process should be the first priority.

---

# Chapter 5

## Outlook

## 5 Outlook

From the variety of comparative experiments performed only few reveal differences between steam treated and raw samples. On the basis of XRD and XPS results, it can be concluded that the steam treatment does not affect the internal structure of the minerals.

The reduced sedimentation volume observed for all samples after exposition to water vapor testifies a successful steam treatment but did not allow an identification of processes.

The measured changes in CEC are only significant in the case of monovalent interlayer cations. This result is in contrast to earlier investigations by Couture (1985b) and Oscarson & Dixon (1989). The fact that cation exchange capacities of samples containing divalent interlayer cations do not change within a 10 % error margin cannot be explained at present and requires further investigation. These differences between mono- and divalent loaded smectites are also indicated by results of time depended VIS spectra of methylene blue clay interaction.

Realizing that sedimentation volume (see for example chapters 2 and 9 of Krut (1952)) and CEC are influenced by the electrokinetic charge density and the surface charge density respectively, strongly suggests that the observed differences are due to changes in the charge distribution at the surface of the minerals. This idea is in qualitative agreement with zeta potentials reported by Bish *et al.* (1997).

The probably negative influence of water vapor on the moulding sand quality and the sand regeneration process could be based on the aforementioned results confirmed. Further experiments therefore included conductometric titrations as well as the determination of zeta potentials or electrophoretic mobilities as a function of pH.

Furthermore, rheological measurements, which could be directly connected to modifications in electrokinetic properties and especially changes of particle shape computed from conductometric titrations (Dukhin & Derjaguin, 1974) were performed. These experiments deliver usable results regarding unprocessed and steam treated samples.

The impact of a hot water vapor treatment on bentonites or smectites, respectively seems to be understood. Smectites with a monovalent interlayer cation showed differences before and after steaming, whereas divalent loaded samples remained mostly unaffected. The bentonite or smectite species exerts no evident influence on the steaming results. As shown in Heuser *et al.* (2014), physical properties (i.e. equivalent sphere diameter) were not systematically changed due to steaming.

Also mineralogy (XRD) and surface near chemical structure (XPS) remained unaffected. However, chemical properties (e.g. sedimentation volume or methylene blue sorption kinetics) react to water vapor. The measurements performed in this work show that the charge conditions at the smectite surface (potentiometric titrations) and especially the surface conductivity (conductometric titrations) were affected by water vapor.

Also the pH of smectite dispersions showed differences between unprocessed and treated samples resulting in a decrease of viscosity and shear stress after steaming. Surface roughness was observed, but in the same order of magnitude for untreated and treated samples. However, the author speculates about a connection between surface roughness and electrokinetics, also with regard to the results of Heuser *et al.* (2014).

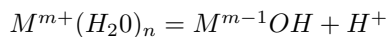
Since the positive properties of smectites (e.g. like interlamellar swelling, low permeability, function as ion exchanger) were not negatively influenced by liquid water, the interaction between the smectite surface and the gaseous phase in the autoclaves should lead to the observed negative results (e.g. lost in swelling capacity).

Other authors i.e. Couture (1985b), Oscarson & Dixon (1989), and Pusch (2000) searching since decades for a possible explanation for changes of parameters and properties observed at clay minerals after a water vapor treatment. However, except Bish *et al.* (1997) other studies mainly examined bulk parameters and properties mostly on macroscopic rather on microscopic scale.



Güven (1990) summarizes, that a steam treatment at enhanced temperatures could affect the (micro-)structure of a bentonite or smectite, respectively, resulting in a disorder of the lamellar ordered framework. Hence, an affection of the grain boundaries between the smectite particles was assumed, that not only could destabilize the microstructure of a smectite, but also the structure of the interlamellar water, that is directly connected to the swelling pressure (Güven, 1990).

Furthermore, Güven (1990) considered another process that could be reduced to a water vapor treatment. This process enclosed a proton dissociation from the hydration shell of the interlayer cations as already introduced by Frenkel (1974):



The proton dissociated by the aforementioned process was firstly assumed to associate with oxygen ions in the smectite layers, resulting in a change of the layer charge and secondly reacted with aluminum ions in the smectite, resulting in the development of hydroxy-aluminum interlayer complexes (Güven, 1990).

Therefore, future investigations should enclose a more detailed examination and clarification of possible surface charge modifying processes.

In this context, some more potentiometric titrations from high to low pH and backwards should be performed, in order to examine possible hysteresis effects and to study the surface acidity of unprocessed and steam treated smectites to a more detailed extent.

The surface roughness and fractality was studied by nitrogen sorption experiments, resulting in a smooth surface with a fractal dimension of  $D = 2.2$ . Differences between unprocessed and steam treated samples were comparable low. Therefore, a further study of the particle surface should clarify, if the surface roughness remains unaffected by steam. Hence, a detailed view on the particle surface by atomic force microscopy (AFM) would deliver real on-sight results (Zabat *et al.*, 1997), which seem to be more probable compared to calculated values from nitrogen sorption.

Finally, it should be considered which other surface sensitive measuring methods could be applied in order to get a closer look to the particle surface, to study its structure and charge conditions.

---

# References

---

## References

- Akin, I. & Likos, W. (2014) Specific Surface Area of Clay Using Water Vapor and EGME Sorption Methods. *Geotechnical Testing Journal*, **37**, 1–12.
- Anbeek, C. (1992) Surface roughness of minerals and implications for dissolution studies. *Geochimica et Cosmochimica Acta*, **56**, 1461–1469.
- Anthony, J., Bideaux, R., Bladh, K. & Nichols, M. (2013) *Handbook of Mineralogy*. Mineralogical Society of America, Chantilly, VA 20151-1110, USA, <http://www.handbookofmineralogy.org>.
- Arroyo, F., Carrique, F., Ahuallia, S. & Delgado, A. (2004) Dynamic mobility of concentrated suspensions - Comparison between different calculations. *Physical Chemistry Chemical Physics*, **6**, 1446–1452.
- Arroyo, F., Carrique, F., Jiménez-Olivares, M. & Delgado, A. (2000) Rheological and Electrokinetic Properties of Sodium Montmorillonite Suspensions - II. Low-Frequency Dielectric Dispersion. *Journal of Colloid and Interface Science*, **229**, 118–122.
- Ashmawy, A., El-Hajji, D., Sotelo, N. & Muhammad, N. (2002) Hydraulic performance of untreated and polymer-treated bentonite in inorganic landfill leachates. *Clays and Clay Minerals*, **50**, 546–552.
- Avnir, D., Farin, D. & Pfeifer, P. (1983) Chemistry in noninteger dimensions between two and three. II. Fractal surfaces of adsorbents. *The Journal of Chemical Physics*, **79**, 3566–3571.
- Baeyens, B. & Bradbury, M. (1997) A mechanistic description of Ni and Zn sorption on Na-montmorillonite Part I: Titration and sorption measurements. *Journal of Contaminant Hydrology*, **27**, 199–222.
- Bagwell, R. & Messing, G. (1999) Effect of Seeding and Water Vapor on the Nucleation and Growth of  $\alpha$ -Al<sub>2</sub>O<sub>3</sub> from  $\gamma$ -Al<sub>2</sub>O<sub>3</sub>. *Journal of the American Ceramic Society*, **82**, 825–832.
- Baier, J. (1991) Griechischer Bentonit für Gießereien. *Giesserei*, **78**, 501–506.
- Beeley, P. (2001) *Foundry technology*. 719 p. Butterworth-Heinemann.
- Benna, M., Kbir-Ariguib, N., Magnin, A. & Bergaya, F. (1999) Effect of pH on Rheological Properties of Purified Sodium Bentonite Suspensions. *Journal of Colloid and Interface Science*, **218**, 442–455.
- Berghof (2012) Homepage of the Berghof Company. visited at 15.01.2012.  
**URL:** [www.berghof.com](http://www.berghof.com)
- Bergmann, J. & Kleeberg, R. (1998) Rietveld analysis of disordered layer silicates. *Material Science Forum*, **278**, 300–305.
- Bish, D. (2006) Parallels and distinctions between clay minerals and zeolites. In: *Handbook of Clay Science* (F. Bergaya, B. Theng and G. Lagaly, editors), Developments in Clay Science, chapter 13.2, 1097–1112. Elsevier.
- Bish, D. & Ming, D. (2001) *Natural zeolithes: occurrence, properties, applications, Reviews in Mineralogy and Geochemistry*, volume 45.
- Bish, D., Wu, W., Carey, J., Constanzo, P., Giese, R., Earl, W. & Oss, C. (1997) Effects of steam on the surface properties of Na-smectite. In: *Proceedings of the 11th International Clay Conference: Clays for our future, Ottawa*, 569–575.
- Breen, C. & Watson, R. (1998) Acid-activated organoclays: preparation, characterisation and catalytic activity of polycation-treated bentonites. *Applied Clay Science*, **12**, 479–494.
- Brigatti, M., Galan, E. & Theng, B. (2006) Structures and Mineralogy of Clay Minerals. In: *Handbook of Clay Science* (F. Bergaya, B. Theng and G. Lagaly, editors), *Developments in Clay Science*, volume 1. Elsevier.

- 
- Brunauer, S., Emmett, P. & Teller, E. (1938) Adsorption of Gases in Multimolecular Layers. *Journal of the American Chemical Society*, **60**, 309–319.
- Bujdák, J., Iyi, N. & Fujita, T. (2002) The aggregation of methylene blue in montmorillonite dispersions. *Clay Minerals*, **37**, 121–133.
- Bujdák, J., Janek, M., Madejová, J. & Komadel, P. (1998) Influence of the layer charge density of smectites on the interaction with methylene blue. *Journal of the Chemical Society, Faraday Transactions*, **94**, 3487–3492.
- Bujdák, J., Janek, M., Madejová, J. & Komadel, P. (2001) Methylene blue interactions with reduced-charge smectites. *Clays and Clay Minerals*, **49**, 244–254.
- Cadene, A., Durand-Vidal, S., Turq, P. & Brendle, J. (2005) Study of individual Na-montmorillonite particles size, morphology, and apparent charge. *Journal of Colloid and Interface Science*, **285**, 719–730.
- Canesson, P. (1982) E.S.C.A. studies of clay minerals. In: *Advanced techniques for clay mineral analysis* (J. Fripiat, editor), *Developments in Sedimentology*, volume 34, chapter 9, 211–236. Elsevier.
- Capek, L., Dedecek, J. & Wichterlova, B. (2004) Co-beta zeolite highly active in propane-SCR-NO<sub>x</sub> in the presence of water vapor: effect of zeolite preparation and Al distribution in the framework. *Journal of Catalysis*, **227**, 352–366.
- Christidis, G. & Huff, W. (2009) Geological Aspects and Genesis of Bentonites. *Elements*, **5**, 93–98.
- Christidis, G., Scott, P. & Dunham, A. (1997) Acid activation and bleaching capacity of bentonites from the islands of Milos and Chios, Aegean, Greece. *Applied Clay Science*, **12**, 329–347.
- Couture, R. (1985a) Rapid increases in permeability and porosity of bentonite-sand mixtures due to alteration by water vapor. *Materials Research Society Symposia Proceedings*, **44**, 515–522.
- Couture, R. (1985b) Steam rapidly reduces the swelling capacity of bentonite. *Nature*, **318**, 50–52.
- Czímerová, A., Jankovic, L. & Bujdák, J. (2003) Effect of the exchangeable cations on the spectral properties of methylene blue in clay dispersions. *Journal of Colloid and Interface Science*, **274**, 126–132.
- Czímerová, A., Jankovic, L. & Bujdák, J. (2004) Effect of exchangeable cations on the spectral properties of methylene blue in clay dispersions. *Journal of Colloid and Interface Science*, **274**, 126–132.
- Damme, H. V. & Fripiat, J. (1985) A fractal analysis of adsorption processes by pillared swelling clays. *The Journal of Chemical Physics*, **82**, 2785–2789.
- Delano, J. W., Tice, S. J., Mitchell, C. E. & Goldman, D. (1994) Rhyolitic glass in Ordovician K-bentonites: A new stratigraphic tool. *Geology*, **22**, 115–118.
- der Linde, A. V. & Bijsterbosch, B. (1990) Zeta potentials as calculated from streaming potential and conductivity data on plugs by means of a number of recent theories. *Croatica Chemica Acta*, **63**, 455.
- Dieng, M. (2005) Der Wasseraufnahmeversuch nach DIN 18132 in einem neu entwickelten Gerät. *Bautechnik*, **82**, 28–32.
- DIN 18129 (2011) DIN 18129:2011-07, Baugrund, Untersuchung von Bodenproben, Kalkgehaltsbestimmung.
- DIN 6174 (2007) *Farbmetrische Bestimmung von Farbmaßzahlen und Farbabständen im angenähert gleichförmigen CIELAB-Farbraum*. Technical report.
-

- 
- Dogan, A., Dogan, M., Onal, M., Sarikaya, Y., Aburub, A. & Wurster, D. (2006) Baseline Studies of the Clay Minerals Society Source Clays: Specific Surface Area by the Brunauer Emmet Teller (BET) Method. *Clays and Clay Minerals*, **54**, 62–66.
- Dohrmann, R., Genske, D., Karnland, O., Kaufhold, S., Kiviranta, L., Olsson, S., Plötze, M., Sandén, T., Sellin, P., Svensson, D. & Valter, M. (2012) Interlaboratory CEC and exchangeable cation study of bentonite buffer materials: I. Cu(II)-Triethylenetetramine method. *Clays and Clay Minerals*, **60**, 162–175.
- Dontsova, K., Norton, L. D., Johnston, C. & Bigham, J. (2004) Influence of Exchangeable Cations on Water Adsorption by Soil Clays. *Soil Science Society of America Journal*, **68**, 1218–1227.
- Dukhin, A. & Goetz, P. (2002) In: *Ultrasound for Characterizing Colloids, Studies in Interface Science*, volume 15. Elsevier.
- Dukhin, S. & Derjaguin, B. (1974) *Equilibrium double layer and electrokinetic phenomena, Surface and Colloid Science*, volume 7, chapter 2, 217 pp. John Wiley and Sons.
- Durán, J., Ramos-Tejada, M., Arroyo, F. & González-Caballero, F. (2000) Rheological and Electrokinetic Properties of Sodium Montmorillonite Dispersions - I. Rheological Properties and Interparticle Energy of Interaction. *Journal of Colloid and Interface Science*, **229**, 107–117.
- Eberl, D., Srodon, J., Kralik, M., Taylor, B. & Peterman, Z. (1990) Ostwald Ripening of Clays and Metamorphic Minerals. *Science*, **248**, 474–477.
- Ebina, T., Iwasaki, T., Chatterjee, A., Katagiri, M. & Stucky, G. (1997) Comparative Study of XPS and DFT with Reference to the Distributions of Al in Tetrahedral and Octahedral Sheets of Phyllosilicates. *Journal of Physical Chemistry B*, **101**, 1125–1129.
- Emmerich, K., Madsen, F. & Kahr, G. (1999) Dehydroxylation behavior of heat-treated and steam-treated homoionic *cis*-vacant montmorillonites. *Clays and Clay Minerals*, **47**, 591–604.
- Erdoğan, B. & Demirci, Ş. (1996) Activation of some Turkish bentonites to improve their drilling fluid properties. *Applied Clay Science*, **10**, 401–410.
- EUBA (2009) Position Paper 9/2009. [www.ima-europe.eu](http://www.ima-europe.eu).
- Fahrenholtz, W. (2008) *Clays. Ceramic and Glass Materials: Structure, Properties and Processing*. Springer.
- Fairley, N. (2009) *CasaXPS Manual - 2.3.15 Introduction to XPS and AES*. 177 p., Casa Software Ltd.
- Frenkel, M. (1974) Surface acidity of motmorillonites. *Clays and Clay Minerals*, **22**, 435–441.
- Galindo-Rosales, F. & Rubio-Hernández, F. (2006) Structural breakdown and build-up in bentonite dispersions. *Applied Clay Science*, **33**, 109–115.
- Genovese, D. B. (2012) Shear rheology of hard-sphere, dispersed, and aggregated suspensions, and filler-matrix composites. *Advances in Colloid and Interface Science*, **171–172**, 1–16.
- Gitipour, S., Bowers, M. & Bodocsi, A. (1997) The Use of Modified Bentonite for Removal of Aromatic Organics from Contaminated Soil. *Journal of Colloid and Interface Science*, **196**, 191–198.
- Gougeon, R., Soulard, M., Miehe-Brendle, J., Chezeau, J.-M., Dred, R. L., Jeandet, P. & Marchal, R. (2003) Analysis of Two Bentonites of Enological Interest before and after Commercial Activation by Solid Na<sub>2</sub>CO<sub>3</sub>. *Journal of Agricultural and Food Chemistry*, **51**, 4096–4100.
- Grefhorst, C. (2006) Prüfung von Bentoniten – Ausführliche Bewertung der Eigenschaften und ihr Wert für die Praxis. *Giesserei*, **93**, 26–31.
-

- 
- Grefhorst, C., Podobed, O. & Böhnke, S. (2005) Bentonitgebundene Formstoffe - Umlaufverhalten von Bentoniten unter besonderer Betrachtung des Kreislaufsystems und der Nasszugfestigkeit. *Giesserei*, **92**, 63–67.
- Grefhorst, C., Podobed, O. & Böhnke, S. (2010) *Handbuch der Gussfehler*, volume 4. S & B Industrial Minerals.
- Grim, R. & Güven, N. (1978) In: *Bentonites—Geology, Mineralogy, Properties and Uses, Developments in Sedimentology*, volume 24. Elsevier.
- Grinsted, R., Jen, H.-W., Montreuil, C., Rokosz, M. & Shelef, M. (1993) The relation between deactivation of CuZSM-5 in the selective reduction of NO and dealumination of the zeolites. *Zeolites*, **13**, 602–606.
- Guggenheim, S. & van Groos, A. K. (2001) Baseline studies of the clay mineral society source clays: Thermal analysis. *Clays and Clay Minerals*, **49**, 433–443.
- Guo, X. (1999) On the degradation of zirconia ceramics during low-temperature annealing in water or water vapor. *Journal of Physics and Chemistry of Solids*, **60**, 539–546.
- Güven, N. (1988) Smectites. In: *Hydrous Phyllosilicates* (S. Bailey, editor), *Reviews in Mineralogy and Geochemistry*, volume 19, 497–559. Mineralogical Society of America.
- Güven, N. (1990) Longevity of Bentonite as Buffer Material in a Nuclear-Waste Repository. *Engineering Geology*, **28**, 233–247.
- Harvey, C. & Lagaly, G. (2006) Conventional applications. In: *Handbook of Clay Science* (F. Bergaya, B. Theng and G. Lagaly, editors), *Developments in Clay Science*, volume 1, chapter 10.1, pp. 506. Elsevier.
- Hasse, S. (2014) *Giesserei-Lexikon*. online available: [www.giessereilexikon.com](http://www.giessereilexikon.com), visited at 28.07.2014.
- Hauser, E. & Reynolds, H. (1939) Alteration of glasses to montmorillonite. 590–597.
- Heuser, M., Andrieux, P., Petit, S. & Stanjek, H. (2013) Iron-bearing smectites: A revised relationship between structural Fe, cell edge length b and refractive indices. *Clay Minerals*, **48**, 97–103.
- Heuser, M., Weber, C., Stanjek, H., Chen, H., Jordan, G., Schmahl, W. & Natzeck, C. (2014) The interaction between bentonite and water vapor. I: Examination of physical and chemical properties. *Clays and Clay Minerals*, **62**, 188–202.
- Hofmann, U. & Klemen, R. (1950) Verlust der Austauschfähigkeit von Lithiumionen an Bentonit durch Erhitzung. *Zeitschrift für anorganische Chemie*, **262**, 95–99.
- Huang, W.-L., Bassett, W. & Wu, T.-C. (1994) Dehydration and hydration of montmorillonite at elevated temperatures and pressures monitored using synchrotron radiation. *American Mineralogist*, **79**, 683–691.
- Jacobs, K. & Schoonheydt, R. (2001) Time dependence of the spectra of methylene blue - clay mineral dispersions. *Langmuir*, **17**, 5150–5155.
- Jones, R. & Uehara, G. (1973) Amorphous coatings on mineral surfaces. *Soil Science Society of America Proceedings*, **37**, 792–798.
- Jordan, G., Eulenkamp, C., Calzada, E., Schillinger, B., Hoelzel, M., Gigler, A., Stanjek, H. & W.W. Schmahl, W. (2013) Quantitative in-situ study on the dehydration of bentonite bonded molding sands. *Clays and Clay Minerals*, **61**, 133–140.
- Jorgensen, P., Wadsworth, M. & Cutler, I. (1961) Effects of Water Vapor on Oxidation of Silicon Carbide. *Journal of the American Ceramic Society*, **44**, 258–261.
-

- 
- Kahr, G. & Madsen, F. (1995) Determination of the cation exchange capacity and the surface area of bentonite, illite and kaolinite by methylene blue adsorption. *Applied Clay Science*, **9**, 327–336.
- Kahr, G. & Madsen, F. (1996) Adsorption of water vapor and specific surface area of clays. *Geosciences*, **27**, 16 p.
- Kaufhold, S., Dohrmann, R. & Klinkenberg, M. (2010) Water-uptake capacity of bentonites. *Clays and Clay Minerals*, **58**, 37–43.
- Kikuchi, E., Ogura, M., Aratani, N., Sugiura, Y., Hiromoto, S. & Yogo, K. (1996) Promotive effect of additives to In/H-ZSM-5 catalyst for selective reduction of nitric oxide with methane in the presence of water vapor. *Catalysis Today*, **27**, 35–40.
- Kitano, T., Kataoka, T. & Shiota, T. (1981) An empirical equation of the relative viscosity of polymer melts filled with various inorganic fillers. *Rheologica Acta*, **20**, 207–209.
- Klinkenberg, M., Rickertsen, N., Kaufhold, S., Dohrmann, R. & Siegesmund, S. (2009) Abrasivity by bentonite dispersions. *Applied Clay Science*, **46**, 37–42.
- Köster, H. (1977) Die Berechnung kristallchemischer Strukturformeln von 2:1-Schichtsilikaten unter Berücksichtigung der gemessenen Zwischenschichtladungen und Kationenumtauschkapazitäten, sowie die Darstellung der Ladungsverteilung in der Struktur mittels Dreieckskoordinaten. *Clay Minerals*, **12**, 45–54.
- Köster, H. (1979) *Die chemische Silikatanalyse: Spektralphotometrische, komplexometrische und flammenspektrometrische Analysenmethoden*. 212 p. Springer.
- Krischey, E., Ohrdorf, K.-H. & Flachberger, H. (2015) Verfahren zur Herstellung von alkalisch und organophil aktiviertem Kalzium-Montmorillonit für den Einsatz in Polymer-Compounds. *BHM*, **160**, 291–299.
- Kruyt, H. (1952) *Colloid Science Volume 1 - Irreversible Systems*. Elsevier.
- Lagaly, G. (1989) Principles of Flow of Kaolin and Bentonite Dispersions. *Applied Clay Science*, **4**, 105–123.
- Lagaly, G., Schulz, O. & Zimehl, R. (1997) *Dispersionen und Emulsionen. Einführung in die Kolloidik feinverteilter Stoffe einschließlich der Tonminerale*. 285–289. Steinkopff-Verlag, 1st edition.
- Lange, H. (1968) Bestimmung von Teilchengrößen aus Trübung und Brechungssinkrement. *Kolloid Zeitschrift und Zeitschrift für Polymere*, **223**, 24–30.
- Lange, H. (1969) Bestimmung der Teilchengröße in ABS-Kunststoffen. *Kolloid Zeitschrift und Zeitschrift für Polymere*, **232**, 753–757.
- Lange, H. (1995) Comparative Test of Methods to Determine Particle Size and Particle Size Distribution in the Submicron Range. *Particle and Particle Systems Characterization*, **12**, 148–157.
- Lee, J.-F., Lee, C.-K. & Juang, L.-C. (1999) Size Effects of Exchange Cation on the Pore Structure and Surface Fractality of Montmorillonite. *Journal of Colloid and Interface Science*, **217**, 172–176.
- Lee, S., Park, Y., Hsu, P. & McNallan, M. (2003) Synergistic Effects of Water Vapor and Alkali Chloride Vapors on the High-Temperature Corrosion of SiC-Based Ceramics. *Journal of the American Ceramic Society*, **86**, 1292–1298.
- Lippens, B. & de Boer, J. (1965) Studies on Pore Systems in Catalysts. V. The t Method. *Journal of Catalysis*, **4**, 319–323.
- Luckham, P. & Rossi, S. (1999) The colloidal and rheological properties of bentonite dispersions. *Advances in Colloid and Interface Science*, **82**, 43–92.
-

- 
- Lyklema, J. (1995) *Fundamentals of Interface and Colloid Science. Solid-Liquid Interfaces*, volume 2. Academic Press.
- Lyklema, J. (2001) Surface conduction. *Journal of Physics: Condensed Matter*, **13**, 5027–5034.
- Lyklema, J. & Minor, M. (1998) On surface conduction and its role in electrokinetics. *Colloids and Surfaces A: Physicochemical and Engineering Aspects*, **140**, 33–41.
- Ma, Y.-L., Xu, Z.-R., Guo, T. & You, P. (2004) Adsorption of methylene blue on Cu(II)-exchanged montmorillonite. *Journal of Colloid and Interface Science*, **280**, 283–288.
- Madsen, F. (1998) Clay mineralogical investigations related to nuclear waste disposal. *Clay Minerals*, **33**, 109–129.
- Malekani, K., Rice, J. & Lin, J.-S. (1996) Comparison of Techniques for Determining the Fractal Dimensions of Clay Minerals. *Clays and Clay Minerals*, **44**, 677–685.
- Malhoukhi, B., Didi, M., Villemain, D. & Azzouz, A. (2009) Acid activation of Bentonite for use as a vegetable oil bleaching agent. *Grasas y aceites*, **60**, 343–349.
- Marchel, C. (2008) Untersuchungen zur Dehydroxilierung dioktaedrischer Smectite. Phd thesis, RWTH Aachen University, Fakultät für Georessourcen und Materialtechnik.
- Meier, L. & Kahr, G. (1999) Determination of the cation exchange capacity (CEC) of clay minerals using the complexes of copper (II) ion with triethylenetetramine and tetraethylenepentamine. *Clays and Clay Minerals*, **47**, 386–388.
- Melik, D. & Fogler, H. (1983) Turbidimetric Determination of Particle Size Distributions of Colloidal Systems. *Journal of Colloid and Interface Science*, **92**, 161–180.
- Mellah, A. & Chegrouche, S. (1997) The removal of zinc from aqueous solutions by natural bentonite. *Water research*, **31**, 621–629.
- Montes-H., G., Duplay, J., Martinez, L., Geraud, Y. & Rousset-Tournier, B. (2003) Influence of interlayer cations on the water sorption and swelling-shrinkage of MX80 bentonite. *Applied Clay Science*, **23**, 309–321.
- Montes-H., G. & Geraud, Y. (2004) Sorption kinetic of water vapour of MX80 bentonite submitted to different physical-chemical and mechanical conditions. *Colloids and Surfaces A: Physicochemical and Engineering Aspects*, **235**, 17–23.
- More, K., Tortorelli, P., Walker, L., Miriyala, N., Price, J. & van Roode, M. (2003) High-Temperature Stability of SiC-Based Composites in High-Water-Vapor-Pressure Environments. *Journal of the American Ceramic Society*, **86**, 1272–1281.
- Mosser, C., Mosser, A., Romeo, M., Petit, S. & Decarreau, A. (1992) Natural and synthetic copper phyllosilicates studied by XPS. *Clays and Clay Minerals*, **40**, 1125–1129.
- Murray, H. (2007) In: *Applied clay mineralogy - Occurrences, Processing and Application of Kaolins, Bentonites, Palygorskite- Sepiolite, and Common Clays, Developments in Clay Science*, volume 2. Elsevier.
- Nadeau, P. (1985) The physical dimensions of fundamental clay particles. *Clay Minerals*, **20**, 499–514.
- Neff, K. (1959) Über die Messung der Wasseraufnahme ungleichförmiger bindiger anorganischer Bodenarten in einer neuen Ausführung des Enslingerätes. *Die Bautechnik*, **39**, 415–421.
- Neimark, A. (1990) Thermodynamic method for calculating surface fractal dimension. *Letters to Journal of Experimental and Theoretical Physics*, **51**, 607–610.
- Neimark, A. V., Hanson, M. & Unger, K. K. (1993) Fractal Analysis of the Distribution of High-Viscosity Fluids in Porous Supports. *Journal of Physical Chemistry*, **97**, 6011–6015.
-



- 
- Neimark, A. V. & Unger, K. K. (1993) Method of Discrimination of Surface Fractality. *Journal of Colloid and Interface Science*, **158**, 412–419.
- O'Brien, R., Jones, A. & Rowlands, W. (2003) A new formula for the dynamic mobility in a concentrated colloid. *Colloids and Surfaces A: Physicochemical and Engineering Aspects*, **218**, 89–101.
- Ohrdorf, K.-H. & Flachberger, H. (2009) Zu Fragen der alkalischen Aktivierung von Bentoniten. *BHM*, **12**, 597–609.
- Ohrdorf, K.-H. & Flachberger, H. (2010) Alkalische Aktivierung von Bentoniten als Beitrag der Aufbereitung zur Ressourcen- und Rohstoffeffizienz. *Chemie Ingenieur Technik*, **82**, 1991–1998.
- Ohtsuka, H. & Tabata, T. (1999) Effect of water vapor on the deactivation of Pd-zeolite catalysts for selective catalytic reduction of nitrogen monoxide by methane. *Applied Catalysis B: Environmental*, **21**, 133–139.
- Opila, E. & Myers, D. (2004) Alumina Volatility in Water Vapor at Elevated Temperatures. *Journal of the American Ceramic Society*, **87**, 1701–1705.
- Oscarson, D. & Dixon, D. (1989) The effect of steam on montmorillonite. *Applied Clay Science*, **4**, 279–292.
- Oscarson, D., Dixon, D. & Gray, M. (1990) Swelling capacity and permeability of an unprocessed and a processed bentonitic clay. *Engineering Geology*, **28**, 281–259.
- O'Brien, R., Cannon, D. & Rowlands, W. (1985) Electroacoustic determination of particle size and zeta potential. *Journal of Colloid and Interface Science*, **173**, 406–418.
- Pabst, W. (2004) Fundamental considerations of suspension rheology. *Ceramics-Silikáty*, **48**, 6–13.
- Pabst, W., Gregorová, E. & Berthold, C. (2006) Particle shape and suspension rheology of short-fiber systems. *Journal of the European Ceramic Society*, **26**, 149–160.
- Parkhurst, D. & Appelo, C. (1994) *User's Guide to PHREEQC (Version 2). A Computer Program for Speciation, Batch Reaction, One-Dimensional Transport, and Inverse Geochemical Calculations*. Water-resources investigations report 99-4259, 312 p., USGS Geological Survey, Denver, Colorado, USA.
- Paterson, E. & Swaffield, R. (1994) X-ray photoelectron spectroscopy. In: *Clay Mineralogy: Spectroscopic and Chemical Determinative Methods* (M. Wilson, editor), chapter 6, 226–259.
- Penner, D. & Lagaly, G. (2001) Influence of anions on the rheological properties of clay mineral dispersions. *Applied Clay Science*, **19**, 131–142.
- Pusch, R. (2000) *On the effect of hot water vapor on MX-80 clay*. TR-00-16 41p., SKB.
- Pusch, R. & Kasbohm, J. (2002) *Alteration of MX-80 by hydrothermal treatment under high salt content conditions*. TR-02-06 39 p., SKB.
- Rasmusson, M., Rowlands, W., O'Brien, R. & Hunter, R. (1997) The Dynamic Mobility and Dielectric Response of Sodium Bentonite. *Journal of Colloid and Interface Science*, **189**, 92–100.
- Recknagel, U. & Dahlmann, M. (2009) Spezialsande-Formgrundstoffe für die moderne Kern- und Formherstellung. *Giesserei-Rundschau*, **56**, 6–17.
- Rouquerol, F., Rouquerol, J. & Sing, K. (1999) Assessment of Surface Area. In: *Adsorption by Powders and Porous Solids*, chapter 6, pp. 165. Academic Press.
- Rowlands, W. & O'Brien, R. (1995) The Dynamic Mobility and Dielectric Response of Kaolinite Particles. *Journal of Colloid and Interface Science*, **175**, 190–200.
-

- 
- Rožić, L., Novaković, T., Petrović, S., Vuković, Z. & Čupić, Ž. (2008) Fractal Analysis of Physical Adsorption on Surfaces of Acid Activated Bentonites from Serbia. *Chemical Industry and Chemical Engineering Quarterly*, **14**, 227–229.
- Sano, T., Yamashita, N., Iwami, Y., Takeda, K. & Kawakami, Y. (1996) Estimation of dealumination rate of ZSM-5 zeolite by adsorption of water vapor. *Zeolites*, **16**, 258–264.
- Scalia, J. & Benson, C. (2011) Hydraulic Conductivity of Geosynthetic Clay Liners Exhumed from Landfill Final Covers with Composite Barriers. *Journal of Geotechnical and Geoenvironmental Engineering*, **137**, 1–13.
- Sing, K., Everett, D., Haul, R., Moscou, L., Pierotti, R., Rouquerol, J. & Siemieniowska, T. (1985) Reporting Physisorption Data for gas/solid Systems with Special Reference to the Determination of Surface Area and Porosity. *Pure and Applied Chemistry*, **57**, 603–619.
- Steudel, A. & Emmerich, K. (2013) Strategies for the successful preparation of homoionic smectites. *Applied Clay Science*, **75–76**, 13–21.
- Thommes, M. (2010) Physical Adsorption Characterization of Nanoporous Materials. *Chemie Ingenieur Technik*, **82**, 1059–1073.
- Träger, H. & Bührig-Polaczek, A. (2000) *Foundry Technology*. Ullmann's Encyclopedia of Industrial Chemistry.
- Ufer, K., Stanjek, H., Roth, G., Dohrmann, R., Kleeberg, R. & Kaufhold, S. (2008) Quantitative phase analysis of bentonites by the rietveld method. *Clays and Clay Minerals*, **56**, 272–282.
- VDG P35 (1999) *Prüfung von tongebundenen Formstoffen. Bestimmung des Anteils an bindetönigem Ton*. Technical report, Verein deutscher Giessereifachleute.
- VDG P69 (1999) *Bindemittelprüfung - Prüfung von Bindetönen*. Technical report, Verein deutscher Giessereifachleute.
- Volzone, C. & Garrido, L. (1991) The effect of some physico-chemical and mineralogical properties on the Na<sub>2</sub>CO<sub>3</sub> activation of Argentine bentonites. *Applied Clay Science*, **6**, 143–154.
- Wang, C., Juang, L., Lee, C.-K., Hsu, T.-C., Lee, J.-F. & Chao, H.-P. (2004) Effects of exchanged surfactant cations on the pore structure and adsorption characteristics of montmorillonite. *Journal of Colloid and Interface Science*, **280**, 27–35.
- Wang, S.-L., Johnston, C., Bish, D., White, J. & Hem, S. (2003) Water-vapor adsorption and surface area measurement of poorly crystalline boehmite. *Journal of Colloid and Interface Science*, **260**, 26–35.
- Weber, C., Heuser, M., Mertens, G. & Stanjek, H. (2013) Determination of clay mineral aspect ratios from conductometric titrations. *Clay Minerals*, **49**, 17–26.
- Wenk, H. & Bulakh, A. (2004) *Minerals - Their Constitution and Origin*. Cambridge.
- Wiederhorn, S. (1967) Influence of Water Vapor on Crack Propagation in Soda-Lime Glass. *Journal of the American Ceramic Society*, **50**, 407–414.
- Wojdyr, M. (2010) Fityk: a general-purpose peak fitting program. *Journal of Applied Crystallography*, **43**, 1126–1128.
- Xu, Y., Sun, D. & Yao, Y. (2004) Surface fractal dimension of bentonite and its application to determination of swelling properties. *Chaos, Solitons and Fractals*, **19**, 347–356.
- Yildiz, N., Aktas, Z. & Calimli, A. (2004) Sulphuric Acid Activation of a Calcium Bentonite. *Particulate Science and Technology*, **22**, 21–33.
- Yildiz, N., Sarikaya, Y. & Calimli, A. (1999) The effect of the electrolyte concentration and pH on the rheological properties of the original and the Na<sub>2</sub>CO<sub>3</sub>-activated Kutahya bentonite. *Applied Clay Science*, **14**, 319–327.
-

- 
- Young, G. (1958) Interaction of water vapor with silica surfaces. *Journal of Colloid Science*, **13**, 67–85.
- Yuan, J. & Murray, H. (1997) The importance of crystal morphology on the viscosity of concentrated suspensions of kaolins. *Applied Clay Science*, **12**, 209–219.
- Zabat, M., Vayer-Besancon, M., Harba, R., Bonnamy, S. & Damme, H. V. (1997) Surface topography and mechanical properties of smectite films. *Progress in Colloid and Polymer Science*, **105**, 96–102.
- Zhu, J., Zhu, L., Zhu, R., Tian, S. & Li, J. (2009) Surface microtopography of surfactant modified montmorillonite. *Applied Clay Science*, **45**, 70–75.
- Zhu, X., Jiang, D. & Tan, S. (2002) Preparation of silicon carbide reticulated porous ceramics. *Materials Science and Engineering A*, **323**, 232–238.

---

# Lebenslauf / Curriculum vitae

## **persönliche Daten / personal data**

Name	Michel Heuser
Geburtstag	09.08.1981
Geburtsort	Wetzlar

## **Ausbildung und Berufstätigkeit / education and professional activity**

1988 - 1992	Grundschule auf dem Falkenflug
1992 - 2002	Gymnasium Phillipinum Weilburg Abschluss: Allgemeine Hochschulreife
2002 - 2005	Studium des Bauingenieurwesens an der RWTH Aachen
2005 - 2010	Studium der Angewandten Geowissenschaften an der RWTH Aachen Abschluss: Master of Science (M.Sc.)
01/2011 - 11/2015	Wissenschaftlicher Angestellter / Doktorand am Lehr- und Forschungsgebiet für Ton- und Grenzflächenmineralogie an der RWTH Aachen
12/2015 - 12/2016	Projektleiter im Ingenieurbüro für Geotechnik und Baugrunduntersuchung Wollenhaupt (IGBW), Wildeck-Hönebach
01/2017 - heute	Ingenieurgeologe bei der TPA Gesellschaft für Qualitätssicherung und Innovation GmbH, Bad Hersfeld